Dynamic Analysis of Slab-on-Grade Systems: Forward and Backcalculation Analyses

A Dissertation
SUBMITTED TO THE FACULTY OF
UNIVERSITY OF MINNESOTA
BY

Abbas Booshehrian

IN PARTIAL FULFILLMENT OF THE REQUIREMENTS
FOR THE DEGREE OF
DOCTOR OF PHILOSOPHY

Lev Khazanovich, Advisor

December 2017

Acknowledgements

This thesis project would not have been possible without the support of a lot of people who helped me along the way. At the very beginning, I would like to express my sincere gratitude to my major advisor, Prof. Lev Khazanovich, for his guidance, support, and technical expertise throughout this process. Also, I would like to express my thanks to the supervisory committee members, Prof. Catherine French, Prof. Henryk Stolarski, and Prof. Ellad Tadmor, for their availability and technical comments. I would like to express my gratitude to my supervisor and friend at VAA, Mr. Chris Broderson, for his understanding and unconditional support. I also thank the Minnesota Department of Transportation (MnDOT) for providing quality field data. Special thanks are due to Prof. Arghavan Louhghalam and Prof. Eyal Levenberg for the fruitful collaboration.

I would like to thank my dear friends and fellow colleagues for the fun memories and emotional support; to you Dr. Vahhab Zarei for the sleepless nights of PES; and to Mr. Samuel Paitich for the long walks of glory.

Finally, “family” is my most valuable asset and the everlasting shelter of unity and love. I would like to thank my beloved parents. Their love has been and will always be the shining light through the darkness, and their sparks of wisdom and affection have ignited the fire of courage and persistence in my career. Since my childhood, I cannot remember even one moment without the scent of your prayers for my well-being, prosperity, and success. All that I am, or hope to be, I owe to my lovely mom and dad. My brothers, Ali and Ammar, you have formed the most beautiful memories of love, joy, and friendship, for which I am grateful and blessed. Finally, thanks to Fatemeh, the dearest little sister, for your sweet smiles, unblemished dreams, and pure wishes. I love you all.

I would like to end with this quote from the famous Persian poet, Hafez, who simply says:

“*If you are not pleased, change your destiny*”

THANK YOU!

To my family and friends, near and far.

Abstract

The problem of calculating the response of a slab-on-grade is of interest for analysis and design of industrial floors, nuclear plants, mat and raft foundations, and pavement systems. These structures are often subjected to complicated external dynamic excitations such as earthquakes, impacts, and moving loads, resulting in a challenging load-structure system to simulate. For design and evaluation purposes, deflection-based non-destructive testing such as falling weight deflectometer (FWD) is often utilized to obtain the design properties of these structures. Typically, this is done in two stages: I) forward analysis in which a mathematical model is used to generate the response of the system to a known FWD load, given the structural properties, and II) inverse analysis (a.k.a. backcalculation) in which a numerical scheme is used to indicate the structural properties, given the response of the system to the known FWD load.

The objective of this study was to develop a computational method based on the plate-on-a-foundation approach to model and characterize the slab-on-grade structures subjected to a short-duration dynamic axisymmetric pressure induced by FWD. The advantage of this approach is that it is simple, efficient, and applicable to both elastic and viscoelastic slabs. Furthermore, this approach is compatible with the recently-developed analysis which estimates the excess vehicular fuel consumed due to the viscous deformation of the pavement under the moving load. Thereby, in addition to the applications for the design and analysis of structures, the backcalculated properties may be employed as inputs for realistic evaluation of the environmental impacts caused by the additional fuel use.

To do so, an efficient numerical forward-solution in the time-domain was developed for the response of a thin and infinite viscoelastic Kirchhoff-Love plate resting on a foundation by making use of a Hankel transform in space and a finite difference method in time. Then, the shortcomings of the traditional foundation models, such as the Winkler, Pasternak, and Vlasov models, in capturing the dynamic behavior of the system were highlighted, and required modifications were made. Next, a gradient-based optimization scheme was employed in conjunction with the forward-solution to develop a fast and reliable dynamic backcalculation. To showcase the ability and applications of the developed analysis, multiple case studies were carried out using the data recorded by the FWDs tested on asphalt and concrete pavements. Finally, the traditional Vlasov foundation model was modified accordingly to accommodate the dynamics of the structure. This reinforced the analysis with the ability to characterize the foundation in addition to the top slab.

Table of Contents

List of Tables

List of Figures

1

Thesis Introduction

The problem of calculating the response of a slab-on-grade is of interest for analysis and design of industrial floors, nuclear plants, mat and raft foundations, and pavement systems. These structures are often subjected to complicated external dynamic excitations such as earthquakes, impacts, and moving loads [*Selvadurai*, 1979; *Maheshwari and Khatri*, 2010]. The slab (top layer) is often fabricated with Portland cement concrete (PCC) or hot mixed asphalt (HMA). In the pavement industry, PCC and HMA pavements are also known as rigid and flexible pavements. Due to the pronounced difference in the rigidity of these materials, different structural responses are observed. As such, depending on the material used for the top layer, different mechanistic models are utilized to mathematically simulate the behavior of the desired structure.

Westergaard [1926] described the concrete slab as a thin elastic plate resting on a Winkler foundation, which is a combination of closely spaced, independent linear springs [*Winkler*, 1867]. This type of model is known as "plate-on-a-foundation" model. On the other hand, for the structures with the HMA as the top layer, the "layered elastic theory" has been traditionally used. This model was originated by Boussinesq, and was later expanded by Burmister [*Huang*, 1993]. In this model, stress, strain, and deflection in the pavement system are calculated by dividing the system into multiple elastic, homogenous, isotropic layers characterized by elastic modulus and Poisson's ratio. This model is often considered as a more realistic representation of the soil behavior; however, it requires more computational effort compared to the Winkler model. Different limitations are associated with these two approaches, for instance, Winkler foundation completely ignores the shear

interaction of the soil grains, while the elastic half-space model ascribes to the foundation a higher degree of shear interaction than is usually observed in the field [*Khazanovich*, 1994].

To address the geometric, mechanical, and loading complexities, the computationally intensive finite-element method (FEM) is often employed to approximate the structural responses. Despite the considerable progress made in the analysis of such structures by making use of the FEM, for many applications and various reasons, simpler analytical and semi-analytical solutions are desirable [*Yin*, 2000; *Tanahashi*, 2004; *Wang et al.*, 2005; *Avramidis and Morfidis*, 2006; *Colasanti and Horvath*, 2010; *Horvath and Colasanti*, 2011; *Worku*, 2013]. To name a few of such applications and reasons, the validation of the FEM approximations, avoiding the difficulties associated with the FEM analysis (mesh dependence, modeling soil and structure together as a unit, analyzing the FEM results), and the high computational cost in relation with the dynamic analysis, can be mentioned [*Worku*, 2014].

Another recent and unique application for simplistic models is the estimation of the excess vehicle fuel use [*Louhghalam et al.*, 2013]. Approximately 10% of fuel consumption for heavy trucks is used to overcome the rolling resistance in the tires at a constant speed of 80 km/h [*Pouget et al.*, 2011]. It has been argued that, in addition to other sources of fuel consumption related to rolling resistance (roughness, friction, and so on), the dissipated energy in the process of viscous deformation of the pavement must be compensated by an external energy provided by fuel [*Pouget et al.*, 2011; *Louhghalam et al.*, 2013].

In order to determine the surface deformation and the resulting dissipated energy through the pavement-vehicle interaction (PVI), *Louhghalam et al.* [2013] described both PCC and HMA pavements as a viscoelastic plate resting on a weightless elastic Winkler foundation. This model is computationally efficient, which makes it an attractive tool for an analysis that up-scales the pavement-scale emission to network level environmental impact

[*Louhghalam et al.*, 2014b]. However, the simplicity of this model does not guarantee its ability to properly describe the pavement behavior. The use of a Winkler foundation model is not a common practice, especially for the case of a HMA pavement. Testing the accuracy of this idealization when pavement is subjected to dynamic (moving) loads is one of the motivations of this study. Furthermore, regardless of the accuracy of the selected model, accurate pavement structural parameters are required as inputs to perform the so-called PVI analysis.

The assessment of foundation models can be done by comparing their response estimations with experimental observations. Deflection-based non-destructive testing (NDT) devices can be utilized for this purpose, as they collect the response of the system in terms of the surface deflections, induced by a controlled external loading [Goktepe et al., 2006]. Among the available deflection-based NDT devices, falling weight deflectometer (FWD) is most commonly used because it emulates the movement of a vehicle on the slab surface more realistically [Tholen et al., 1985; Sebaaly et al., 1985; Stolle, 1991; Goktepe et al., 2006; Howard and Warren, 2008]. This is done by applying sinusoidal loads to the slab surface, similar in magnitude and duration to that of a single heavy moving axle [Tholen et al., 1985; Nazarian and Stoke, 1986; Irwin et al., 1989]. The loading plate is circular and multiple sensors are located at different distances radiating away from the center of the loading plate. The apparatus can record the applied loading pressure and the deflection of the pavement surface with respect to time (Figure 1a). A sample FWD time history of the surface deflection and the applied sinusoidal load is shown in Figure 1b. The deflection profiles with smaller magnitudes are collected by sensors positioned at farther radial distances.

Typically, the process of analyzing the FWD data consists of two main components: I) *forward analysis* in which a mathematical model is used to generate the response of the system to a known FWD load, given the structural properties, and II) *inverse analysis (a.k.a. backcalculation)* in which a numerical scheme is used to indicate the structural properties, given the response of the system to the known FWD load. The system response,

in terms of the surface deflections, is measured by the FWD sensors. The search scheme typically adopts techniques such as nonlinear regression, iterative methods, closed-form solutions, and database search to find the combination of the sought properties that leads to the least discrepancy between the model estimations and the FWD measurements (field observations) [*Dong et al.*, 2002; *Xu*, 2014; *Varma*, 2015; *Von Quintus et al.*, 2015]. If the fit is acceptable and the backcalculated properties are reasonable, it validates the adopted model. Then, the analysis is used to indicate the structural properties of the system in a non-destructive manner.

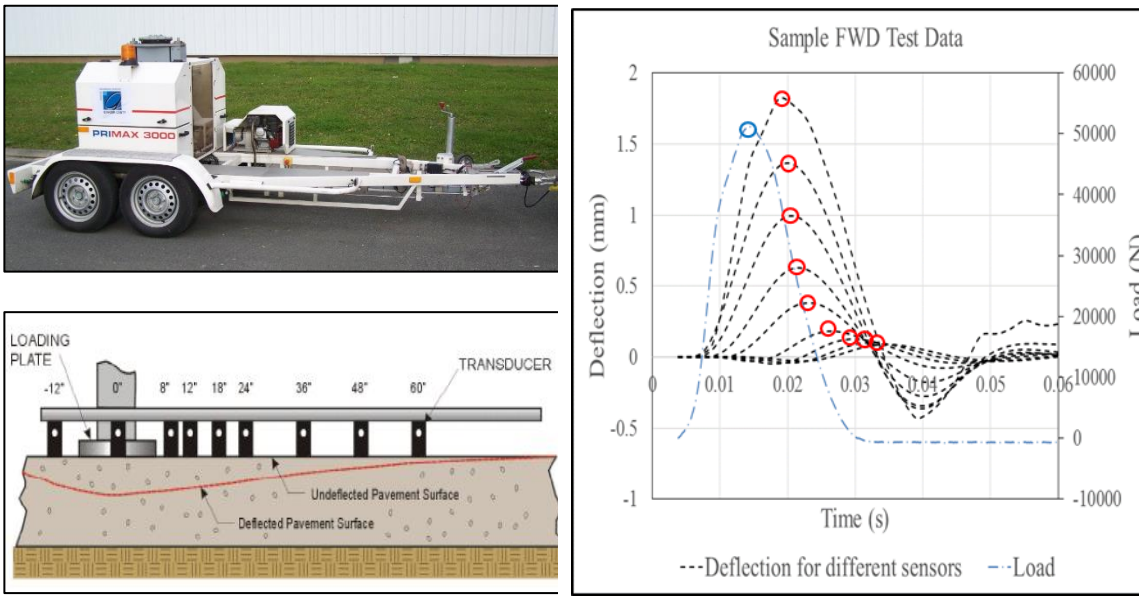

(a) (b)

Figure 1. FWD: (a) equipment (adapted from [*Elseifi et al.*, 2012]), (b) measured load and surface deflection at different distances from the center of loading versus time (Data is provided by Minnesota Department of Transportation)

Although FWD can record loading pressure and the deflection history, the most common approach for interpreting FWD data is static backcalculation, which determines the layer elastic properties by neglecting the time effects and matching only the measured maximum

deflections with the deflections calculated from the layered elastic, Westergaard model, or FEM. The circles in Figure 1b highlight the peaks of each deflection profile and the FWD load. Dynamic backcalculation, unlike the static backcalculation, aims to match the entire sensor deflection history under the FWD load [*Lytton*, 1989; *Uzan*, 1994a; *Goktepe et al.*, 2006]. The disadvantages of the dynamic backcalculation are the more computational efforts and numerical complexity, and the fact that it is not conventionally used for design purposes as compared with the static backcalculation [*Goktepe et al.*, 2006, *Varma*, 2015]. The advantages, on the other hand, are notable. First, it is appropriate for the inherent nature of the problem, i.e., the analysis takes into consideration the observed time-dependent behavior of the structure under the FWD dynamic loading. In addition, it matches the entire deflection profiles, which assures better correlation between the model predictions and the in-situ behavior. Furthermore, viscoelastic properties of the system can be efficiently considered in dynamic analysis [*Uzan*, 1994a; *Kang*, 1998; *Ullidtz*, 2000; *Goktepe et al.*, 2006; *Xu*, 2014]. As such, dynamic backcalculation has been the subject of many research activities in the recent past.

The available dynamic backcalculation analyses often use the layered elastic theory or FEM as their forward analysis [*Foinquinos et al.*, 1993; *Wang and Lytton*, 1993; *Uzan*, 1994a, 1994b; *Kang*, 1998; *Ullidtz*, 2000; *Al-Khoury et al.*, 2001a, 2001b, 2002; *Dong et al.*, 2002; *Chatti*, 2004; *Goktepe et al.*, 2006; *Grenier and Konrad*, 2009; *Hadidi and Gucunski*, 2010; *Kutay et al.*, 2011; *Lee*, 2014; *Xu*, 2014; *Varma*, 2015; *Chatti et al.*, 2017, etc.]. Even though several researchers have studied the dynamics of beams and plates on foundations for different applications [*Auersch*, 1996; *Khazanovich*, 2000; *Kim and Yun*, 2000; *Silva et al.*, 2001; *Wang et al.*, 2005; *Calim*, 2009; *Xing and Liu*, 2009; *Horvath and Colasanti*, 2011; *Maheshwari and Khatri*, 2010, 2012; *Patil et al.*, 2012*; Hasheminejad and Gheshlaghi*, 2012; *Tornabene et al.*, 2014; *Maheshwari*, 2014; *Swaminathan et al.*, 2015; *Pradhan et al.*, 2016, etc.], no significant effort has been made to perform a dynamic backcalculation using the plate on a foundation approach. This can be attributed to various reasons: I) the capability of these idealizations to capture the dynamic behavior observed in the field is not well established, and II) the foundation model parameters can only be

used to compute the surface deflection and consequently the plate stress and strain, while they fail to provide similar information for the soil stratum.

Since the PVI analysis deals with moving loads and hence is dynamic in nature, and due to the absence of a compatible dynamic backcalculation that follows the plate on a foundation approach, the author was motivated to develop the tools required to address the recognized issues.

1.1. Thesis Objectives

The overall goal of this research was to develop a computationally-efficient dynamic forward- and inverse-solution for the analysis of infinite elastic (PCC) and viscoelastic (HMA) slab-on-grade structures following the plate-on-a-foundation approach. This allows for better understanding of the dynamic response of the structures, and provides the input model parameters required to obtain precise estimations for PVI analysis and life-cycle assessments. To advance this goal, the following main objectives were pursued:

i. Evaluate the classic mechanical models (such as the Winkler model) by comparing their predictions with the field measurements recorded by the FWD testing device; if the models were proven to be insufficient, make modifications to improve the plate on a foundation model.
ii. Make the PVI analysis compatible with the model modifications so that the obtained backcalculated parameters can be used as inputs to estimate the deflection-induced excess fuel consumption.
iii. Investigate the possibility of using the Vlasov approach to perform the dynamic backcalculation. This permits the inverse-solution to characterize the physical properties of the soil stratum, which addresses one of the major drawbacks of the mechanical models.

1.2. Thesis Organization

The dissertation covers the following contents, divided into six chapters:

Chapter 1 introduces the research problems and objectives.

Chapter 2 studies the response of the traditional Winkler model to the dynamic FWD circular pressure. Through an experimental study and a simple factorial-based inverse analysis, the shortcomings of this model are recognized. Improvements are made accordingly by introducing the generalized Winkler model (also known as generalized Westergaard model) which accounts for damping and inertia of the foundation.

Chapter 3 makes the so-called pavement-vehicle interaction analysis compatible with the generalized Winkler model. A gradient-base optimization scheme is employed to make the backcalculation program more efficient. A case study is conducted to showcase the ability of the proposed procedure to link the structural performance of the pavement, evaluated by the FWD testing device, to the fuel consumption of moving vehicles.

Chapter 4 discusses the concern raised in chapters 2 and 3 regarding the fit obtained for the asphalt pavements which was not as good as that of the concrete pavements. The Pasternak foundation model accounts for the shear resistance of the soil medium, which is the more realistic representation of the soil behavior. In this chapter, this model is extended to the generalized Pasternak model by accounting for damping and inertia effects. A field study is performed to investigate whether the inclusion of the shear parameter improves the correlation between the model-predicted and field-measured deflections, as well as, the obtained backcalculated properties.

Chapter 5 modifies the Vlasov model to account for damping and inertia of the soil stratum. The advantage of the Vlasov approach is that it makes connection between the model parameters and the soil properties, which addresses one of the limitations of the mechanical models. A study conducted in this chapter on several pavement sections comprised of different soil types allows for comprehensive evaluation of this model.

Chapter 6 presents a brief conclusion of the main findings and discusses future research.

The introduction sections of chapters *2, 3, 4, and 5,* provide a review on the literature relevant to the topic discussed in each chapter. Chapters *2, 3, and 4* are published and presented studies with minor modifications to maintain the integrity of the publication. Thus, some overlapping information may be seen.

2

Dynamic Visco-Elastic Analysis of Falling Weight Deflectometer Deflections for Rigid and Flexible Pavements

Published as Khazanovich, L., and A. Booshehrian (2015), Dynamic Viscoelastic Analysis of Falling Weight Deflectometer Deflections for Rigid and Flexible Pavements, *Transportation Research Record: Journal of the Transportation Research Board*, 2525, 31–39.

2.1. Summary

This chapter investigates the ability of a generalized Westergaard model, consisting of a viscoelastic plate on a viscoelastic Winkler foundation, to describe deflections of both rigid and flexible pavements under dynamic loading. The pavement response to Falling Weight Deflectometer (FWD) loading was simulated, and a semi-analytical solution involving the use of a Hankel transform in space and a finite difference method in time was developed. The obtained solution was used to interpret FWD data collected at the Minnesota Road Research facility. It was shown that a good match between the simulated and measured response data could be obtained for both rigid and flexible pavements if inertia and viscoelastic effects are accounted for. This makes the proposed model an attractive tool for pavement-vehicle interaction analysis.

2.2. Introduction

The Falling Weight Deflectometer (FWD) is the most commonly used device for non-destructive pavement characterization. FWD loading simulates conditions experienced by a pavement under a moving axle load [*Tholen et al.*, 1985; *Nazarian and Stokoe*, 1986; *Irwin et al.*, 1989]. Although FWD can record loading pressure and the deflection history, it is primarily used to collect the peak load and sensor deflections. The most common approach for interpreting FWD data is static backcalculation, which determines the layer elastic properties by matching the measured maximum deflections with the deflections calculated from the layered elastic or Westergaard model. The popularity of static backcalculation is largely due to the fact that current pavement design procedures, including the Mechanistic–Empirical Pavement Design Guide (MEPDG), use static structural analysis for pavement response calculations.

Nevertheless, dynamic backcalculation has been the subject of many research activities in the past. Dynamic backcalculation, unlike the static backcalculation, aims to find model parameters that match the entire sensor deflection history under the FWD load. Many researchers used the viscoelastic layered analysis to explain the lag in the maximum responses for the outer sensors [*Kim and Kim*, 1998; *Kutay et al.*, 2011]. *Sebaaly et al.* [1986] found that inertial effects are also important. *Khazanovich* [2000] modeled the behavior of the rigid pavement under dynamic loading as an elastic plate resting on a viscoelastic Winkler foundation, and highlighted the inertial and damping effects of subgrade.

Two common approaches are implemented in the backcalculation process:

1) the frequency domain approach, in which the time and deflection history are transformed into the frequency domain using fast Fourier transform and matched to responses in the frequency domain, and
2) the time domain approach, which matches the measured and calculated deflections in the time domain.

Multiple researchers employed the frequency domain approach. *Kim and Kim* [1998] employed numerical solutions of a multilayered half-space based in frequency domain and Hankel transforms in space as a forward model, and used an artificial neural network (ANN) for the inversion process. *Kang* [2001] also developed a frequency domain backcalculation program by modeling the pavement as a layered elastic system resting over a rigid bedrock or half-space. In another attempt, *Chatti and Kim* [2001] introduced a semi-analytical method in frequency domain for backcalculation of the dynamic subgrade stiffness and damping coefficients from FWD deflection basin. The elastic modulus of the pavement was then backcalculated using static backcalculation method. *Guzina and Osburn* [2002] transferred the load and deflection records into frequency domain to determine zero-frequency force and deflection values and used conventional static backcalculation afterwards. Backcalculation in frequency domain requires caution as this method is very sensitive to signal noise and truncation of the tail of the deflection basin might be required [*Kutay et al.*, 2011].

Some researchers adopted time domain to approach the dynamic backcalculation problem. Khazanovich modeled the behavior of the rigid pavement under dynamic loading as an elastic plate resting on a viscoelastic Winkler foundation, and highlighted that the inertia and damping effects of subgrade should be accounted for [*Khazanovich*, 2000]. In a recent study conducted by Zaabar et al., a solution in the time domain was developed for flexible pavements that was able to backcalculate the time-dependent layer properties of pavement [*Zaabar et al.*, 2014]. *Kutay et al.* [2011] utilized the time domain approach to backcalculate the elastic modulus of asphalt layer.

Uzan [1994b] compared the two backcalculation common approaches, meaning, the frequency domain and time domain. This comparison illustrated that the frequency-domain scheme requires a tail correction that may be unjustified and may induce distorting effects in the deflection time histories. Therefore, considering the advantages and disadvantages of both methods, the time domain approach was preferred [*Uzan*, 1994a]. *Zaabar et al.*

[2014] also pointed out that the use of the time domain approach makes the backcalculation insensitive to truncation in deflection time histories.

In either case, one challenging issue relevant to dynamic analysis has been the existence of a time lag between the load and deflection peaks. *Kutay et al.* [2011] identified this time delay and offered a solution by shifting the load to match the same peaks (see Figure 2). The reason for the time delay in deflection history was attributed to dynamic behavior (wave propagation), while their solution was only based on linear viscoelastic formulations.

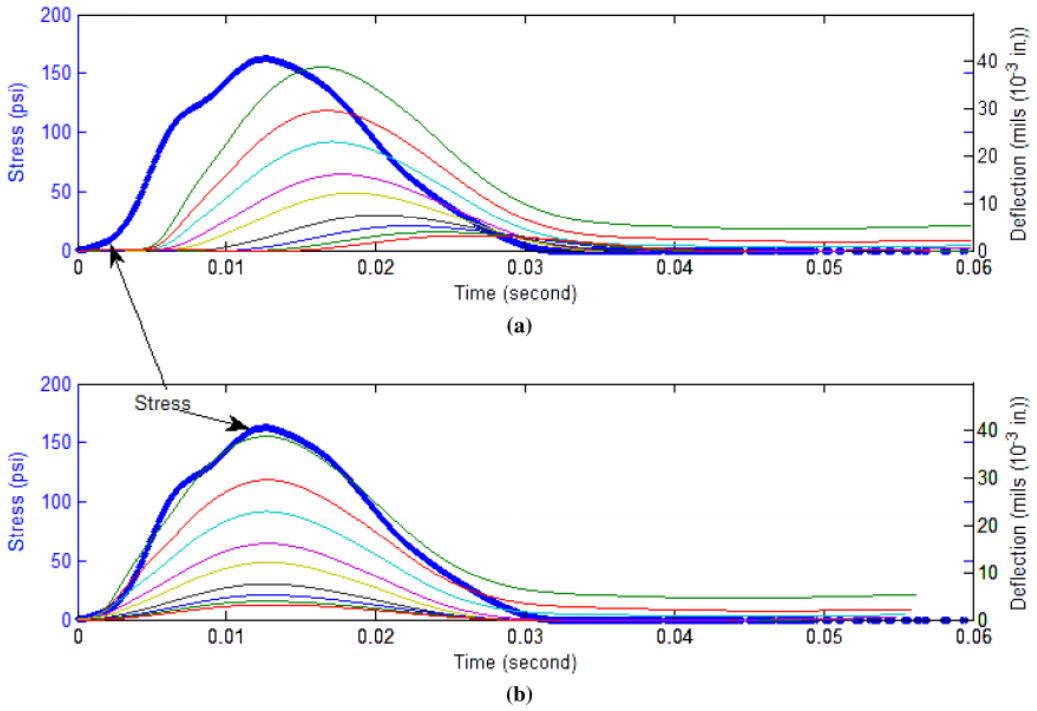

FIGURE 8 Load (stress) and deflection time histories for Lane 11 (SBS-LG): (*a*) original data (station = 1; dropID = 8) and (*b*) deflection data shifted.

Figure 2. Shifting the applied stress to address the time lag (reproduced from [*Kutay et al.*, 2011])

Kim and Kim [1998] used the viscoelastic layered analysis to explain the lag in the maximum responses for the outer sensors. *Sebaaly et al.* [1986] found that inertia effects

are also important. *Khazanovich* [2000] included the inertia effects of subgrade and pavement and was able to predict the time shift in the deflection peaks of different sensors and the time lag between the load peak and deflection measurements. This highlighted that the inertia and damping effects are the main sources for the time shifts.

Recently, efforts to reduce fuel consumption and carbon dioxide (CO_2) emissions have encouraged researchers to investigate the possibility of designing pavements that can reduce the fuel consumed by moving traffic. Approximately 10% of fuel consumption for heavy trucks is used to overcome the rolling resistance in the tires at a constant speed of 80 km/h [*Pouget et al.*, 2011]. Many studies have tried to identify the connection between extra fuel consumption and structural behavior of the pavement [*Chupin et al.*, 2013; *Louhghalam et al.*, 2013; *Louhghalam et al.*, 2014]. It has been argued that, in addition to other sources of fuel consumption related to rolling resistance (roughness, friction, and so on), the dissipated energy in the process of deforming the pavement must be compensated by an external energy provided by fuel [*Chupin et al.*, 2013; *Louhghalam et al.*, 2014]. It is preferred that the model for this type of study be as simple as possible yet be able to accurately capture pavement surface deflections under dynamic loading.

In a recent study conducted at the Massachusetts Institute of Technology, a procedure for an energy dissipation calculation under a moving load was developed. Both rigid and flexible pavements were modeled using a viscoelastic plate resting on an elastic Winkler foundation [*Louhghalam et al.*, 2014], which permitted obtaining simple semi-analytical solutions, making it an attractive tool for evaluation of fuel consumption caused by pavement deformation. However, the simplicity of the model raises concerns about its ability to properly describe surface deflections, especially for flexible pavements. FWD time history deflection data provide an opportunity to evaluate the ability of the model to describe pavement deflection, and to provide a rational approach for the model parameter assignment.

This study considers a generalized Westergaard model consisting of a viscoelastic plate resting on a viscoelastic subgrade. The objective of the study is to evaluate the ability of this model to describe time histories of sensor deflections for both rigid and flexible pavements and, if so, determine a procedure for backcalculating model parameters that closely matches the deflection histories. The importance of subgrade characteristics, such as damping and inertia, will also be evaluated.

2.3. Generalized Westergaard Model

Consider an infinite, linear viscoelastic, homogeneous, and isotropic plate resting on a viscoelastic, dense liquid foundation (Figure 3). The dynamic behavior of such a system under FWD loading is described here.

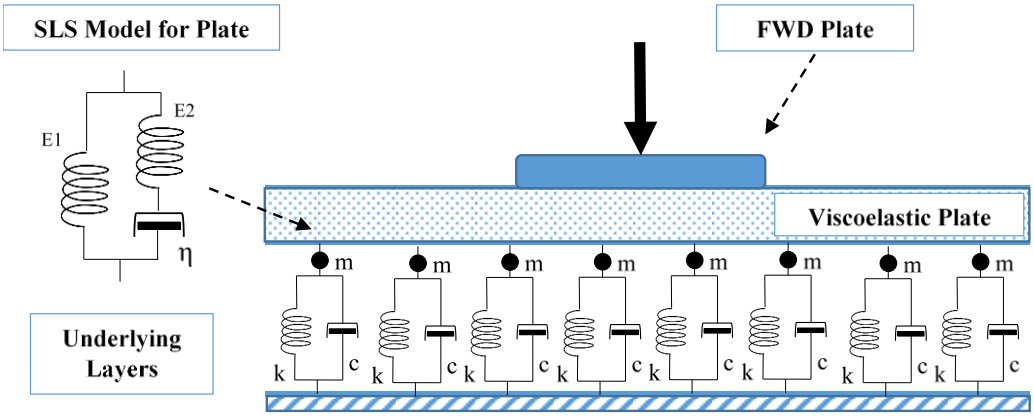

Figure 3. Generalized Westergaard model

$$D\left(\tilde{I}-\tilde{R}\right)\nabla^4 w(r,t)+k\,w(r,t)+c\frac{\partial w(r,t)}{\partial t}+m\frac{\partial^2 w(r,t)}{\partial t^2}=p(r,t) \tag{2-1}$$

where

D = slab instantaneous flexural stiffness, defined as:

$$D=\frac{Eh^3}{12(1-\mu^2)} \tag{2-2}$$

h = slab thickness

μ = slab Poisson's ratio

E = slab instantaneous modulus of elasticity

$\tilde{I}$ = identity operator: $\tilde{I}f(t) = f(t)$

$\tilde{R}$ = relaxation operator (defined later)

$w(r,t)$ = slab deflection

r = distance from the center of FWD load

t = time

k = coefficient of subgrade reaction

c = damping parameter for the unit area of the foundation

m = mass of the unit area of the plate and the moveable portion of the underlying layers

$p(r,t)$ = history of applied pressure

∇^4 = Laplace operator, defined as:

$$\nabla^2 = \frac{1}{r}\frac{\partial}{\partial r} + \frac{\partial^2}{\partial r^2} \tag{2-3}$$

If the viscoelastic behavior of the plate is described by the three parameter Standard Linear Solid (SLS) model (see Figure 3), then the stress-strain relationship can be described as follows [*Christensen*, 1982]:

$$\frac{d\sigma}{dt} + \frac{E_2}{\eta}\sigma = \frac{E_1 E_2}{\eta}\epsilon \tag{2-4}$$

where

η = damper viscosity in SLS model for the plate

E_1 , E_2 = spring stiffnesses in SLS model for the plate, and the instantaneous modulus of elasticity for the plate is

E = $E_1 + E_2$

The differential equation (2-4) can be re-written in the form of Volterra's integral equation:

$$\sigma(r,t) = E\ (\epsilon(t) - \frac{\beta}{E}\int_0^t e^{-\lambda(t-\tau)}\epsilon(\tau)d\tau) = E(\tilde{I} - \tilde{R})\epsilon(t) \tag{2-2}$$

where

σ = stress

ϵ = strain

β = $\frac{{E_2}^2}{\eta}$

λ = $\frac{E_2}{\eta}$

$\tilde{R}$ = relaxation operator defined as

$$\tilde{R}\epsilon(t) = \frac{\beta}{E}\int_0^t e^{-\lambda(t-\tau)}\epsilon(\tau)d\tau \tag{2-3}$$

In equation (2-1), assume that at any time, the applied pressure is uniformly distributed over the surface of the contact between FWD plate and the pavement. The history of applied pressure can be presented in the following form.

$$p(r,t) = \frac{P}{\pi a^2}H(r-a)g(t) \tag{2-4}$$

where

P = total applied load

a = FWD plate radius

H(r) = Heaviside function

g(t) = an arbitrary function of time

The number of parameters in equation (2-1) can be reduced by transferring the coordinates into a nondimensional domain. The following is the rewritten representation of equation (2-1) in terms of nondimensional deflection (w^*), pressure (p^*), time (t^*), damping (c^*), and mass (m^*).

$$\left(\tilde{I}-\tilde{R}\right)\nabla^4 w^*(s,t^*) + w^*(s,t^*) + c^*\frac{\partial w^*(s,t^*)}{\partial t^*} + m^*\frac{\partial^2 w^*(s,t^*)}{\partial {t^*}^2} = p^*(s,t^*) \tag{2-5}$$

The nondimensional terms are defined as:

$$w^*(s,t^*) = \frac{kl^2}{P}w(r,t) \tag{2-6}$$

$$p^*(s,t^*) = \frac{l^2}{P} p(r,t) \tag{2-7}$$

$$t^* = 2\pi \frac{t}{T} \tag{2-8}$$

$$c^* = \frac{2\pi}{T} \frac{c}{k} \tag{2-9}$$

$$m^* = (\frac{2\pi}{T})^2 \frac{m}{k} \tag{2-10}$$

where

T = duration of the applied load (period)

l = the radius of relative stiffness, defined as:

$$l = \sqrt[4]{\frac{D}{k}} \tag{2-11}$$

s = nondimensional distance from the center of the applied load, defined as:

$$s = \frac{r}{l} \tag{2-12}$$

The following approach was proposed to solve equation (2-1).

1. Apply the zero order Hankel transform to equation (2-5) with respect to nondimensionalized coordinate *s*.
2. Using the finite difference method, solve the transformed differential equation, with respect to time, to obtain the transformed nondimensional deflection, W^*.
3. Apply the inverse Hankel transform to obtain nondimensional deflection, w^*.
4. Convert the obtained nondimensional deflection to dimensional deflection, *w*.

Step 1

The zero order Hankel transform of a function, *f(s)*, is defined as follows:

$$(H_0 f)(\alpha) = \int_0^\infty s f(s) J_0(\alpha \cdot s) ds \tag{2-13}$$

where

J_n = Bessel function of order n

An application of the Hankel transform to the left-hand and right-hand sides of equation (2-5) leads to the following linear ordinary differential equation.

$$\alpha^4 \left(\tilde{I} - \tilde{R}\right) W^*(\alpha, t^*) + W^*(\alpha, t^*) + c^* \frac{\partial W^*(\alpha, t^*)}{\partial t^*} + m^* \frac{\partial^2 W^*(\alpha, t^*)}{\partial {t^*}^2} = \frac{J_1(\alpha a_l)}{\pi a_l \alpha} g(t^*) \tag{2-17}$$

where α is a parameter of the Hankel transform, and $a_l = a/l$.

Step 2

To solve equation (2-**Error! Reference source not found.**) using the central finite difference method, the first and second derivatives are approximated by:

$$\frac{\partial W^*(\alpha, t^*)}{\partial t^*} \approx \frac{{W^*}_{i+1} - {W^*}_{i-1}}{2\Delta t^*} \tag{2-14}$$

$$\frac{\partial^2 W^*(\alpha, t^*)}{\partial {t^*}^2} \approx \frac{{W^*}_{i+1} - 2{W^*}_i + {W^*}_{i-1}}{\Delta {t^*}^2} \tag{2-15}$$

Substitutions of equations (2-14) and (2-15) into equation (2-**Error! Reference source not found.**) lead to a system of linear equations for each time step t_i. In order to solve this system, two initial conditions are required. Initial deflection and slope are simply equal to zero as expressed here:

$$w^*(\alpha, 0) = 0 \tag{2-16}$$

$$\frac{\partial w^*(\alpha, t^*)}{\partial t^*}\Big|_{t^*=0} = 0 \tag{2-17}$$

Step 3

As a result of step 2, for each value of α, the transformed nondimensional deflections (W^*) can be calculated. By applying the inverse Hankel transform with respect to α, the nondimensional deflection (w^*) may be obtained.

$$w^*(s,t^*) = \int_0^\infty W^*(\alpha,t^*)J_0(\alpha s)\alpha d\alpha \tag{2-18}$$

The improper integral of equation (2-18) can be solved numerically using an appropriate quadrature rule.

Step 4

The final step is to convert the nondimensional deflection (w^*) obtained from step 3 to a dimensional deflection (w) as expressed in equation (2-23).

$$w(r,t) = \frac{P}{kl^2}w^*(s,t^*) \tag{2-19}$$

2.4. Verification of The Numerical Solution

The procedure described above permits the numerical calculation of the FWD deflections under an arbitrary FWD-type load history. To verify the solution, a series of sensitivity analyses were conducted. First, for the elastic plate on viscoelastic foundation, the solution was compared with analytical solutions reported by *Khazanovich* [2000]. Due to a lack of space, the comparison is not presented here; however, the numerical solutions obtained using the described methods agreed with the analytical solutions. Next, the viscoelastic plate was considered to verify that in limit cases, it approaches known elastic solutions.

In the viscoelastic plate analysis, the viscoelastic model parameters were set such that $E_1 = E_2 = 0.5*E$, while the relaxation time (η/E_2), which is associated with the viscosity parameter η, was varied. For constant E_1 *and* E_2, it is expected that when relaxation time approaches zero, the plate should behave as an elastic plate with modulus of elasticity E_1. When relaxation time takes on large values, the behavior of the plate should be that of an elastic plate with modulus of elasticity E. Figure 4a shows the relaxation curves for various viscosities, while Figure 4b provides the response of the plate in terms of deflection for the same ratios. The solid lines on Figure 4b show the limiting elastic cases. One can observe that the numerical solution properly captures the transition from one elastic model to the other as viscosity varies.

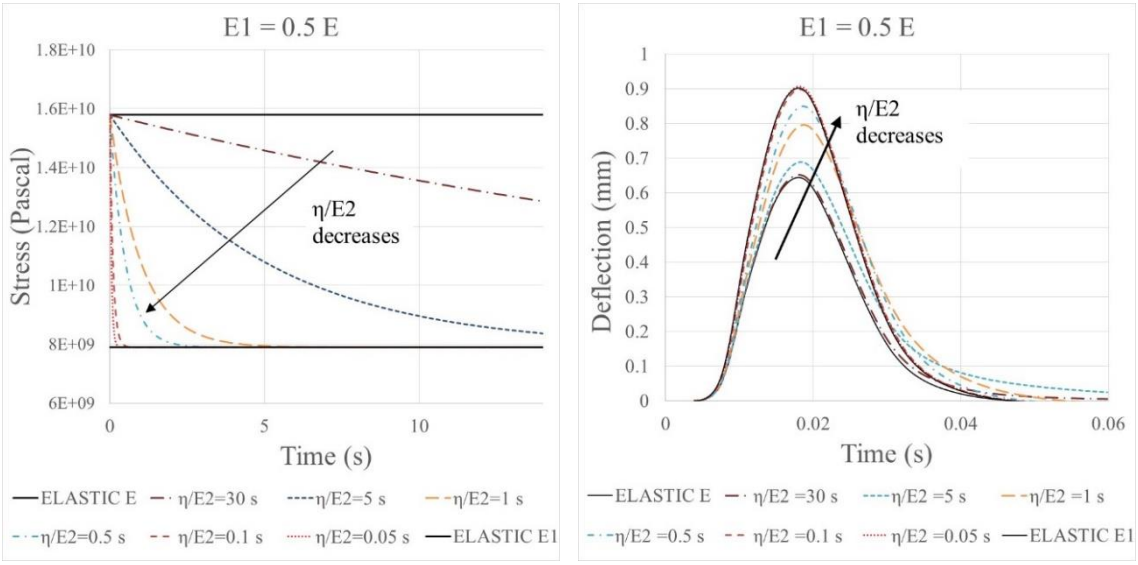

(a) (b)

Figure 4. (a) Relaxation curves for varying values of relaxation time (η/E_2), (b) Deflection profiles for varying values of relaxation time (η/E_2)

2.5. Backcalculation

The numerical solution described above is used as a forward calculation solution in the backcalculation procedure developed in this study. Since the objective is to assess the ability of the model to capture the physical behavior of the pavement, a very simple

backcalculation scheme is adopted; this scheme involves a simulation of the pavement responses for a given FWD load history for a wide range of the model parameters (factorial method). For each set of model parameters, the following measure of the discrepancy between measured and calculated deflections is determined.

$$SSE = (\frac{1}{w_{max}^{M}})^2 \sum_{i=1}^{n} \sum_{j=1}^{m} (w_{ij}^{M} - w_{ij}^{C})^2 \quad (2\text{-}20)$$

where

n = number of sensors

m = number of time steps in the FWD deflection history

w_{ij}^{M} = measured deflection for sensor i at time j

w_{ij}^{C} = calculated deflection for sensor i at time j

w_{max}^{M} = the maximum measured deflection in the FWD deflection history

SSE = the normalized sum of squared errors normalized by the maximum measured deflection in the FWD deflection history. The normalization term is included to eliminate the effect of different deflection values for different pavements, so that their non-dimensional SSE values can be compared.

The set of parameters that minimize the error function SSE is determined. The variables considered in the backcalculation procedure are as follows:

1. The mass ratio of the moveable layers (θ), where

$$\theta = \frac{m}{m_{plate}} \quad (2\text{-}21)$$

   θ varies between 1 and 13.

2. The elastic modulus of the plate (E) that varies between 1,000 MPA (= 0.15 x 10^6 psi)

   and 52,000 MPA (= 7.54 x 10^6 psi).

3. The coefficient of subgrade reaction (k) that varies between 25 KPa/mm (= 92.25 psi/in) and 135 KPa/mm (~ 498.15 psi/in).

4. The nondimensional damping ratio of the subgrade (c^*) that varies between 0.0 and 10.0.
5. The ratio of E_1/E as one of the viscoelastic parameters of the plate that varies between 0.05 and 0.9.
6. The ratio of η/E_2 as another viscoelastic parameter of the plate that varies between 0.05 s and 30 s.

The backcalculation was initially performed for a simulated pavement deflection to examine whether the procedure is able to reliably predict the characteristics of the simulated pavement. After it was verified that the backcalculation procedure is able to estimate the pavement characteristics for a simulated FWD deflection history, backcalculation was performed for field FWD data collected as explained in the following section.

2.6. Field FWD Deflection History

Two sets of FWD deflection time histories were analyzed in this study, both of which were collected at the Minnesota Road Research (MnROAD) test facility in July 2008. Two adjacent pavement sections at the MnROAD low-volume loop were selected: a rigid slab (MnROAD cell 37) and a flexible pavement (MnROAD cell 33). The rigid section has PCC slab thickness of 162 mm on a 125 mm aggregate base. The flexible pavement has HMA layer thickness of 100 mm and a 300 mm aggregate base. PCC slab is undoweled and conventional and innovative grinds (TS1, TS2, and TS3) were applied on it prior to the time of FDW testing. The HMA layer is a 12.5 mm dense graded superpave mixture fabricated with PG 58-34 asphalt binder. The air temperature at the time of the FWD testing was 31 °C (88 °F), and the surface temperature for the flexible pavement was 52 °C (125 °F). Both sections have the same subgrade and were in a good condition. Further information about MnROAD test facility and the details on the selected two cells can be found in *MnROAD* [2017]. The FWD tests were performed at a location away from the edges for both pavements. The tests were performed with four drops with different

maximum load values, and the deflection history of the test with highest maximum load was employed in the analysis. The collected FWD dataset consists of time, load, and the deflection response for 9 sensors located at distances ranging from 0 to 1.8 m from the center of the FWD loading plate.

To investigate the importance of accounting for viscoelastic and inertial properties of the base and subgrade, the following scenarios were considered for both sections:

- CASE 01 → where the subgrade is assumed to be elastic and weightless.
- CASE 0m → where the subgrade is assumed to be elastic and the mass contribution of the underlying layers is taken into account.
- CASE c1 → where the subgrade is assumed to be viscoelastic and weightless.
- CASE cm → where the subgrade is assumed to be viscoelastic and the mass contribution of the underlying layers is taken into account.

For each case, a backcalculation was performed to obtain the best fit between the measured and calculated deflections. Table 1 provides the summary of the values estimated by the backcalculation procedure for each case.

Table 1. Backcalculation analysis summary results for HMA and PCC pavements

Case ID	θ	E (MPa)	k (KPa/mm)	c*	$\frac{E_1}{E}$	$\frac{\eta}{E_2}$ (s)	SSE
HMA 01	1.0*	31,500	70.0	0.0*	0.05	0.10	67.53
HMA c1	1.0*	6,250	50.0	1.0	0.26	0.50	29.14
HMA 0m	11.0	10,000	85.0	0.0*	0.05	1.00	29.29
HMA cm	7.0	3,400	60.0	1.0	0.48	0.50	8.02
PCC 01	1.0*	52,000**	85.0	0.0*	0.26	1.00	69.70
PCC c1	1.0*	52,000**	40.0	1.0	0.9**	1.00	8.07
PCC 0m	1.0	52,000**	85.0	0.0*	0.26	1.00	69.70
PCC cm	2.0	40,000	55.0	1.0	0.9**	0.50	5.84

- Note: * fixed parameter
** denotes that the value is the upper boundary of the selected range.

The relaxation curves, normalized to the instantaneous backcalculated elastic modulus, for each case are illustrated in Figure 5. One can observe in Figure 5b that modeling the subgrade as elastic (cases PCC 01 and PCC 0m) leads to unrealistic viscoelastic behavior of the concrete plate. On the other hand, accounting for viscoelastic behavior of the subgrade results in much less pronounced viscoelastic response for concrete, which is as expected. At the same time, the asphalt layer still behaves in a more noticeable and characteristic viscoelastic manner. It must also be noted that exaggerated viscoelastic behavior of the concrete layer for cases PCC c1 and PCC cm is a result of a coarse search scheme in which the upper-limit value of E_1/E is reached. An additional discussion of this topic follows in the remaining sections.

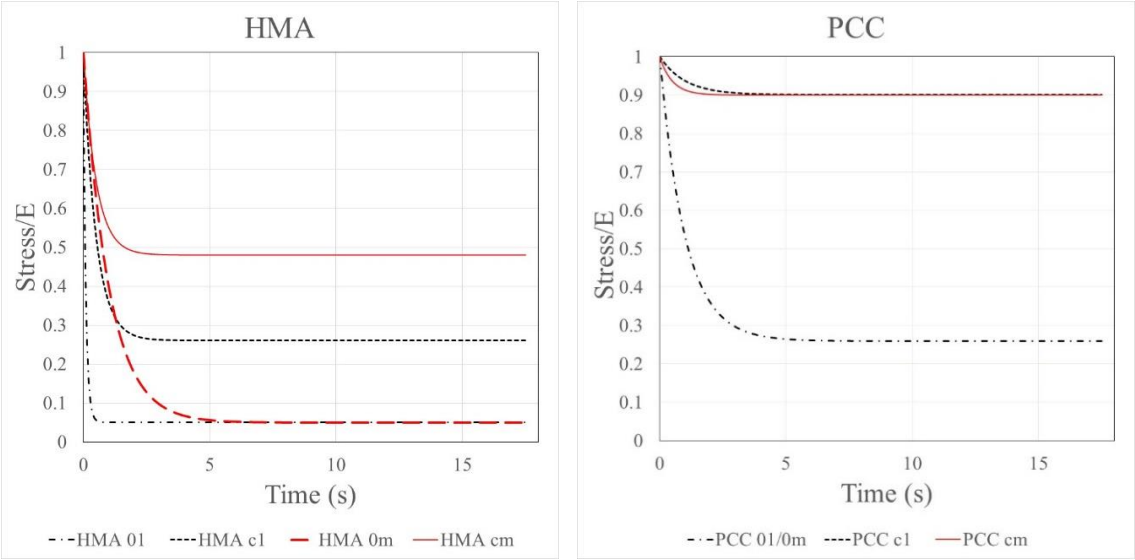

(a) (b)

Figure 5. Relaxation curves for different case scenarios for (a) HMA, (b) PCC

A comparison of the obtained SSE values in Table 1 for each pavement section shows that the models with weightless elastic subgrades have the highest SSE; in contrast, the models that account for damping and inertia exhibit the lowest SSE. This is as expected given that

the introduction of additional parameters to the model quantitatively improves the accuracy of the estimations.

Figure 6 and Figure 7 present the best fit found using the different foundation models for HMA and PCC pavements, respectively. The calculated (predicted) deflection profiles were generated using the backcalculated pavement parameters listed in Table 1.

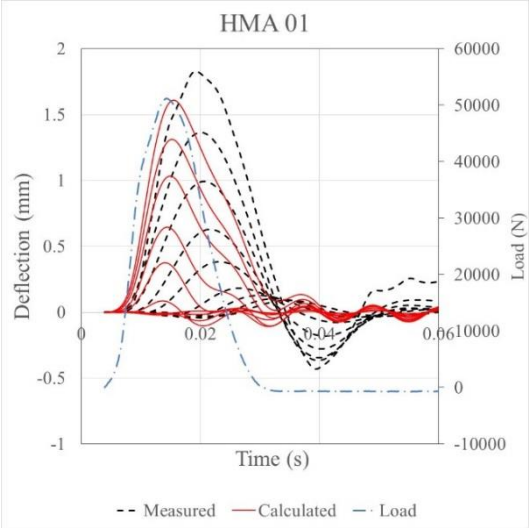

(a)

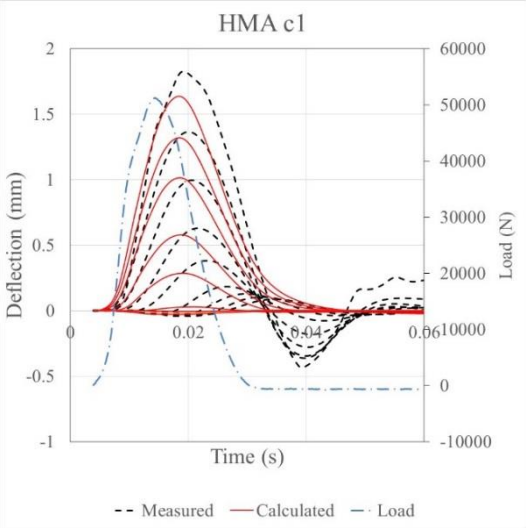

(b)

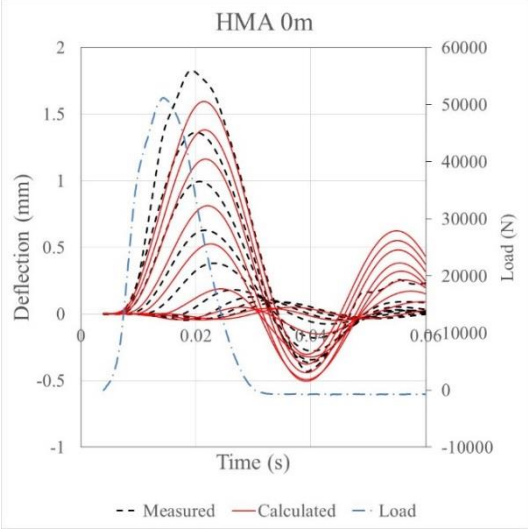

(c)

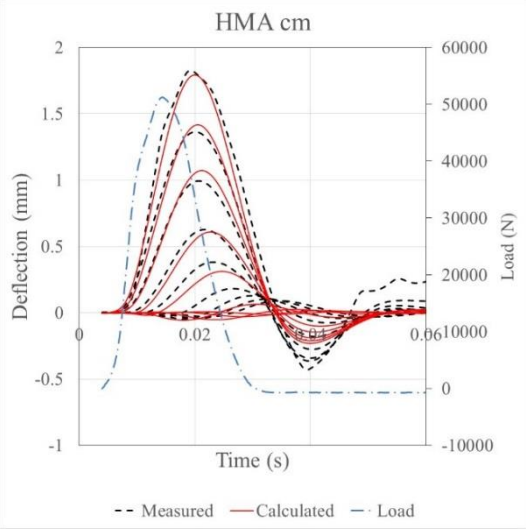

(d)

Figure 6. Different case scenarios for HMA backcalculation: (a) HMA 01, (b) HMA c1, (c) HMA 0m, (d) HMA cm

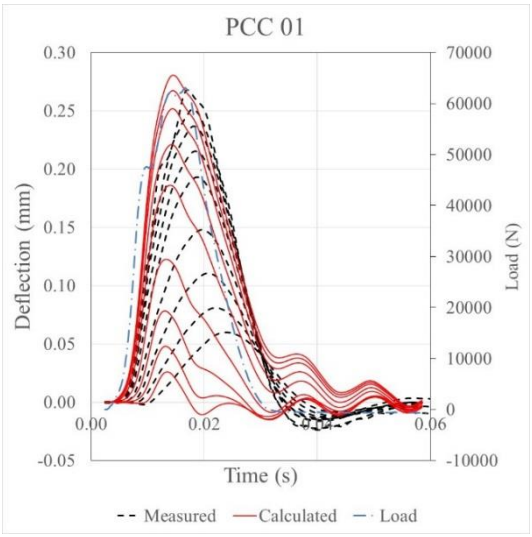

(a)

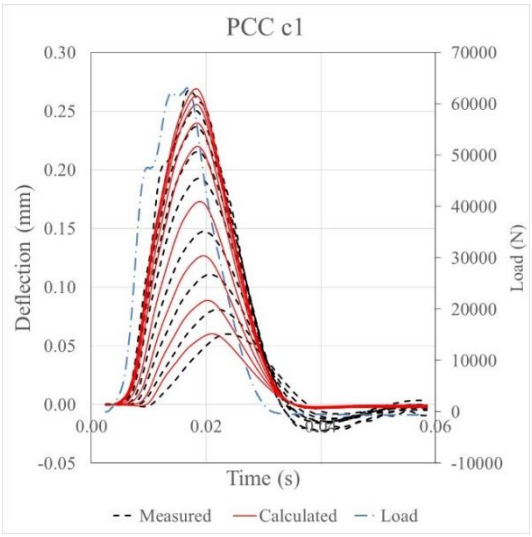

(b)

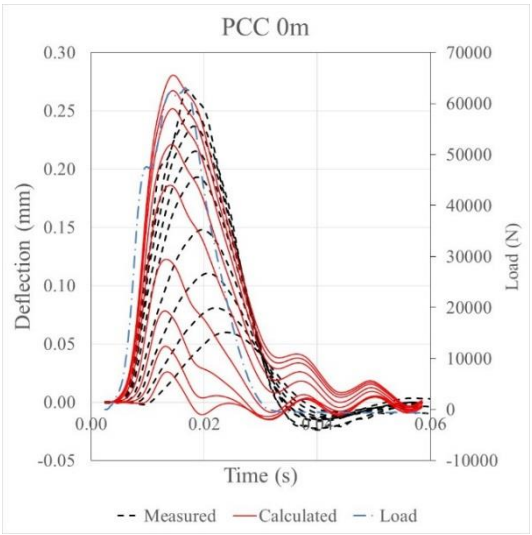

(c)

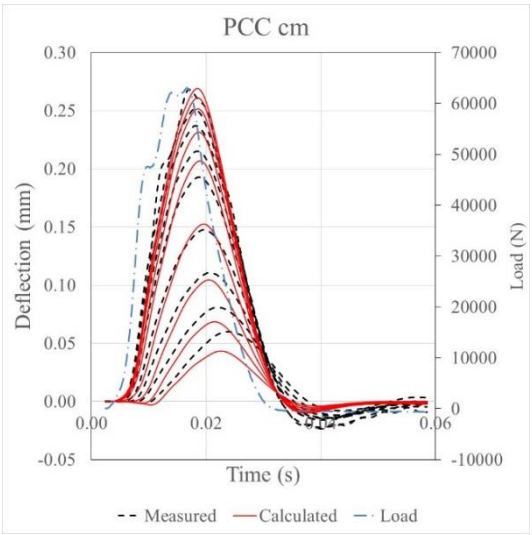

(d)

Figure 7. Different case scenarios for PCC backcalculation: (a) PCC 01, (b) PCC c1, (c) PCC 0m, (d) PCC cm

The visual inspection of Figure 6 and Figure 7, which present measured and simulated responses, indicates that accounting for viscoelastic and inertia properties of the subgrade leads to qualitative improvements in the model prediction.

As it can be seen in Figure 6a and Figure 7a, the assumption of weightless elastic subgrade leads to significant underestimation of the time lag between peak load and deflection peaks. Moreover, the deflection peaks for the inner and outer sensors occurred at almost the same time. This effect has been previously discussed by *Kutay et al* [2011].

Figure 6c and Figure 7c show the simulated deflections if the subgrade is considered to be elastic, but inertia effects are taken into account. One can observe significant improvement in time lag prediction for the asphalt pavement, but poor qualitative and quantitative match of deflections for the concrete pavement. Moreover, even for the asphalt pavement, the oscillation of deflections after the end of the loading impulse is exaggerated.

When the subgrade is weightless but viscoelasticity is accounted for, as shown in Figure 6b and Figure 7b, there is improved agreement between measured and simulated responses. However, the predicted responses do not change sign, which clearly contradicts the measured responses that take place after the end of the load impulse (tail behavior).

Figure 6d and Figure 7d present the simulated deflections for the cases when both subgrade inertia and damping effects are considered. One can observe a good qualitative and quantitative agreement between the measured and simulated responses for both types for pavements. For both pavement types, no issues associated with time lag or deflection oscillation are observed. A final comment on the backcalculated results in Table 1 is that the values for the asphalt and concrete instantaneous moduli are within expected ranges for these parameters. Moreover, the backcalculated subgrade properties for both types of pavements (the coefficient of subgrade reaction, k, and damping, c^*) are very similar. This is a positive sign considering that the sections are adjacent and thus share the same subgrade. This indicates that the simple model of a plate on a Winkler foundation can

accurately describe dynamic pavement deflections if the viscoelastic, inertial properties are taken into account.

One of the limitations of the analysis presented above was that the backcalculation for rigid pavements reached the upper-limit value (E_1/E). Although the resulting concrete behavior was the least "viscoelastic" of the cases considered, the relaxation curves in Figure 5b indicates that it behaves more viscous than expected for concrete. This was not observed for the asphalt layer, in which E_1/E was in the middle of the considered range of values, indicating that no problems existed for the search scheme for this type of pavement. To address this limitation, additional analysis was performed in which the concrete was considered as a purely elastic layer. Figure 8 presents the resulting simulated deflections for the backcalculated parameters determined in this analysis.

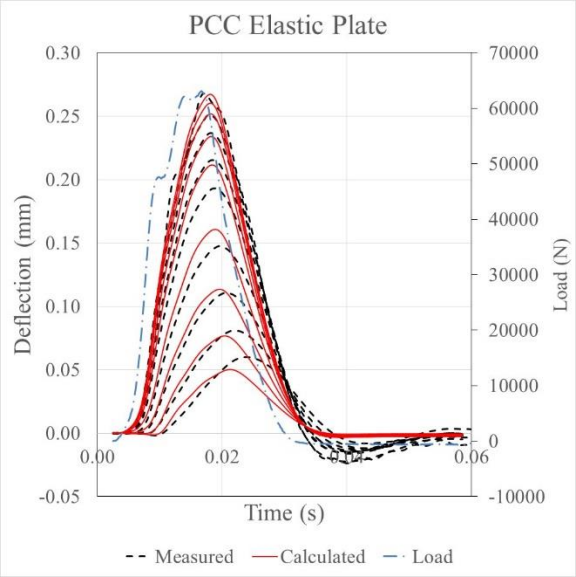

Figure 8. Case scenario with elastic plate and viscoelastic subgrade for PCC

One can observe that the predicted deflections are almost identical to the calculated deflections presented in Figure 7d. Also, the computed SSEs are very similar (5.84 for viscoelastic PCC and 6.40 for purely elastic PCC). This indicates that the assumption of an

elastic plate for the concrete layer is a valid assumption and can lead to realistic estimations for pavement characteristics.

2.7. Conclusions

In this study, a generalized Westergaard model consisting of a viscoelastic plate on a viscoelastic subgrade with inertia effects was considered. A semi-analytical solution for the simulation of FWD loading was obtained. The combined application of Hankel transform in space and finite difference method in time eliminated any need for tail correction. The developed solution was used to interpret FWD time history data collected at MnROAD. The following observations were made:

- The generalized Westergaard model, in spite of its simplicity, can adequately describe pavement deflections for both rigid and flexible pavements.
- Viscoelastic behavior and inertial effects of base and subgrade layers must be accounted for.

The simplicity of the Westergaard model makes it an attractive tool for pavement-vehicle interaction analysis. However, as there are no guidelines currently available to assess the inertia and damping of subgrade, the FWD testing and subsequent backcalculation should be used to estimate these parameters.

This study has implications for pavement design and analysis. In the AASHTO M-E procedure for flexible pavements, the viscoelasticity of the system is accounted for through the HMA complex modulus only. At the same time, the subgrade is assumed to behave as an elastic body. This study indicates that viscoelastic properties of the subgrade may affect the responses of flexible pavements, which has implications for both pavement-vehicle interaction and pavement design. This highlights the need for further investigation of this phenomenon.

3

Assessment of Pavement Deflection-Caused Fuel Consumption via FWD Data

Booshehrian, A., Louhghalam, A., Khazanovich, L. and F.J. Ulm (2016), Assessment of Pavement Deflection-Caused Fuel Consumption via FWD Data, *Transportation Research Board 95th*, No. 16-6246.

3.1. Summary

The recently developed deflection-induced pavement-vehicle interaction analysis links the structural performance of the pavement to the fuel consumption of moving vehicles and the subsequent greenhouse gas emissions during the pavement use-phase. Accurate estimations of these impacts are tightly dependent on the proper evaluation of pavement structural parameters, including the properties of the surface course and underlying layers. A recent study demonstrated that inertia and damping effects of underlying layers must be taken into account for pavements subjected to dynamic loads, and that accurate parameters of pavement model could be backcalculated using the falling weight deflectometer measurements. In this chapter, the pavement-vehicle interaction analysis is modified accordingly. Then, a case study is performed using multiple time histories of falling weight deflectometer deflections collected over a year's time for a rigid and a flexible pavement. Analysis of deflection basins showcases how falling weight deflectometer measurements can be used for estimating the deflection-induced vehicle fuel consumption for both rigid and flexible pavements. The simplicity and accuracy of the demonstrated analyses show great promise for wider application of this methodology, especially regarding sustainable development of pavement network.

3.2. Introduction

It is well established that road properties affect rolling resistance, and thus, fuel consumption and corresponding environmental footprint [*Ardekani and Sumitsawan*, 2010; *Gschsser and Wallbaum*, 2013; *Chatti and Zaaber*, 2012; *Louhghalam et al.*, 2015a]. Alongside pavement roughness and texture [*Louhghalam et al.*, 2015b; *Zaaber and Chatti*, 2010; *Zaaber and Chatti*, 2011; *Wang et al.*, 2014], dissipation of energy due to pavement deformation is an important contributor to rolling resistance [*Pouget et al.*, 2011]. The deflection-induced dissipated energy contributes to excess fuel consumption and use-phase greenhouse gas emission. In order to develop sustainable transportation systems, it is necessary to develop quantitative tools that establish the link between pavement deformation and life-cycle energy consumption, which has been the topic of few recent studies [*Zaaber and Chatti*, 2010; *Pouget et al.*, 2011; *Chupin et al.*, 2013; *Pouget et al.*, 2014]. Some quantitative tools have been proposed. For instance, deflections recorded by Benkelman beam rebound were used by Zaabar and Chatti as an indicating factor in estimating the fuel consumption [*Zaaber and Chatti*, 2010]. Another approach was the deflection-induced pavement-vehicle interaction (PVI) model proposed by *Louhghalam et al.* [2013; 2014a]. PVI quantifies the dissipated energy due to viscous deformation of pavement under a moving load and evaluates the related fuel consumption and environmental footprint as functions of structural and material properties of pavement.

In order to determine the surface deformation and the resulting dissipated energy, the PVI model proposed by *Louhghalam et al.* [2013] describes both rigid and flexible pavements as a viscoelastic plate resting on a weightless elastic Winkler foundation. This model is computationally efficient, and so it is an attractive tool for an analysis that up-scales the pavement-scale emission to network level environmental impact [*Louhghalam et al.*, 2014b]. However, the simplicity of this model does not guarantee its ability to properly describe the pavement behavior. Especially for the case of a flexible pavement, the use of a Winkler foundation model is not a common practice. Therefore, the accuracy of this idealization must be tested when pavement is subjected to dynamic loads. Also, regardless

of the accuracy of the selected model, pavement structural parameters are needed to perform the PVI analysis.

The dynamic nature of the falling weight deflectometer (FWD) loading mechanism and its similarity with moving loads make the FWD time history deflection data a viable source for 1) evaluation of the ability of the selected model in describing the pavement behavior, and 2) development of a rational approach for the assignment of model parameters for PVI analysis. Since FWDs are commonly used by roadway agencies, the FWD deflection data could be used for rational analysis of vehicles fuel consumption on roadways in network planning and pavement management decision-making.

A numerical-based dynamic backcalculation method was developed in previous chapter to analyze the FWD deflection time histories and indicate the pavement model parameters. As the forward model of this backcalculation method, the generalized Westergaard model was used which accounts for the inertia and damping effects of foundation as well as the viscoelasticity of the plate. By performing a field study on two FWD deflection basins obtained from adjacent rigid and flexible pavements in Minnesota, it was shown that including both inertia and damping effects of foundation is substantial for accurate description of the behavior of both rigid and flexible pavements under dynamic loading. Therefore, in order to obtain realistic estimations for the dissipated energy, the deflection-induced PVI model needs to be modified to account for foundation inertia and damping.

The purpose of this chapter is to demonstrate how FWD measurements can be used by transportation agencies to evaluate deflection-induced vehicle fuel consumption. To this end, the PVI analysis is modified first to account for inertia and damping effects of the layers underlying the road surface. This modification makes the analysis compatible with the generalized Westergaard model. Next, one flexible and one rigid pavement section are selected from the database provided by the Long-Term Pavement Performance (LTPP) program, each of which were tested multiple times at different months of a year. The model parameters were backcalculated for the selected pavement sections, and then employed as inputs to estimate the resulting fuel consumption. The variation in energy dissipation due

to seasonal changes was also studied. The results confirm that the proposed methodology can be a reliable tool to evaluate deflection-induced vehicle fuel consumption and environmental footprint.

3.3. Theoretical Background

The plate-on-a-foundation model has been commonly used for structural modeling of rigid pavements. *Westergaard* [1926] described the rigid slab as a thin elastic Kirchhoff-Love plate resting on a Winkler foundation, which is a combination of closely spaced, independent elastic linear springs. Various researchers emphasized the more complex behavior of the foundation and added a dashpot to the Westergaard model to account for viscoelastic behavior of foundation [*Kutay et al.*, 2011; *Kue and Tsai*, 2014; *Kue et al.*, 2015; *Sebaaly et al.*, 1986]. Also, the importance of foundation inertia effects was pointed out [*Khazanovich*, 2000] by demonstrating that the integrated inertia and damping effect can more accurately explain the behavior of pavement under dynamic loading, in particular, the time shift between the applied FWD load and the recorded deflection peaks [*Pozhuev*, 1986]. Chapter 2 proposed a generalized Westergaard model to account for viscoelasticity of the plate and the inertia and damping effects of foundation. They were able to show this model could accurately capture the pavement behavior under dynamic FWD loading for both flexible and rigid pavements.

The generalized Westergaard model consists of an infinite viscoelastic plate resting on a foundation that takes into account inertia and damping effects of the foundation (Figure 9). The plate is modeled with a three-parameter standard linear solid (SLS) model to capture the viscoelastic behavior of flexible pavement. The damping and inertia effects of foundation are accounted for by the addition of dashpot and mass elements to the Winkler foundation. The mass element represents the mass of the plate and the moving portion of the underlying layers under applied dynamic loads. The combination of the spring and dashpot simulates the viscoelastic behavior of the underlying layers based on the Kelvin-Voigt model.

In the following section, the generalized Westergaard model is incorporated into the PVI frameworks [*Pouget et al.*, 2014; *Louhghalam et al.*, 2013; *Louhghalam et al.*, 2014a, 2014b]

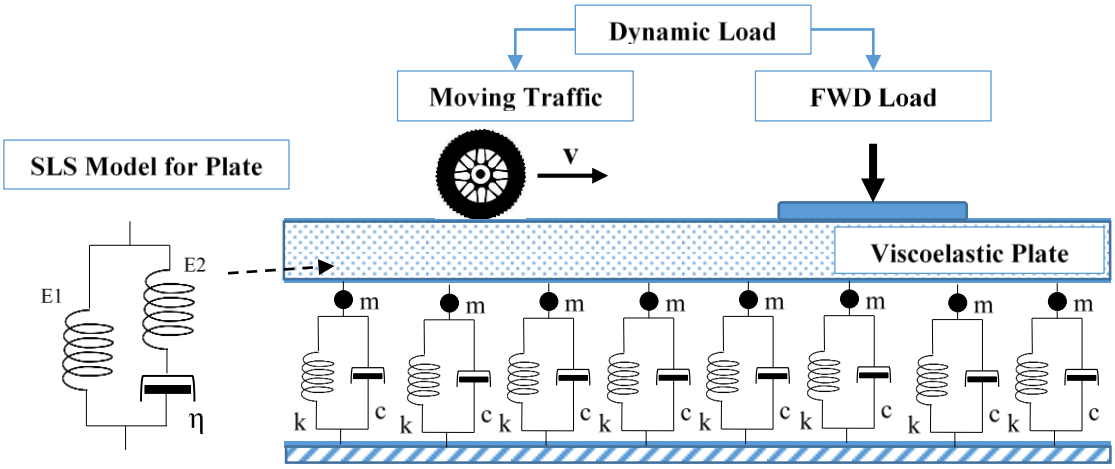

Figure 9. Generalized Westergaard model subjected to FWD dynamic load or moving vehicle

Deflection-Induced PVI Model

Consider an infinite plate subjected to a moving load $P = pS$ representing the wheel load, with S rectangular area of tire-road contact trajectory. Herein, we consider a moving coordinate system $X = x - Vt$, attached to the load traveling with constant speed V. For any viscoelastic material in this reference frame, it can be shown that the dissipated energy within the material is related to the slope in the moving direction at the road-tire contact trajectory [*Louhghalam et al.*, 2013]. Assuming a uniformly distributed load, the dissipated energy per distance traveled, δU, reads:

$$\delta U = -P \left\langle \frac{dw}{dX} \right\rangle \tag{3-1}$$

where w is the plate deflection and $\langle dw/dX \rangle$ is the average slope along the area of tire-road contact surface in X-direction. Hence, to evaluate the energy dissipation one needs to evaluate plate deflection and its spatial derivative in the moving coordinate system. Herein,

we employ the elastic-viscoelastic correspondence principle [*Read*, 1950; *Christensen*, 1982; *Uzan*, 1994b] to evaluate deflection. The principle allows for finding the solution of a viscoelastic problem from the solution of a corresponding elastic problem in the frequency domain, by substituting the complex modulus of the viscoelastic material with its elastic counterpart.

Using the elastic-viscoelastic correspondence principle, first the solution to equation of motion of an elastic plate on an elastic foundation subjected to a moving load needs to be obtained in the frequency domain. Assuming a steady-state condition (constant speed), and noting that in the moving coordinate system $\partial/\partial t = -V\partial/\partial X$, the equation of motion in this reference frame reads:

$$D\left(\frac{\partial^2}{\partial X^2}+\frac{\partial^2}{\partial y^2}\right)^2 w + mV^2\frac{\partial^2 w}{\partial X^2} + kw = p \tag{3-2}$$

where $D = Eh^3/12(1-\nu^2)$ is plate's instantaneous flexural stiffness and m is mass per unit area of the plate and moving portion of foundation; *E, h,* and *v* are instantaneous modulus of elasticity, thickness, and Poisson's ratio of the surface layer (plate), respectively. Taking the Fourier transformation of the above solution in frequency domain gives:

$$\widehat{w} = \widehat{p}\,(D(\lambda_1^2+\lambda_2^2)^2 - mV^2\lambda_1^2 + k)^{-1} \tag{3-3}$$

where $\lambda_1$and λ_2 are respectively the transformed fields of X and y.

To find the solution of a viscoelastic plate on a viscoelastic foundation, the following approach was taken. The stress-strain relationship of the viscoelastic top layer is according to the constitutive equation of a standard linear solid (SLS) model (illustrated in the inset of Figure 9).

$$\frac{\partial \varepsilon}{\partial t} = \frac{1}{E_1+E_2}\left(\frac{\partial \sigma}{\partial t}+\frac{1}{\eta}(E_2\sigma - E_1E_2\varepsilon)\right) \tag{3-4}$$

where E_1, E_2 are two stiffness parameters of the model. In addition, η is the material viscosity parameter, and therefore, $\tau = \eta/E_2$ is the relaxation time of the viscoelastic top-layer. Damping of foundation is modeled via a Kelvin-Voigt viscoelastic foundation with stiffness k and relaxation time $\tau_s = c/k$, where c is viscous damping coefficient of foundation as illustrated in Figure 9. To incorporate the viscoelasticity of foundation, the elastic foundation modulus k is replaced with the complex modulus of a Kelvin-Voigt model in the moving coordinate system, i.e. $\hat{k} = k(1 - i\lambda_1 V\tau_s)$.

For the SLS model representing the material of surface layer (plate), we first rewrite equation (3-4) in the moving coordinate system:

$$-V\frac{d\varepsilon}{dX} = \frac{1}{E_1 + E_2}\left(-V\frac{d\sigma}{dX} + \frac{1}{\eta}(E_2\sigma - E_1E_2\varepsilon)\right) \tag{3-5}$$

Here we assume a three-dimensional creep behavior characterized by constant creep Poisson's ratio such that $\widehat{D} = \hat{E}h^3/12(1-\nu^2)$. Then, taking Fourier transform of equation (3-5), the complex modulus can be obtained $\widehat{D} = D_1(1 - i\lambda_1 V\tau(D_2/D_1 + 1))/(1 - i\lambda_1 V\tau)$ where $D_1 = E_1h^3/12(1-\nu^2)$ and $D_2 = E_2h^3/12(1-\nu^2)$. The solution for the viscoelastic problem in the frequency domain is expressed as:

$$\widehat{w} = \widehat{p}\left(\frac{1 - i\lambda_1 V\tau(D_2/D_1 + 1)}{1 - i\lambda_1 V\tau}D_1(\lambda_1^2 + \lambda_2^2)^2 - mV^2\lambda_1^2 + k(1 - i\lambda_1\tau_s)\right)^{-1} \tag{3-6}$$

The viscoelastic plate deformation is obtained by taking the inverse Fourier transformation of above equation. The slope dw/dX is also similarly calculated from $\mathcal{F}^{-1}(-i\lambda V\widehat{w})$ with $\mathcal{F}^{-1}$ denoting the inverse Fourier transformation.

The procedure above offers a computationally efficient approach for determining pavement deflections and energy dissipation under a moving load using the generalized Westergaard model. However, to ensure that the estimation of the energy dissipation is realistic, it is important to select appropriate values for model parameters that will result in calculated deflections similar to those exhibited by the pavement system. These quantities can be obtained from the dynamic backcalculation analysis of FWD data as explained below.

Dynamic Backcalculation of Pavement Parameters Using FWD Data

FWD measures the time histories of the applied load and surface deflections at different distances from the center of a circular FWD applied pressure. Thus, the governing differential equation for an infinite, homogeneous, isotropic, and linearly viscoelastic plate on a viscoelastic foundation subjected to axisymmetric FWD loading is:

$$\widetilde{D}\left(\frac{1}{r}\frac{\partial}{\partial r}+\frac{\partial^2}{\partial r^2}\right)^2 w(r,t)+k\,w(r,t)+c\frac{\partial w(r,t)}{\partial t}+m\frac{\partial^2 w(r,t)}{\partial t^2}=p(r,t) \tag{3-7}$$

where $\widetilde{D}$ is the viscoelastic rigidity of the plate that can be calculated based on stress-strain relationship of the viscoelastic top layer given in equation (3-4), $w(r,t)$ is the surface deflection, $p(r,t)$ is the applied pressure in the FWD test, r is the distance from the center of FWD load, and *t* is the time. The pressure, $p(r,t)$, is obtained from measurements in the FWD tests, and is not necessarily a mathematical function, therefore equation (3-7) must be solved numerically. Chapter 2 proposed a numerical solution for this equation using a combined application of Hankel transform in space and finite difference method in time. Taking advantage of the time domain approach prevents the potential problems of using frequency domain such as the need for tail correction [*Uzan*, 1994a; *Zaabar et al.*, 2014].

The obtained semi-analytical solution is used as a forward solution in the backcalculation procedure. A normalized sum of squared errors (SSE) is defined to quantify the difference between the measured and calculated FWD deflections. A combination of quasi-Newton method and a finite-difference gradient is employed to find the solution to the inverse problem, which is to find the set of parameters that minimizes the following error function.

$$SSE=\left(\frac{1}{W_{max}^{M}}\right)^2\sum_{i=1}^{n}\sum_{j=1}^{m}(w_{ij}^{M}-w_{ij}^{C})^2 \tag{3-8}$$

where n is the number of sensors, m is the number of time steps in the FWD deflection time history, w_{ij}^{M} and w_{ij}^{C} are the measured and calculated deflections for sensor i at time j, respectively, while w_{max}^{M} is the maximum measured deflection in the FWD deflection history. The error is normalized by dividing by w_{max}^{M}, so that their non-dimensional SSE values can be compared. The parameters to be determined from the backcalculation procedure are 1) the plate's instantaneous flexural stiffness, E, 2) the ratio E_1/E, and 3) the relaxation time of the plate material, τ, 4) foundation stiffness ,k, 5) foundation inertia ,m, and 6) damping coefficient of the foundation, c.

3.4. Case Studies

The previous section describes how the pavement-vehicle interaction (PVI) model was modified according to the generalized Westergaard model to account for inertia and damping effects of underlying layers. This section illustrates how the model parameters, backcalculated using the FWD data, can be used in the implementation of the PVI model to estimate the vehicle fuel consumption due to pavement deformation for both rigid and flexible pavements. This section also examines if the developed procedure is able to address the seasonal variations in pavement system and provide acceptable estimations of fuel consumption. Especially when considering flexible pavements fabricated with a hot mix asphalt (HMA) course as the surface layer, temperature variation could considerably influence the viscoelastic properties of the asphaltic material, and thus, the amount of energy dissipated through PVI.

The FWD data collected through the "Seasonal Monitoring Program (SMP)" of the Long Term Pavement Performance (LTPP) program were used in this study [*FHWA*, 2017]. The SMP study did not contain a set of flexible and rigid pavements located in fairly similar locations, so pavements with relatively similar foundations were chosen: a flexible pavement located in Nevada (ID = 320101) and a rigid pavement located in North Carolina (ID = 370201). Both sections were in good condition in year 2000. Details of the pavement sections are described in Table 2.

Table 2. Detailed information on the selected pavement sections

Location / Section ID	Pavement Type	Surface Layer	Thickness (m) / Density (kg/m^3)	Base layer / Thickness (m)	Subbase layer / Thickness (m)	Subgrade Type
NV / NV0101	Flexible	HMA	0.1829 / 2234	Agg. / 0.208	Agg./ 0.579 + Treated/ 0.305	Coarse Grained
NC / NC0201	Rigid	PCC	0.2337/ 2240	Agg. / 0.236	Treated/ 0.203	Fine Grained

A Poisson's ratio of 0.15 was assumed for the rigid pavement and 0.35 for the flexible pavement. FWD tests were performed at the center of the slab, away from the pavement edge (J1 loading). The same location of the pavement section was investigated at different times of the year. Further information on the two sections studied here can be found on InfoPave™, the online LTPP database [*FHWA*, 2017].

3.5. Results

Six FWD deflection measurements for the flexible section (NV0101) and five FWD deflection measurements for the rigid section (NC0201) collected in year 2000 were used for this study. The sections were analyzed using the dynamic backcalculation procedure described in the previous section, and are summarized in Table 3 along with the month and surface temperature of the FWD testing. The backcalculated parameters were then used to calculate the deflection basins. The time history of measured and calculated surface deflections at different sensor locations (0.0 to 1.5 m) are shown in Figure 10 (sections NV0101) and Figure 11 (section NC0201).

The backcalculated model parameters were ultimately used in the modified PVI model to compute the dissipated energy and fuel consumption under a moving vehicle load. The analysis was performed at typical highway speed of 100 Km/hr for an HS-20 (a 20 ton semi-trailer truck). The tire-road contact surface was assumed to be a square with dimension of 0.15 x 0.15 m. The dissipated energy per distance traveled was calculated

based on equation (3-1). The associated fuel consumption is obtained by dividing the dissipated energy by the energy content of fuel which is equal to 38.74 MJ/liter for Diesel [*Ardekani and Sumitsawan*, 2010]. The results of this analysis are summarized in Table 4 together with the month and surface temperature at the time of FWD tests.

Table 3. Backcalculated pavement parameters based on the FWD deflection basins

Pavement Type	ID	Month	Surface Temp.	Foundation Parameters			Plate Parameters			Error
				k	m	c	E	E_1/E	τ	
			˚C	KPa/mm	kg/m^2	$Ns/m/m^2$	GPa	-	s	-
Flexible (NV0101)	A1	Feb	1.4	92.83	1102.2	7.07E+05	26.53	1.00	-	6.98
	B1	Mar	16.5	92.93	822.2	7.08E+05	22.05	1.00	-	7.04
	C1	May	18.2	96.50	662.0	6.87E+05	18.95	0.93	4.95	6.71
	D1	Aug	34.9	143.59	408.8	7.77E+05	8.63	0.51	2.28	9.41
	E1	Sep	23.7	102.87	408.8	7.31E+05	13.90	0.81	6.31	7.50
	F1	Nov	3.9	91.24	998.3	6.64E+05	23.80	1.00	-	7.25
Rigid (NC0201)	B1	Feb	11.2	32.46	838.2	3.47E+05	34.73	1.00	-	1.88
	C1	Mar	13.8	34.25	1158.7	3.98E+05	34.93	1.00	-	2.44
	E1	May	26.5	30.09	1529.9	3.59E+05	33.80	1.00	-	6.81
	F1	Aug	36.2	30.16	1308.0	3.52E+05	33.17	1.00	-	3.07
	G1	Sep	32.7	32.46	963.9	3.75E+05	33.83	1.00	-	2.73

Table 4. Results of energy dissipation analyses using the backcalculated pavement parameters

Pavement Type	ID	Month	Surface Temp.	Dissipation Rate	Dissipation	Fuel Consumption
			˚C	(J/Sec)	(MJ/Km)	(Gal/mile)
Flexible (NV0101)	A1	Feb	1.4	163.22	5.88E-03	6.45E-05
	B1	Mar	16.5	195.82	7.05E-03	7.74E-05
	C1	May	18.2	212.14	7.64E-03	8.38E-05
	D1	Aug	34.9	362.40	1.30E-02	1.43E-04
	E1	Sep	23.7	293.28	1.06E-02	1.16E-04
	F1	Nov	3.9	173.23	6.24E-03	6.84E-05
Rigid (NC0201)	B1	Feb	11.2	87.61	3.15E-03	3.46E-05
	C1	Mar	13.8	108.11	3.89E-03	4.27E-05
	E1	May	26.5	103.80	3.74E-03	4.10E-05
	F1	Aug	36.2	101.94	3.67E-03	4.03E-05
	G1	Sep	32.7	104.60	3.77E-03	4.13E-05

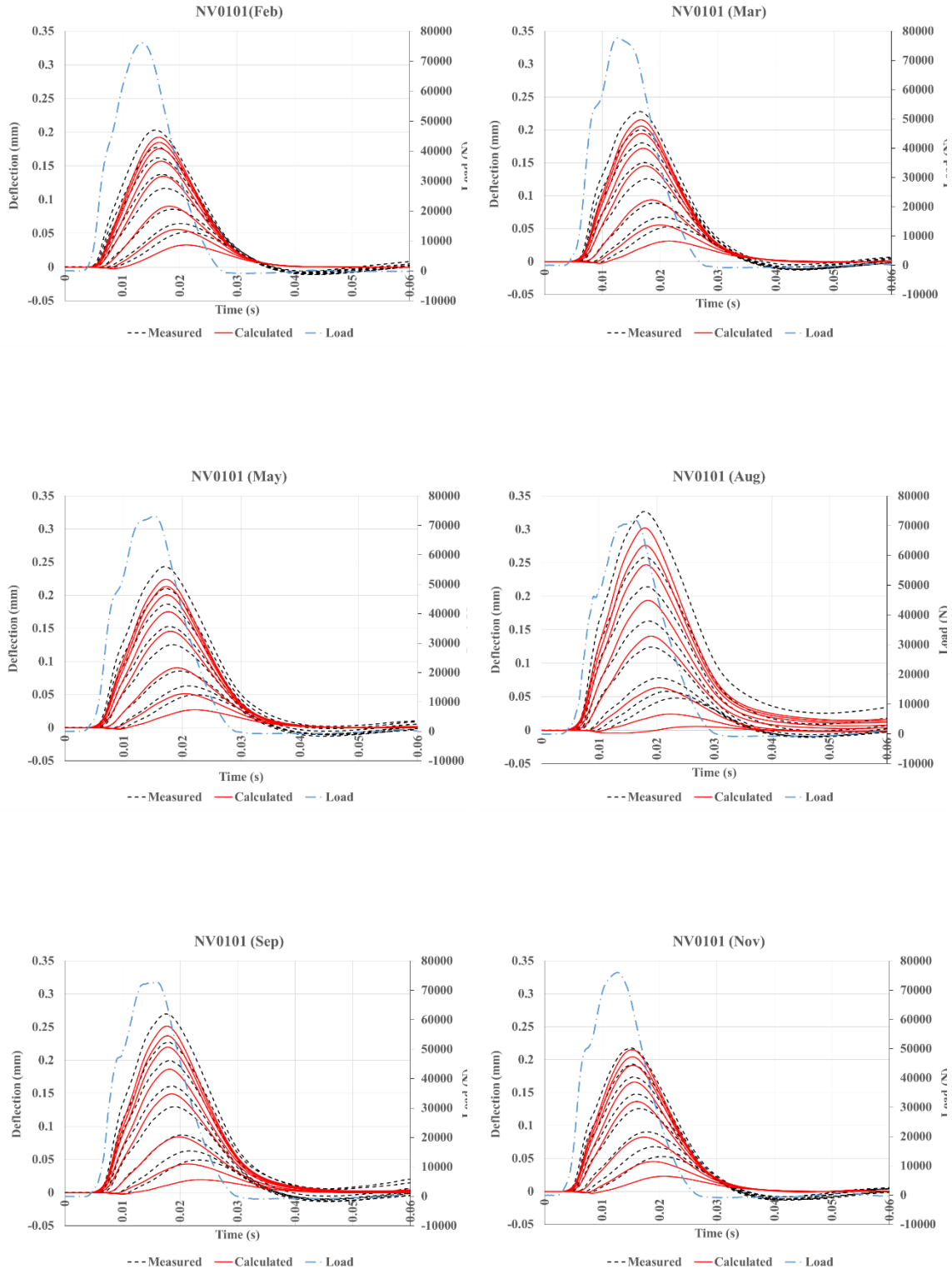

Figure 10. Measured and calculated FWD deflection basins for flexible pavement (NV0101) in Nevada at different months

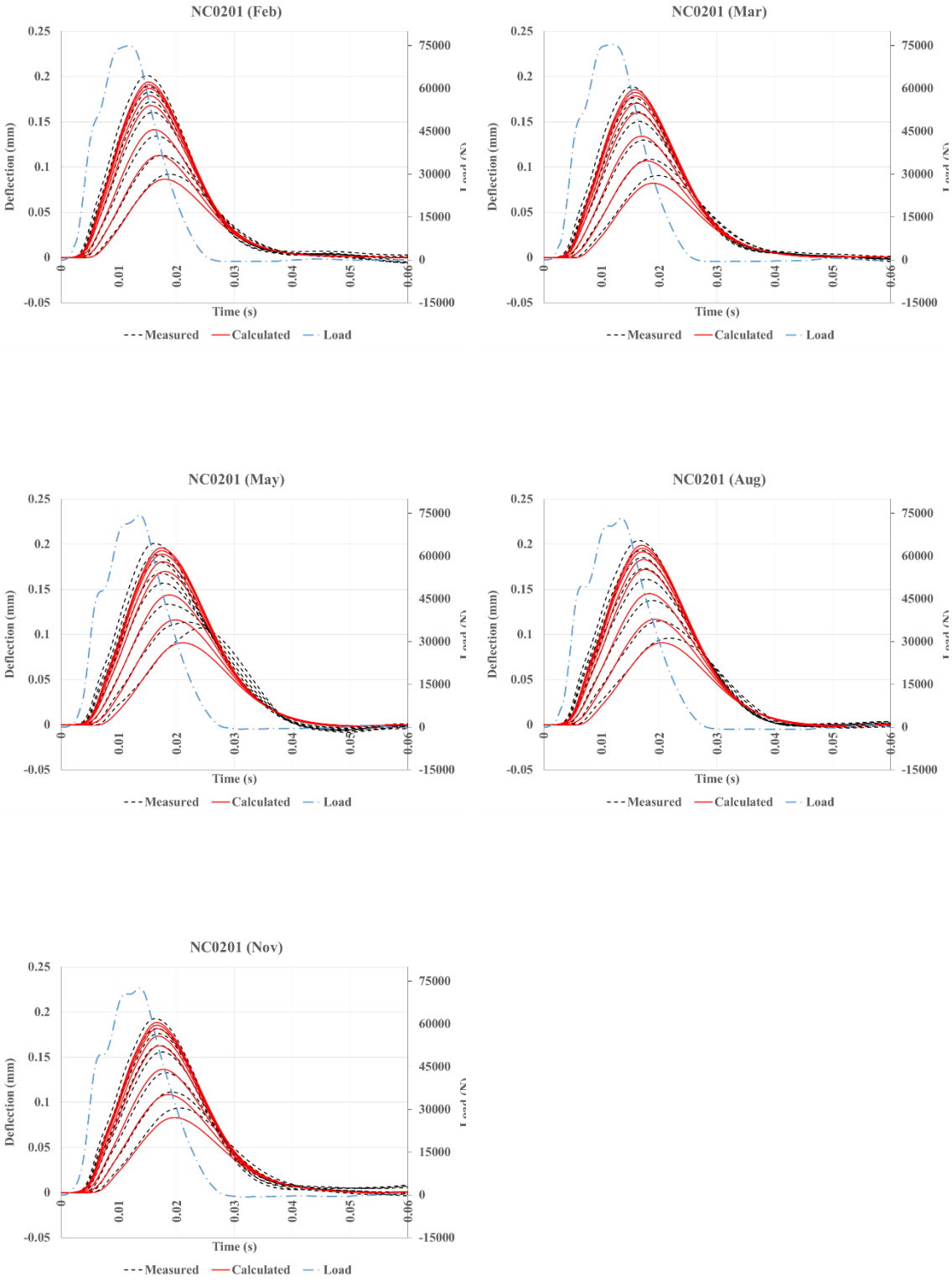

Figure 11. Measured and calculated FWD deflection basins for rigid pavement (NC0201) in North Carolina at different months

3.6. Discussion

The backcalculated pavement parameters are reliable if the measured and calculated FWD deflection basins are in close agreement with each other, confirming that the backcalculated parameters are capable of appropriately describing the pavement behavior under dynamic loading. The agreement of the measured and calculated results illustrated in Figure 10 and Figure 11 indicates that the proposed method is an effective tool for evaluating the properties of pavement sections.

The results of the analyses on the SMP sections (NV0101 and NC0201), shown in Table 3, reveals that the properties of the PCC layer in the selected rigid pavement remained almost constant and the PCC plate behaved elastically regardless of the seasonal/temperature variations. The foundation properties, except for foundation viscosity exhibited relatively higher variability, in particular the foundation inertia effect. On the other hand, for flexible pavement, the temperature variation and seasonal changes caused considerable changes in the properties of both the plate (HMA course) and the foundation (underlying layers). Both coefficients of subgrade reaction and foundation inertia effect varied significantly with the temperature change while the foundation viscosity did not encounter significant changes. The instantaneous elastic modulus of the HMA plate altered proportionally with the surface temperature change. The plate behaved elastically at the colder periods of the year (Feb, Mar, and Nov) and became more viscous as the temperature increased. The obtained backcalculated parameters were in line with the expectations of the behavior of rigid and flexible pavements.

Figure 12 depicts the variation of fuel consumption and testing temperature throughout the year 2000. Figure 12 clearly demonstrates the dependency of the vehicle energy consumption on the temperature change for flexible pavements. An increase in the temperature made the HMA surface more viscous, resulting in more viscoelastic deformation and a higher amount of deflection-induced dissipation of energy. In contrast,

based on the backcalculated plate parameters, shown in Table 3, the PCC layer behaved elastically regardless of the seasonal variation, and the dissipation due to the plate deformation is insignificant. Interestingly, the consumed fuel for rigid pavements plotted in Figure 12 was a consequence of viscoelastic properties of the underlying layer and not the surface layer. The backcalculated damping coefficient of foundation showed minor variation in the pavement section in North Carolina (see Table 3), which made the vehicle fuel consumption independent from temperature variation for the selected rigid pavement in this region. It is important to note that the fuel consumption caused by foundation viscoelasticity might vary considerably in regions that encounter considerable seasonal variation in the soil properties.

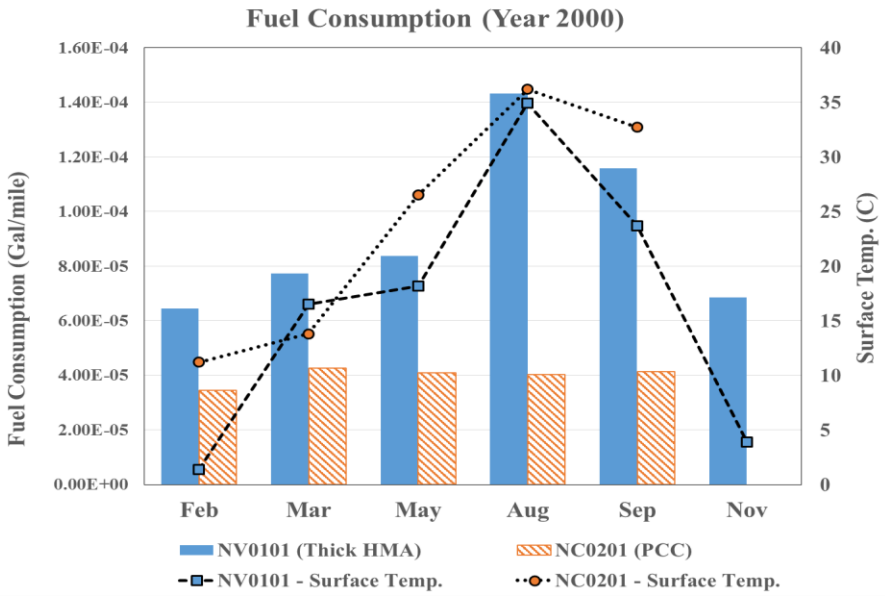

Figure 12. Effect of seasonal variation on the dissipation rate for both flexible and rigid pavements

Overall, based on the observations made in this study, the proposed method — dynamic backcalculation analyses using FWD time history data followed by the modified deflection-induced PVI analyses — provided reasonable results, which are in agreement with realistic expectations and field observations. Since FWD testing is a common pavement evaluation practice, the proposed method could be used widely to perform network scale analyses. The estimated deflection-induced energy dissipation and vehicle

fuel consumption could potentially be incorporated as a factor in pavement management and in future network planning to reduce greenhouse gas (GHG) emissions and design more sustainable roads. It is necessary to note that the proposed approach still has to be tested and validated via field measurements of fuel consumption for various site conditions and pavement structures.

The proposed tool shows reasonable results for the sections analyzed in this study, yet the model can still benefit from improvement. A few possible improvements are discussed here. The results in Figure 10 and Figure 11 show that the discrepancy between the curves is smaller for the rigid section than for a relatively thick flexible pavement. One reason might be that the generalized Westergaard model employed in this study ignores the shear resistance of the underlying layers. While this assumption may be realistic for rigid pavements, it may not hold true for flexible pavements, especially when the top layer is thin. Thus, one important adjustment to the model could be including shear resistance in the foundation model, especially for flexible pavements. Making use of the Pasternak model could be a solution to this issue.

In addition, the viscoelastic Kirchhoff-Love plate adopted in this study does not account for shear deformation and compressibility of the surface layer, which might be important properties for HMA layers. However, these properties are more influential in flexible pavements constructed with thicker HMA layers as seen in full-depth asphalt pavements. Those pavements were not the topic of this study. Another important factor to improve is accounting for the effect of daily temperature change on the properties of the flexible pavement and on fuel consumption. This effect could have considerable impact on estimating the use-phase GHG emissions. One solution for addressing this issue is to perform similar analyses on multiple sets of FWD tests conducted on the same day to capture the effect of daily temperature variation on the properties of pavement system, and to define/introduce correction factors.

It is worth noting that the PVI analysis herein assumes an infinite plate and does not consider the impact of joint spacing and characteristics on vehicle fuel consumption. Neglecting the joints impact might underestimate the deflection-induced energy dissipation for rigid pavements. However, this impact is local and can only be considerable at locations very close to the joints. Further investigation is required to quantify the variation in fuel consumptions close to the joints.

3.7. Conclusions

In this study, the structural parameters of the tested pavement sections are backcalculated by minimizing the difference between the time histories of deflections measured via FWD and the deflections calculated using the generalized Westergaard model. The backcalculated parameters are then used to estimate the vehicle fuel consumption due to deflection-induce pavement-vehicle interaction. The described procedure allows for establishing a link between the structural parameters of rigid and flexible pavements, and vehicle fuel consumption and greenhouse gas (GHG) emissions during the pavement use-phase. The purpose of this study is to show that the proposed method can be used to estimate the fuel consumption related to both asphalt and concrete pavements. Since the two tested pavement sections were not structurally equivalent, direct comparison is not possible. The following general conclusions can be drawn from this study:

- Modifying the PVI model to be compatible with the generalized Westergaard model allows it to take into account the impact of foundation damping and inertia.
- It is shown that the generalized Westergaard model is able to capture the behavior of both rigid and flexible pavements under dynamic loading with good accuracy, which makes the assignment of model parameter for PVI analysis more reliable.
- The proposed methodology is able to describe the pavement structural changes due to seasonal variation for the selected rigid and flexible pavement sections. The energy is dissipated through the viscous deformation of both the surface layer and underlying layers.

- Seasonal variations affects the amount of fuel consumption throughout a year for flexible pavement mainly due to the noticeable variation in the temperature and the corresponding change in viscoelastic properties of the HMA surface course.
- A significant portion of energy dissipation occurs in the foundation. Thus, ignoring this effect may lead to underestimation of the energy dissipation, especially for rigid pavements.
- The simplicity of the described model and the availability of FWD measurements makes the proposed methodology an attractive tool for performing network scale analyses and, potentially, for designing more sustainable roads.

Good fit was obtained in the performed analyses for the two tested pavement sections; however, there is still a room for improvement of the generalized Westergaard model, in particular for flexible pavements. One possible modification is to use a foundation model that incorporates the shear contribution of the foundation. The applicability of this model for a wider range of pavement systems and climatic conditions, such as a thin HMA layer, should be further investigated. The effect of daily temperature change on the viscoelastic properties of the HMA layer and energy dissipation must be evaluated in future studies. Further studies should investigate the contribution of joint spacing and joint characteristics to the energy dissipation.

4

Dynamic Analyses of a Viscoelastic Plate on a Generalized Pasternak Foundation

Published as Booshehrian, A., & Khazanovich, L. (2017). Dynamic analyses of a viscoelastic plate on a generalised Pasternak foundation. International Journal of Geotechnical Engineering, 1-13.

4.1. Summary

This chapter studies the problem of a slab-on-grade subjected to short-duration dynamic loading. The slab-on-grade system is modeled as a viscoelastic plate resting on a generalized Pasternak foundation, which accounts for the effects of inertia, damping, and shear resistance. A semi-analytical forward-solution is proposed by making the use of a Hankel transform in space and a finite difference method in time. To evaluate the ability of the considered model to describe the response of slab-on-grade systems, the behaviors of several pavement sections under dynamic loading are examined. A quasi-Newton inverse analysis is employed to find the model parameters by comparing the field-measured and model-calculated responses. The results show that the generalized Pasternak model can simulate the behavior of slab-on-grade systems with a wide range of slab and grade properties.

4.2. Introduction

Modeling of a slab-on-grade is an important problem for analysis and design of industrial floors, nuclear plants, mat and raft foundations, and pavement systems. These structures are often subjected to complicated external dynamic excitations such as earthquakes, impacts, and moving loads [*Selvadurai*, 1979; *Maheshwari and Khatri*, 2010]. To address the geometric and mechanical complexities of these structures, the computationally intensive finite-element method (FEM) is often employed. However, for many applications, simpler semi-analytical solutions are desirable [*Wang et al.*, 2005; *Worku*, 2013].

Various foundation models have been used for describing the slab-on-grade systems. One of the commonly used approaches was proposed by Westergaard [*Westergaard*, 1926]. It describes the subgrade as a Winkler foundation, which is a combination of closely spaced, independent linear springs. Another frequently used model for the foundation is the layered elastic half-space model, which is often considered as a more realistic representation of soil behavior [*Huang*, 1993]. However, it requires more computational effort compared to the Winkler model. Different limitations are associated with these two approaches, for instance, Winkler foundation completely ignores the shear interaction of the soil grains, while the elastic half-space model ascribes to the foundation a higher degree of shear interaction than is usually observed in the field [*Khazanovich*, 1994].

A variety of foundation models has been proposed to include the shear resistance in the Winkler foundation and to make the predictions of this model agree with the field observations [*Filonenko-Borodich*, 1940; *Hetenyi*, 1950; *Pasternak*, 1954; *Kerr*, 1965]. Among those, Pasternak foundation model is the most natural extension of the Winkler model and has been more widely adopted by researchers [*Selvadurai*, 1979]. In the Pasternak approach, the shear contribution of the foundation is incorporated by including

an elastic shear layer connected consequently to the vertical elastic springs in the foundation model [*Pasternak*, 1954].

The Pasternak foundation has been previously utilized by many authors for different applications. Several researchers have considered the elastic weightless two-parameter Pasternak foundation and offered mathematical forward solutions for the problem of slab-on-grade with various boundary conditions and loading mechanisms [*Pronk*, 1993; *Shi et al.*, 1994; *Van Cauwelaert*, 2003; *Tanahashi*, 2004; *Ferreira et al.*, 2010; *Worku*, 2013; *Worku*, 2014; *Sireesh et al.*, 2016). One of the main applications of the slab resting on a two-parameter Pasternak foundation is to simulate the behavior of pavements (*Shi et al*., 1993; *Uzan*, 1994a; *Fwa et al.*, 1996; *Van Cauwelaert*, 2003; *Patil et al.*, 2012). This model has been employed as part of the standardized pavement condition assessment in the Netherlands (*Stet et al.*, 2002).

Several researchers made use of a viscoelastic weightless Pasternak foundation by accounting for the damping effects of the foundation to simulate the behavior of an Euler-Bernoulli or a Timoshenko beam under dynamic loads [*Saito and Terasawa*, 1980; *Zheng et al.*, 2000; *Kargarnovin and Younesian*, 2004; *Younesian et al.*, 2006; *Yang et al.*, 2013]. *Hasheminejad and Gheshlaghi* [2012] found a semi-analytical solution for an arbitrary thick plate resting on a viscoelastic weightless foundation. *Basu and Kameswara* [2013] obtained the analytical solution for a point load moving on an elastic Euler-Bernoulli beam resting on a viscoelastic Pasternak foundation which accounts for the inertial effects of the beam and the foundation. Regardless of the selection of the foundation model and the robust mathematical approaches, assigning reasonable values to the model parameters is an essential and challenging task for analysis and evaluation purposes [*ARA*, 2003].

Recent research on linking the energy dissipated through the pavement deformation to vehicle consumption adds to the importance of the model selection [*Louhghalam et al.*, 2014; *Coleri et al.*, 2016]. The dissipated energy (excess fuel consumption) estimated by

the deflection-induced pavement-vehicle interaction (PVI) analysis was formulated using a viscoelastic plate on a Winkler foundation. This foundation model was used because of its simplicity and computational efficiency [*Louhghalam et al.*, 2014]. It is self-evident that the precision of PVI analyses is tightly dependent on the accuracy of the pavement surface deformations estimated by the selected model under a moving vehicle.

Chapter 2 questioned the ability of the Winkler foundation to properly describe the behavior of slab-on-grade under dynamic loading. This speculation was put to the test by examining the response of pavements (such as slab-on-grade systems) subjected to short-duration loading of falling weight deflectometer (FWD). The discrepancies observed between the pavement deflections measured by the FWD sensors and those calculated by the model demonstrated that the Winkler foundation cannot properly simulate the behavior of the grade under short-duration loading. The results suggested that the inclusion of inertia and damping effects of the foundation is fundamental in obtaining realistic predictions of the pavement behavior.

Despite the considerable improvements made by accounting for the damping and inertia of the foundation, the fit found for the asphalt pavement was not as accurate as that for the concrete pavement with the stiffer and elastic surface layer, especially for the deflections recorded by sensors that were located farther away from the center of FWD loading plate. This motivated the author to investigate whether the inclusion of shear (based on the Pasternak foundation) could provide more reasonable predictions for describing behavior of a general slab-on-grade system under dynamic loading while maintaining the computational efficiency. Obtaining realistic model parameters by developing a robust inverse analysis is another rational motivation of this chapter.

In this study, a viscoelastic plate resting on a generalized Pasternak foundation is considered. The generalized Pasternak model (GPM) accounts for the effects of inertia, damping, and shear resistance of the foundation. The forward- and inverse-solutions under

the dynamic circular pressure are developed. To evaluate the ability of the GPM in modeling the behavior of a general slab-on-grade system, the responses of pavement systems under short-duration loading of FWD test are considered. The inverse analysis was performed on the measured time histories of FWD deflections obtained from pavement sections with various properties. The mathematical approach and the results of the analyses are presented below.

4.3. Generalized Pasternak Model

Consider an infinite, homogeneous, isotropic, and linearly viscoelastic Kirchhoff-Love plate on a generalized Pasternak foundation (Figure 13). The viscoelasticity of the plate is simulated using the three-parameter standard linear solid (SLS) (Christensen 1982) model as illustrated in the inset of Figure 13.

The generalized Pasternak foundation is a four-parameter model consisting of:

1) linear Winkler springs representing the subgrade coefficient of reaction, *k*,
2) linear dashpots representing the damping coefficient of the foundation, *c*,
3) mass elements representing the mass of the unit area of the viscoelastic plate and the moving portion of foundation, $m = m_{plate} + m_{foundation}$, and
4) an incompressible shear layer representing the shear resistance of the foundation with elastic shear modulus *G*.

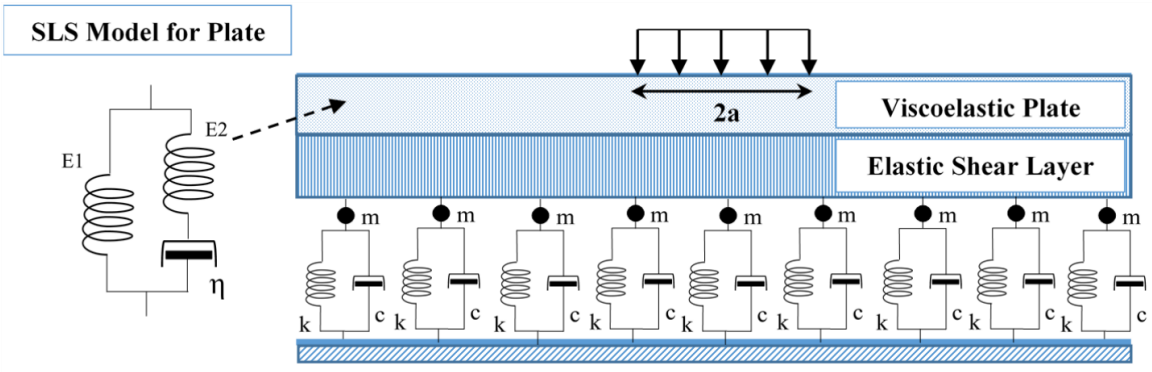

Figure 13. Viscoelastic plate resting on a generalized Pasternak foundation

The generalized Pasternak foundation model is an extension of Pasternak model that takes into account the effects of inertia and damping. If the shear modulus, G, is set to be equal to zero then the model is reduced to the extension of the Winkler model that accounts for the effects of inertia and damping. If zero values were assigned to mass elements and dashpots, the generalized Pasternak foundation model is reduced to the classic two-parameter Pasternak model.

If a viscoelastic plate supported by the generalized Pasternak foundation is subjected to a time-dependent circular pressure, then the equation of motion of the plate has the following form:

$$D\left(\tilde{I}-\tilde{R}\right)\nabla^4 w(r,t) - G\nabla^2 w(r,t) + kw(r,t) + c\frac{\partial w(r,t)}{\partial t} + m\frac{\partial^2 w(r,t)}{\partial t^2} = p(r,t) \tag{4-1}$$

where $D = Eh^3/12(1-\nu^2)$ is the plate's instantaneous flexural stiffness; and E, h, and ν are instantaneous modulus of elasticity, thickness, and Poisson's ratio of the plate, respectively. $w(r,t)$ is the surface deflection at distance r from the center of the circular pressure, and t is the time; ∇^2 is the Laplace operator defined as $\nabla^2 = \frac{1}{r}\frac{\partial}{\partial r} + \frac{\partial^2}{\partial r^2}$; $p(r,t)$ is the time-dependent applied pressure which can be presented as $p(r,t) = \frac{P}{\pi a^2}H(r-a)g(t)$ where P is the maximum total applied load, a is the radius of the circular contact area, $H(r)$ is the Heaviside function, $g(t)$ is an arbitrary function of time that represents the change of pressure with respect to time t; $\tilde{I}$ is the identity operator, and $\tilde{R}$ is the relaxation operator found based on the stress-strain relationship (constitutive equation) of the SLS model used for the viscoelastic plate, defined as:

$$\tilde{R}\epsilon(t) = \frac{1}{\tau}\left(1 - \frac{E_1}{(E_1+E_2)}\right)\int_0^t e^{\frac{(t-x)}{-\tau}}\epsilon(x)dx \tag{4-2}$$

where E_1, E_2 are two stiffness parameters of the SLS model (see inset of Figure 13). In addition, η is the material viscosity parameter, and therefore, $\tau = \eta/E_2$ is the relaxation

time of the viscoelastic plate. The detailed steps for deriving equation (4-2) can be found in Chapter 2. The three plate parameters used in this study, based on the SLS model, are:

1) the instantaneous modulus of elasticity of the plate, $E = E_1 + E_2$;
2) the ratio of E_1/E; and
3) the plate relaxation time, $\tau = \eta/E_2$.

4.4. Forward Analysis

The governing differential equation (4-1) can be re-written in a non-dimensional form:

$$\left(\tilde{I} - \tilde{R}\right)\nabla^4 w^*(s,t^*) - G^*\nabla^2 w^*(s,t^*) + w^*(s,t^*) + c^*\frac{\partial w^*(s,t^*)}{\partial t^*} + m^*\frac{\partial^2 w^*(s,t^*)}{\partial {t^*}^2} = p^*(s,t^*) \tag{4-3}$$

The terms with asterisk represent the non-dimensional variables defined as $w^*(s,t^*) = \frac{kl^2}{P}w(r,t)$; $p^*(s,t^*) = \frac{l^2}{P}p(r,t)$; $t^* = 2\pi\frac{t}{T}$; $G^* = \frac{G}{kl^2}$; $c^* = \frac{2\pi}{T}\frac{c}{k}$; $m^* = (\frac{2\pi}{T})^2\frac{m}{k}$; where l is the radius of relative stiffness, defined as $l = \sqrt[4]{\frac{D}{k}}$; s is the nondimensional distance from the center of the applied load, defined as $s = \frac{r}{l}$; and *T* is the loading duration of the applied pressure.

In order to solve the non-dimensional governing differential equation (4-3), a semi-analytical approach similar to the approach used in Chapter 2 is adapted. This approach makes use of the combined application of Hankel transform in space, and finite difference method in time.

The zero order Hankel transform is applied with respect to the space variable, *s*. The zero order Hankel transform of a function, *f(s)*, is defined as:

$$(H_0 f)(\alpha) = \int_0^\infty s f(s) J_0(\alpha \cdot s) ds \tag{4-4}$$

where J_0 is the zero order Bessel function, and α is a parameter of the Hankel transform. An application of the zero Hankel transform to Equation (4-3) yields:

$$\alpha^4\left(\tilde{I}-\tilde{R}\right)W^*(\alpha,t^*)+\alpha^2G^*W^*(\alpha,t^*)+W^*(\alpha,t^*)+c^*\frac{\partial W^*(\alpha,t^*)}{\partial t^*} + m^*\frac{\partial^2 W^*(\alpha,t^*)}{\partial {t^*}^2}=\frac{J_1(\alpha a_l)}{\pi a_l \alpha}g(t^*) \tag{4-5}$$

where $W^*(\alpha,t^*)$ is the nondimensional Hankel transformed surface deflection, a_l = *a/l*, and J_1 is the Bessel function of order one.

The first and second derivatives in time at each time step, t_i, are approximated using principles of finite difference as follows:

$$\frac{\partial W^*(\alpha,t^*)}{\partial t^*}\approx\frac{{W^*}_{i+1}-{W^*}_{i-1}}{2\Delta t^*} \tag{4-6}$$

$$\frac{\partial^2 W^*(\alpha,t^*)}{\partial {t^*}^2}\approx\frac{{W^*}_{i+1}-2{W^*}_{i}+{W^*}_{i-1}}{\Delta {t^*}^2} \tag{4-7}$$

Substituting equations (4-6) and (4-7) into equation (4-5) leads to a system of linear equations. The introduction of the following two initial conditions allows for solving this system of equations and obtaining ${W^*}_i$ at each time step, t_i.

$$W^*(\alpha,0)=0 \tag{4-8}$$

$$\frac{\partial W^*(\alpha,t^*)}{\partial t^*}\Big|_{t^*=0}=0 \tag{4-9}$$

The obtained $W^*(\alpha,t^*)$ for each value of α can be transferred back to the nondimensional space using the inverse zero order Hankel transform, defined as:

$$w^*(s,t^*) = \int_0^\infty W^*(\alpha,t^*)J_0(\alpha s)\alpha d\alpha \tag{4-10}$$

Finally, the obtained nondimensional values, $w^*(s,t^*)$, are converted back into dimensional term, $w(r,t)$, using the following equation:

$$w(r,t) = \frac{P}{kl^2}w^*(s,t^*) \tag{4-11}$$

Since this analysis is performed in the time domain, it prevents the potential problems associated with the use of the frequency domain [*Uzan*, 1994b; *Chatti*, 2004; *Zaabar et al.*, 2014).

Based on the explained procedure, the forward analysis was implemented into a Fortran program. In order to verify the numerical analysis, the closed-form solution for a simpler case of an elastic plate resting on the generalized Pasternak foundation was obtained following the analytical procedure proposed by *Khazanovich* [2000]. The applied dynamic load was assumed sinusoidal to simulate the movement of a vehicle or an impact load. Thus, the time-dependent function of the applied load was defined as $g(t) = \frac{1}{2}(1 - \cos(t))$ for $0 < t < T$ and $g(t) = 0$ for $T > 0$. The slab-on-grade system and the loading configuration simulated here have the following properties:

$E = 34.5\ GPa, \nu = 0.15, h = 0.225\ m, k = 27.1 KPa/mm, P = 45\ KN, T = 0.02\ s, a = 0.15\ m$. Here, the response of the plate at $r = 0.1\ m$ away from center of loading was considered.

A comparison of the numerical and closed-form solutions for four sets of non-dimensional parameters is presented in Figure 14. Case 1 is related to the Winkler foundation. Case 2 represents an elastic weightless Pasternak foundation with $G^* = 2$. In Case 3, the inertial effect of the plate and foundation is added (assuming $m/m_{plate} = 2$) to the elastic weightless Pasternak foundation. Finally, Case 4 is a generalized Pasternak foundation with

$c^* = 2$. These examples demonstrate that the numerical and closed-form solutions match perfectly.

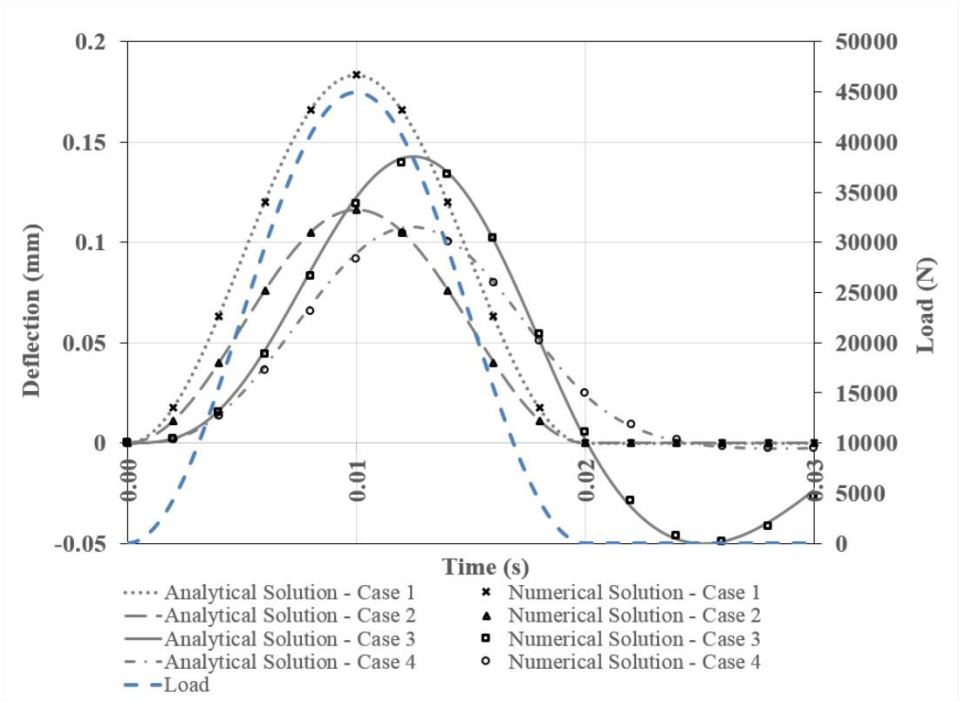

Figure 14. Verification of the numerical solution for an elastic plate on various foundation models subjected to a sinusoidal load

To verify that the viscoelasticity of the plate is properly implemented based on the principles of the standard linear solid model, a slab-on-grade system with a viscoelastic slab consisting of the following parameters was considered: $E = 10\ GPa, E_1 = 3\ GPa, E_2 = 7\ GPa, \nu = 0.35, h = 0.183\ m, k = 100\frac{KPa}{mm}, G^* = 2, m/m_{plate} = 2, c^* = 2, P = 76\ KN, T = 0.023\ s, a = 0.15\ m, r = 0.0\ m$. The response of the system under an arbitrary impact load was generated for various values of viscosity, η, (or relaxation time, τ) (Figure 15).

The extreme case responses are related to the elastic behavior with $E = E_1 = 3\ GPa$ when τ approaches zero, and the elastic behavior with $E = E_1 + E_2 = 10\ GPa$ when τ approaches infinity. The surface deflections for the two elastic limit cases were computed

using the obtained closed-form solutions. Figure 15 shows that, in line with the expectation, the numerical solutions for the slab-on-grade systems incorporating viscoelastic slabs were enclosed by the solutions for the elastic limit cases.

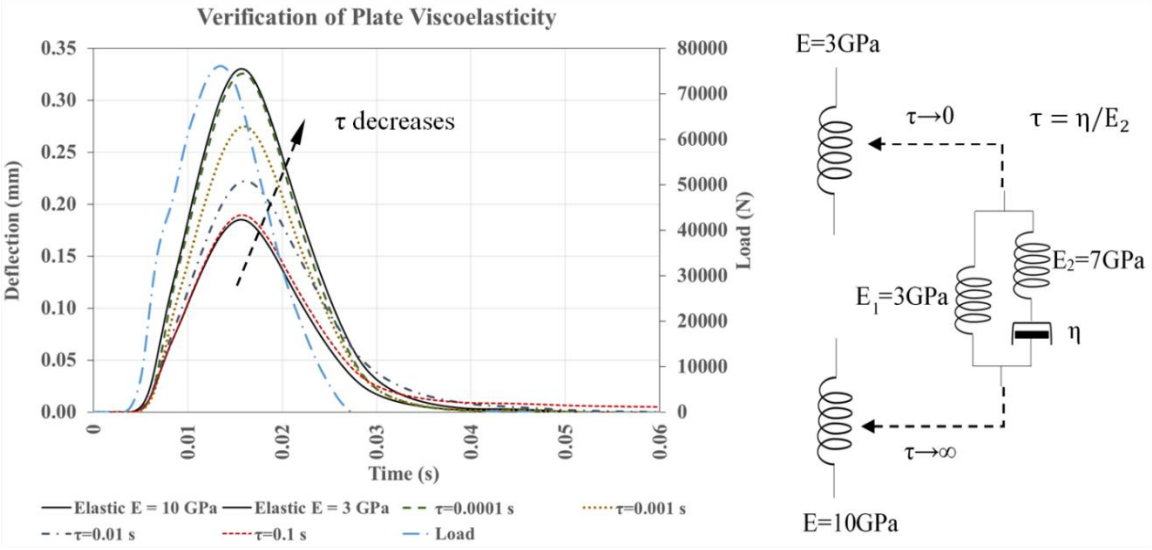

Figure 15. Comparison of the response for elastic plates with response for viscoelastic plates with various viscosities subjected to a dynamic load

4.5. Inverse Analysis (Backcalculation)

One major issue associated with the models developed for slab-on-grade systems is selection of the model parameters. A common solution is to use non-destructive testing (NDT) methods that can introduce a known excitation to the system and record the system response. This allows for finding the model parameters by solving an inverse problem. A deflection-based NDT device commonly used for pavements and industrial floors is the falling weight deflectometer (FWD). FWD applies a user-specified sinusoidal load pulse to the slab surface and records the time history of the surface deflections using an array of sensors located at various distances radiating from the center of the circular FWD base plate [*Uzan*, 1994b; *Howard and Warren*, 2008]. Therefore, to illustrate the ability of the generalized Pasternak model in describing the behavior of a slab-on-grade system subjected to a dynamic loading, the pavement responses to the applied dynamic loads of the Falling Weight Deflectometer (FWD) can be considered as an example.

The numerical analysis described earlier offers a computationally efficient approach for determining the surface deflections under a time-dependent circular pressure - here, the time history of the FWD pressure - for a given set of parameters (forward solution). A backcalculation procedure can be developed to find the model parameters by matching the model-calculated deflections under FWD load with those measured by FWD sensors (inverse solution). In the inverse problem, the plate is subjected to a time-varying circular pressure. The thickness, *h*, the Poisson's ratio, *v*, and the mass of the plate, m_{plate}, are known values. FWD provides the loading plate radius, *a*, the loading duration, *T*, the location of the sensors, and the time histories of the applied pressure and surface deflections at the location of each sensor, all of which are required for the backcalculation.

The solution to the inverse problem can be found by minimizing the defined error function through iteration. The error function used in this study is defined as the normalized sum of square of errors (SSE) normalized by the maximum deflection in the FWD deflection profiles:

$$SSE = \left(\frac{1}{w_{max}^{M}}\right)^2 \sum_{i=1}^{n}\sum_{j=1}^{m}(w_{ij}^{M} - w_{ij}^{C})^2 \tag{4-12}$$

where *n* is number of sensors, *m* is number of time steps, w_{max}^{M} is the maximum measured deflection in the FWD deflection history, and w_{ij}^{M} and w_{ij}^{C} are the FWD-measured and model-calculated deflection for sensor *i* at time *j*, respectively.

Seven parameters must be backcalculated: four parameters are related to the generalized Pasternak foundation, and three parameters are associated with the model for the plate viscoelastic material. A combination of quasi-Newton method and a finite-difference gradient has been employed to improve and expedite the search scheme. A common issue associated with a gradient-based search scheme is the problem of finding the local minimum instead of the global minimum. This issue is addressed by generating multiple

random seeding values and comparing the obtained backcalculation solutions and the corresponding error values.

The inverse analysis was implemented into Fortran program and tested using multiple synthetic FWD deflection basins. Figure 16 provides an example of the calculated versus synthetically generated deflection profiles. As shown in Figure 16, the FWD applies a short duration (between 0.012s to 0.035s) sinusoidal pressure to the surface of the layered structure. The pavement properties for this synthetic FWD deflection profile are: $E = 1.42\ GPa, E_1/E = 0.69, \tau = 0.010\ s, \nu = 0.3, h = 0.071\ m, k = 110\frac{KPa}{mm}, G^* = 7.27, m/m_{plate} = 2.45, c^* = 1.07, P = 58\ kN, T = 0.014\ s, a = 0.15\ m.$ In this example, FWD sensors are located at 0.0, 0.2, 0.3, 0.45, 0.6, 0.9, and 1.5 m away from the center of loading. Deflection profiles with smaller values correspond to the sensors located farther away from the center of loading. It can be observed from Figure 16 that the synthetic deflections and the model-calculated deflections using the backcalculated parameters fit perfectly. The backcalculated parameters were in close agreement with the mentioned assigned parameters with no significant difference.

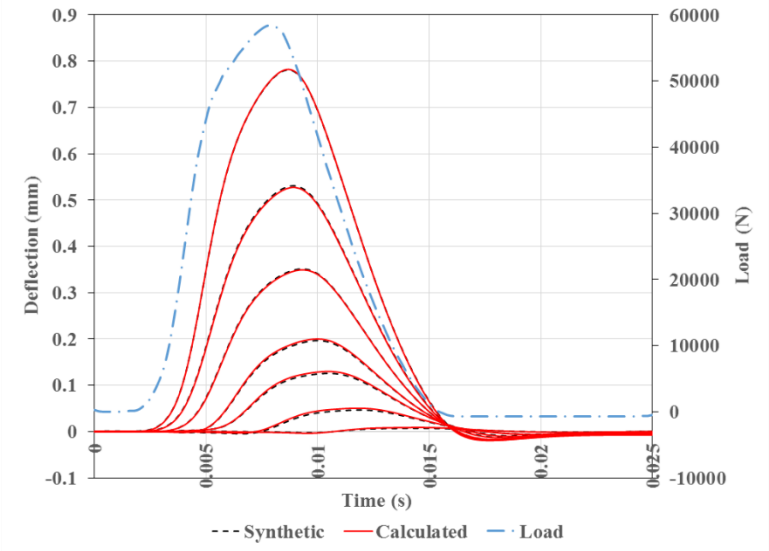

Figure 16. Verification of the developed gradient-based backcalculation procedure using synthetic data

4.6. Case Studies

To examine the importance of various foundation parameters in modeling the slab-on-grade systems, FWD deflection basins collected for four pavements under the Long-Term Pavement Performance (LTPP) program [*FHWA*, 2017] were considered. Cases A, B, and C are located on the highway I-80 in Nevada, and the studied test data are collected in the year 2000. The fourth section, Case D, is located on the highway US-14 in Wyoming, and the data collected in the year 1994 were employed in this study. These test data were selected because the pavements were in good condition at the time of testing and the number of major treatments performed on these pavements were limited.

The layers description of the four selected pavement sections are listed in Table 5. Case A has a 234-mm thick concrete top surface, while Cases B and C are asphalt pavements with a top layer thickness of 109 and 183 mm, respectively. These three sections incorporate similar aggregate base as well as aggregate and lime stabilized subbase layer and coarse grained subgrade. Case D consists of a 71-mm thick asphalt layer with a relatively thin base layer placed directly on a coarse grained subgrade. Further information on these sections can be found on InfoPave™, the online LTPP database [*FHWA*, 2017]. The Poisson's ratio of the plate, v, can be taken into account as an additional plate variable; however, assuming that the Poisson's value is known does not result in serious errors [*Uzan*, 1994a; *Von Quintus and Simpson*, 2002] while the advantage would be reduction of the computational efforts. Here, in the forward and inverse analysis, the Poisson's ratio of the plate was assumed to be constant and equal to 0.15 for concrete. For asphalt sections, depending on the test temperature, a reasonable value of 0.20 to 0.40 was assigned using the laboratory tested values reported in the literature [*Von Quintus and Simpson*, 2002].

The inverse analyses were performed on the FWD deflection profiles for the selected sections to determine three SLS model parameters for the plate and the foundation model parameters. The following four foundation models were considered:

- Winkler Model with one parameter: the coefficient of subgrade reaction, k.

- Pasternak Model with two parameters: k and the foundation shear modulus, G.
- Generalized Winkler Model (GWM) with three-parameters: k, the mass of the unit area of the moving portion of foundation, $m_{foundation,}$ and the damping coefficient of the foundation, c.
- Generalized Pasternak model (GPM) with four-parameters: k, $m_{foundation}$, c, and G.

The objective was to examine what foundation model is most suitable in describing the dynamic response of the selected pavement sections. Needless to say, the only difference in the inverse analyses for the mentioned models is forcing the additional parameter(s) equal to zero (i.e. the G-value is equal to zero for GWM).

To minimize the effects of pavement joints and edges, the analysis used the FWD data collected at the center of the slab and away from the pavement edges (interior loading). For Cases A and B, the LTPP database provides only one FWD visit in several years; thus, only one FWD data set was analyzed for each case. For Cases C and D, the FWD test data from different times throughout a year are available. Several FWD data sets were analyzed to investigate the effect of climatic conditions. The surface layer temperatures at the time of FWD testing are listed in Table 6, Table 7, and Table 8.

Table 5. Detailed information on the selected pavement sections

Case	Top Layer				Base Layer		Subbase Layer	
	Material	Thickness (m)	Density (kg/m^3)	Plate Mass (kg/m^2)	Material	Thickness (m)	Material	Thickness (m)
A	Concrete	0.234	2222	0.520	CA[1]	0.150	A[2]/LTS[3]	0.551/0.305
B	Asphalt	0.109	2234	0.244	CA	0.208	A/LTS	0.579/0.305
C	Asphalt	0.183	2234	0.409	CA	0.297	A/LTS	0.544/0.305
D	Asphalt	0.071	2250	0.160	CA	0.157	-	-

[1] Crushed Aggregate
[2] Aggregate
[3] Lime Treated Soil

4.7. Results

Table 6, Table 7, and Table 8 present the backcalculated model parameters and the associated error values computed using Equation (4-12) for the above-mentioned foundation idealizations. As expected, regardless of the foundation model used in the analysis, the concrete layer exhibited an elastic behavior as indicated by the backcalculated E_1/E ratio equal to 1. The asphalt layer exhibited viscoelastic properties in all three asphalt sections used in this study, unless the testing was conducted at a low temperature. For example, the asphalt layer in Case C exhibited mostly elastic behavior, i.e. backcalculated E_1/E = 1, from the testing in February and November with the surface temperature equal to 1.4 ^{o}C and 3.9 ^{o}C, respectively. The asphalt layer in Case C exhibited a strong viscoelastic behavior in August when the surface temperature was 34.9 ^{o}C.

Figure 17 shows the fit between the measured deflections at the location of the FWD sensors and the corresponding model-calculated deflections for the elastic slab-on-grade system with portland cement concrete surface layer (Case A). The elastic weightless Winkler model provided a very poor fit (Figure 17a). The addition of the shear parameter to the foundation model (the elastic weightless Pasternak model) did not improve the fit considerably (Figure 17b). In contrast, the use of the generalized Winkler model improved the fit significantly (Figure 17c). No difference was witnessed between the generalized Winkler and Pasternak models for the concrete pavement (Figure 17d). The considerable visual enhancement of the fit and the much smaller error values (see Table 6) obtained by the addition of the inertia and damping parameters underline the importance of including these mechanical elements in the foundation model for short-duration loading.

Similar observation was made for a viscoelastic slab-on-grade system with a thin asphaltic surface layer (Case B). Similar to Case A, using the Winkler and Pasternak model led to a very poor fit (see Figure 18a and Figure 18b) and large error values (see Table 6). The addition of the foundation inertia and damping effects, however, significantly improved the predictions as can be observed in Figure 18c and Figure 18d. The GPM resulted in a slight improvement in the fit for the outer sensors (recorded deflection profiles with smaller

deformation) compared to the GWM. Table 6 shows that the smaller SSE associated with the GPM supports this argument (7.85 versus 11.49).

Table 6. Backcalculated pavement parameters for Cases A, and B

Surface Type	Model	Month	Surface Temp.	Foundation Parameters				Plate Parameters				Error (SSE)
				K	$m_{Foundation}$	c	G	m_{Plate}	E	E_1/E	τ	
			˚C	KPa/mm	kg/m^2	Pa.s/m	MPa	kg/m^2	GPa	-	s	-
Concrete (Case A)	GPM[1]	June	40.1	51.80	140	0.371	0.00	520	18.14	1.00	-	2.42
	GWM[2]	June	40.1	51.80	140	0.371	-	520	18.14	1.00	-	2.42
	PM[3]	June	40.1	16.51	-	-	139.98	520	4.66	1.00	-	129.00
	WM[4]	June	40.1	134.88	-	-	-	520	10.66	1.00	-	137.23
Thinner Asphalt (Case B)	GPM	June	50.0	108.11	0	1.084	19.67	244	1.02	0.00	0.010	7.85
	GWM	June	50.0	201.13	0	0.940	-	244	5.50	0.39	0.016	11.49
	PM	June	50.0	217.60	0	-	10.09	244	16.91	0.00	0.002	13.60
	WM	June	50.0	245.60	0	-	-	244	17.85	0.09	0.002	14.31

[1] Generalized Pasternak Model (GPM)
[2] Generalized Winkler Model (GWM)
[3] Pasternak Model (PM)
[4] Winkler Model (WM)

Table 7. Backcalculated pavement parameters for Case C

Surface Type	Model	Month	Surface Temp.	Foundation Parameters				Plate Parameters				Error (SSE)
				K	$m_{Foundation}$	c	G	m_{Plate}	E	E_1/E	τ	
			˚C	KPa/mm	kg/m^2	Pa.s/m	MPa	kg/m^2	GPa	-	s	-
Thicker Asphalt (Case C)	GPM	Feb	1.4	91.99	704	0.699	0.00	409	27.06	1.00	-	6.95
		Mar	16.5	84.97	749	0.692	15.90	409	17.54	0.92	0.041	7.04
		May	18.2	86.42	501	0.662	21.83	409	14.43	0.84	0.034	5.97
		Aug	34.9	84.06	204	0.675	43.32	409	5.26	0.00	0.008	4.79
		Sep	23.7	89.63	611	0.668	29.81	409	9.70	0.46	0.014	6.12
		Nov	3.9	91.06	620	0.663	0.00	409	23.99	1.00	-	7.10
	GWM	Feb	1.4	91.99	693	0.699	-	409	27.06	1.00	-	6.95
		Mar	16.5	92.93	413	0.708	-	409	22.05	1.00	-	7.14
		May	18.2	96.50	253	0.687	-	409	18.95	0.93	0.034	6.71
		Aug	34.9	143.59	0	0.777	-	409	8.63	0.47	0.014	9.41
		Sep	23.7	102.87	0	0.731	-	409	13.90	0.81	0.035	7.50
		Nov	3.9	91.06	589	0.663	-	409	23.99	1.00	-	7.10

Table 8. Backcalculated pavement parameters for Case D

Surface Type	Model	Month	Surface Temp.	Foundation Parameters				Plate Parameters				Error (SSE)
				K	$m_{Foundation}$	C	G	m_{Plate}	E	E_1/E	τ	
			˚C	KPa/mm	kg/m^2	Pa.s/m	MPa	kg/m^2	GPa	-	s	-
Thinner Asphalt (Case D)	GPM	Jan	4.4	30.84	173	0.197	42.36	160	15.01	0.00	0.012	3.55
		Mar	27.2	45.35	32	0.167	18.88	160	5.84	0.00	0.006	2.01
		Apr	19.4	54.92	72	0.160	20.21	160	7.81	0.00	0.006	1.80
		Jun	16.1	55.10	0	0.183	19.20	160	7.11	0.00	0.009	2.03
		Jul	22.2	72.68	0	0.207	16.97	160	6.84	0.00	0.008	2.48
		Sep	12.8	57.96	22	0.175	20.06	160	7.90	0.00	0.008	1.84
		Dec	-6.1	24.54	252	0.157	83.71	160	21.90	0.38	0.012	3.47
	GWM	Jan	4.4	147.27	0	0.546	-	160	35.10	1.00	-	19.17
		Mar	27.2	101.09	0	0.214	-	160	22.08	0.60	0.016	5.26
		Apr	19.4	103.80	0	0.224	-	160	24.92	1.00	-	5.47
		Jun	16.1	113.40	0	0.206	-	160	28.80	0.53	0.015	4.79
		Jul	22.2	125.33	0	0.211		160	25.03	0.44	0.011	5.15
		Sep	12.8	122.33	0	0.214	-	160	26.33	0.49	0.017	4.72
		Dec	-6.1	288.10	0	0.953	-	160	45.00	1.00	-	59.50

Table 9. Alternative backcalculated pavement parameters for Case D

Surface Type	Model	Month	Surface Temp.	Foundation Parameters				Plate Parameters				Error (SSE)
				K	$m_{Foundation}$	C	G	m_{Plate}	E	E_1/E	τ	
			˚C	KPa/mm	kg/m^2	Pa.s/m	MPa	kg/m^2	GPa	-	s	-
Thinner Asphalt (Case D)	GPM	Jul	22.2	72.68	0	0.207	16.97	160	6.84	0.00	0.008	2.48
				65.09	32	0.215	18.51	160	7.09	0.00	0.007	2.51
				66.15	24	0.205	21.09	160	7.10	0.00	0.005	2.58

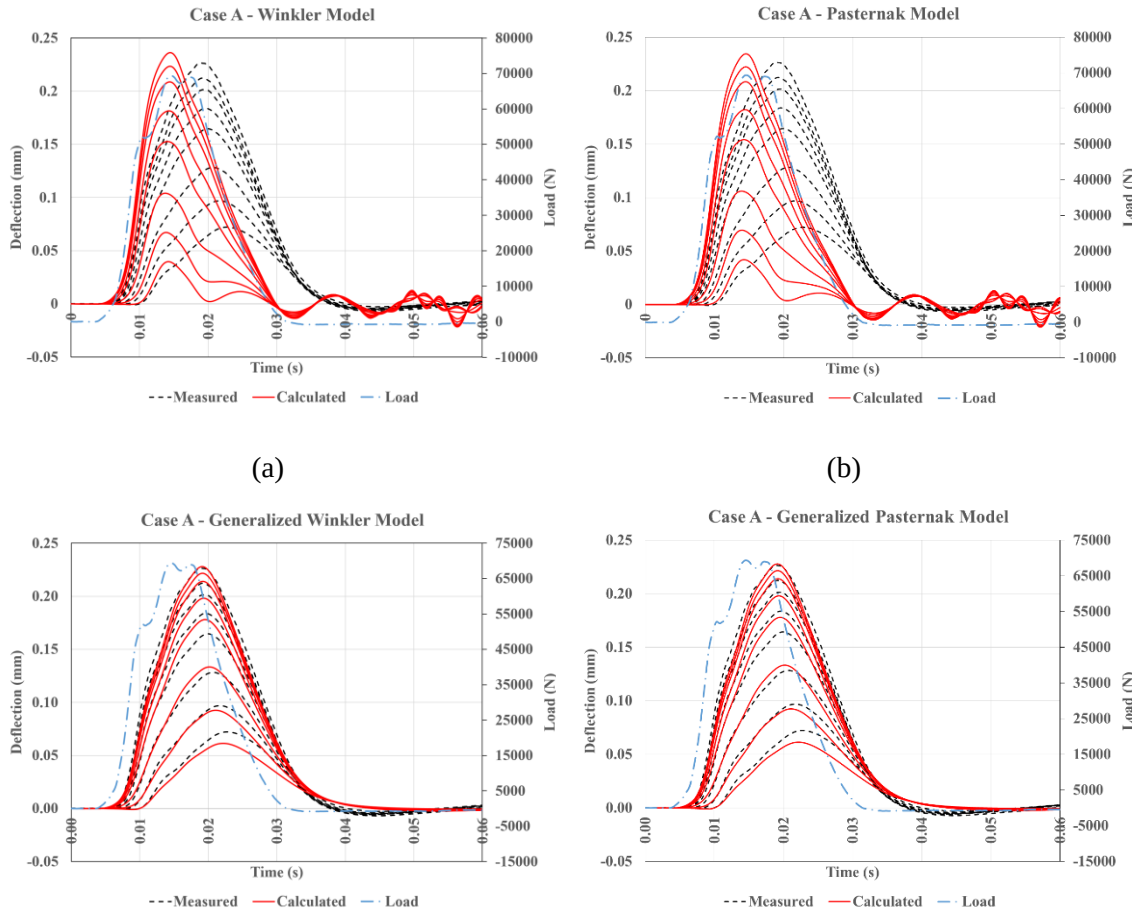

Figure 17. Measured and calculated FWD deflection basins for concrete section (Case A) modeled with (a) Winkler model, (b) Pasternak model, (c) generalized Winkler model, and (d) generalized Pasternak model

Based on the observations from Figure 17 and Figure 18, it can be clearly inferred that the idealization of the grade as an elastic and weightless medium is inaccurate when the structure is subjected to a dynamic load. However, the importance of accounting for the shear resistance of the subgrade requires a more detailed analysis. This was done by comparing backcalculation results for asphalt sections, Cases C and D, in multiple site visits.

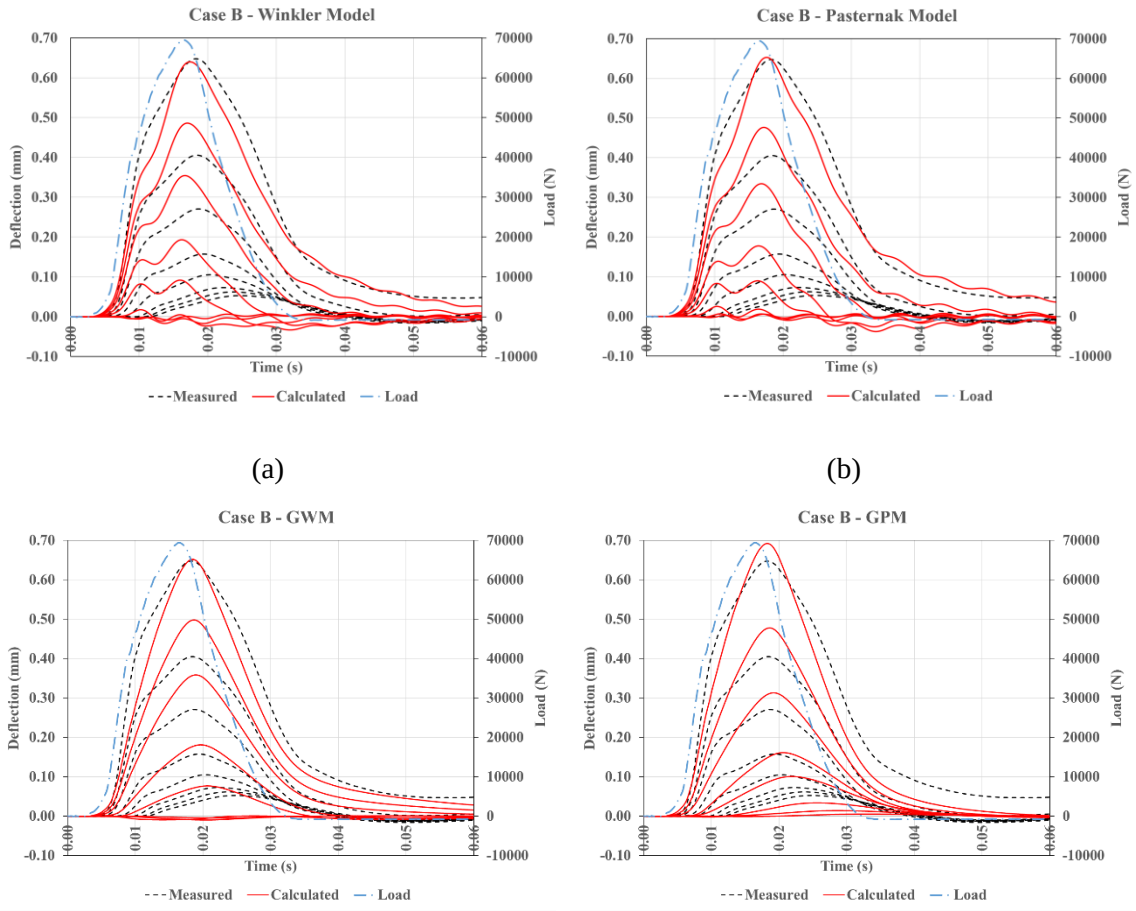

Figure 18. Measured and calculated FWD deflection basins for pavement section with thinner asphalt layer (Case B) modeled with (a) Winkler model, (b) Pasternak model, (c) generalized Winkler model, and (d) generalized Pasternak model

Case C is a pavement constructed with thicker asphalt layer (183 mm). Six FWD deflection data measured in one year were analyzed. Figure 19 presents the FWD-measured versus the GPM-calculated deflections in various months using the backcalculated model parameters listed in Table 7. A good fit for this pavement section is obtained regardless of the test temperature or season, and the various surface deformation profiles.

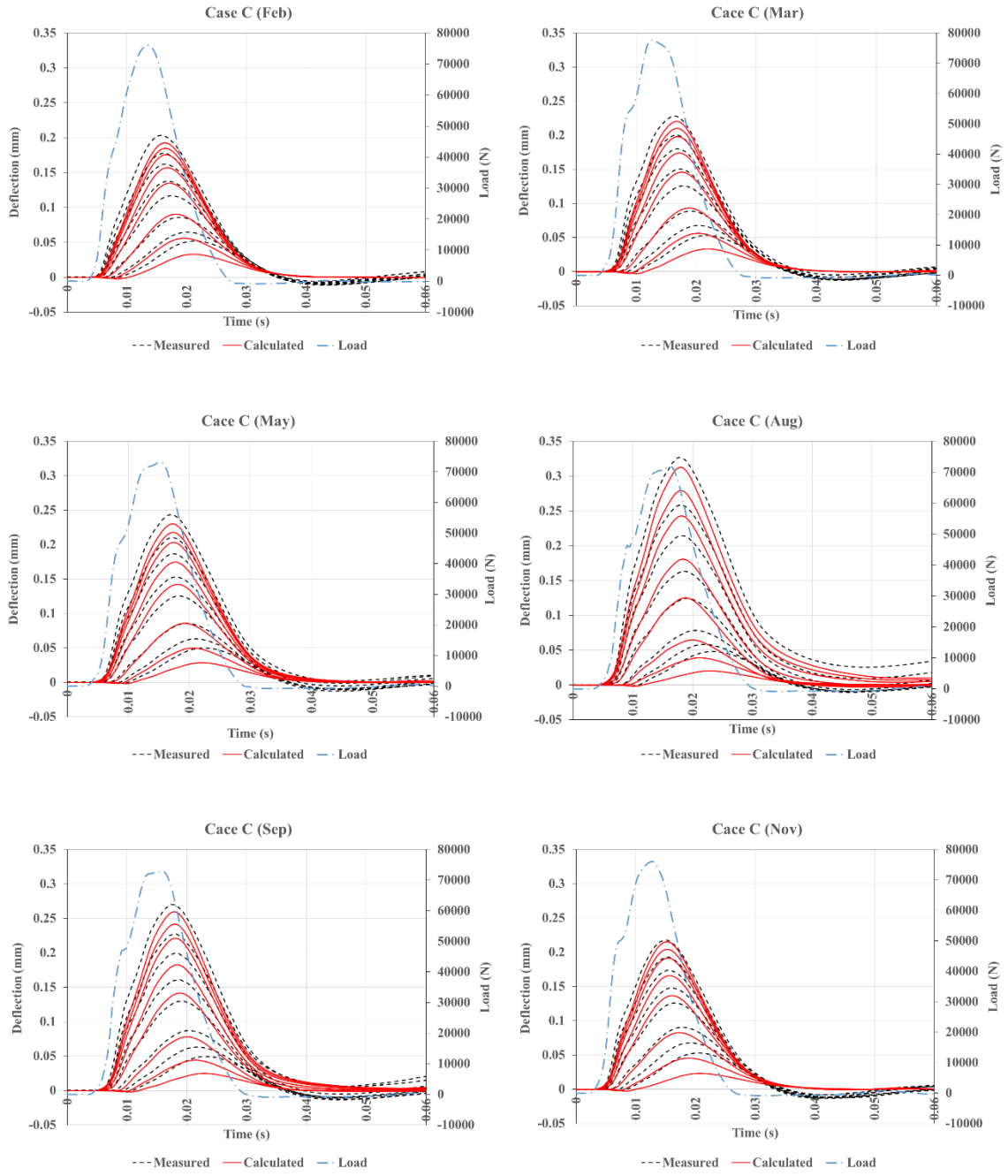

Figure 19. Measured and calculated FWD deflection basins for pavement section with thicker asphalt layer (Case C) at various months using generalized Pasternak model

Figure 20 illustrates a comparison between the match found for the warmest test temperature (34.9 ˚C) in the month of August using the GWM and GPM. Month of August

was selected because the largest difference in the error value between GWM and GPM predictions occurred at this field observation. The visual comparison of Figure 20a and Figure 20b indicates that a slightly better match for the deflections associated with the outer sensors can be obtained using the GPM. This observation is confirmed by the reduction of the error values listed in Table 7 (9.41 versus 4.79). Similarly, slight improvement of the error values was achieved by the addition of the shear parameter in the foundation model (GPM) during the warmer periods of the year for this pavement section (see Table 7).

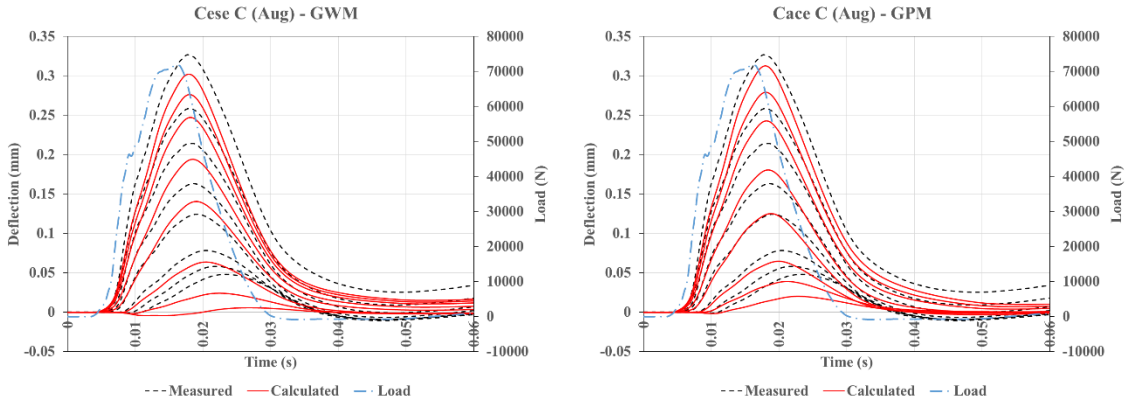

(a) (b)

Figure 20. Measured and calculated FWD deflection basins for pavement section with thicker asphalt layer (Case C) at high ambient temperature modeled with (a) generalized Winkler model, and (b) generalized Pasternak model

Similar seasonal study was performed for the asphalt section with a 0.071-m thick top layer, Case D. This test section is thinner compared to the Case C (0.071 m versus 0.183 m). The foundation models GWM and GPM were utilized to simulate the behavior of this pavement. Figure 21 shows the measured and simulated deflection time histories for the warmest month (March), coldest month (December), and the month of September (see Table 8). It can be observed that the GPM resulted in significantly better fit than that of the GWM. Similar improvement was observed for the FWD data obtained for other periods of the year. Analysis of the error values reported in Table 8 quantifies this considerable improvement (e.g. 3.47 versus 59.50 in the month of December).

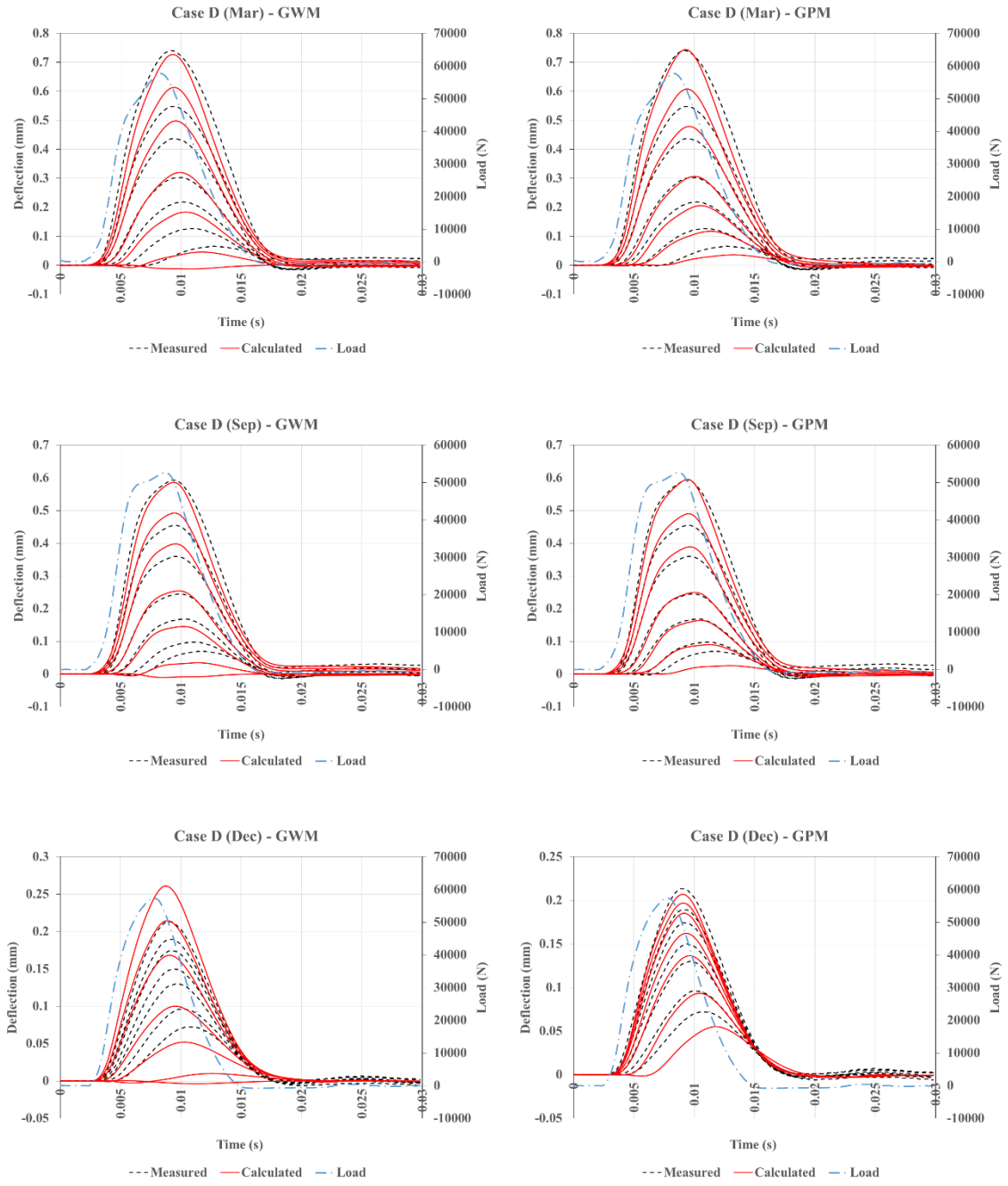

Figure 21. Comparison of the fits between measured and calculated FWD deflection basins for pavement section with thin asphalt layer (Case D) at various months using GWM and GPM

The collective visual comparison based on Figure 18, Figure 20, and Figure 21 suggests that the improvements made by GPM over GWM are greater when the top asphalt layer becomes thinner and more compliant (less rigid).

4.8. Discussion

The results of this study permitted evaluation of the following key issues regarding the analysis of the slab-on-grade subjected to a short-term loading:

- Accounting for the inertia and viscoelasticity
- Accounting for the shear resistance of the subgrade

The graphs presented in the previous section (Figure 17 and Figure 18) indicate that the elastic and weightless Winkler and Pasternak models are incapable of simulating the behavior of the slab-on-grade subject to short-duration dynamic loading. These foundation models fail to describe a time lag between the applied load and the resulting surface deflections. Ignoring the foundation inertia and damping terms from equation (4-1) leads to the fact that the only parameters that can originate a time lag between the excitation and the response of the system are the plate relaxation operator, $\tilde{R}$, and the mass of the plate. Inadequacy of these two parameters is especially clear from the analysis of the behavior of the concrete slab, for which the relaxation operator is reduced to the elastic constant. This explains why the peaks of the calculated deflections and the load for the concrete pavement occur roughly at the same time (see Figure 17). The presence of a time delay between the peak of the applied dynamic pressure and the surface deformation in FWD field measurements, as well as the notable differences in the tail behavior suggest that a proper slab-on-grade model must account for the inertia and viscoelastic behavior of the subgrade.

Both GPM and GWM resulted in a reasonably good fit between measured and simulated deflection basins for majority of the studied sections. This confirms the earlier findings in Chapter 2 of importance of inclusion of subgrade inertia and damping in describing the

behavior of a slab-on-grade subjected to a short-duration loading. Accounting for subgrade shear resistance also increased goodness of fit, but the degree of improvement varied.

It could be noted that the inclusion of the Pasternak's shear layer did not result in the improvement of goodness of fit for the concrete section, Case A, and a 183-mm thick asphalt section, Case C, when the test temperature is low. The presence of a stiff surface layer capable of distributing the load over a relatively wide area of subgrade diminishes the need to account for the subgrade shear resistance. Therefore, the GWM that models the subgrade using the independent viscoelastic elements reacting only to the applied vertical pressure is capable of adequately describing the subgrade support to the constructed layer. A support for the validity of this model is the close agreement between the average in-situ modulus of elasticity, E_{ave} = 19.13 GPa, measured through LTPP and the backcalculated modulus of elasticity of 18.14 GPa.

Asphalt is a temperature-dependent material. Its behavior becomes closer to elastic at low temperatures and almost viscous at relatively high temperatures. As can be seen from Table 7, when the surface temperature for Case C increased, the backcalculated stiffness of the asphalt layer decreased. In August, when the surface temperature was 34.9 ^{o}C, the initial stiffness of the asphalt layer was less than 20% of its initial stiffness in February when the surface temperature was 1.4 ^{o}C (see Table 7). As a result, the ability of the asphalt layer to distribute the load was reduced. Thus, accounting for the ability of the subgrade to redistribute the load becomes more important. As can be seen from Figure 20, the GPM led to an enhanced fit of the deflection profiles compared to the GWM. Moreover, the backcalculated foundation shear modulus, *G*, from the August testing was significantly higher than the shear moduli backcalculated for this section from the test results in May and September when the surface temperature was lower, but the backcalculated subgrade k-values were very similar. At the same time, the backacualted subgrade k-value for the GWM for August was much higher than that for May and September (143.59 kPa/mm vs 96.50 kPa/mm and 102.87 kPa/mm, respectively). The unrealistically high k-value for the

GWM is another indicator that the GPM is better suited for describing subgrade support for the asphalt layer than the GWM.

The analysis of the backcalculation results for the thinnest asphalt Case D suggests that accounting for the shear resistance of the subgrade is even more crucial for a thinner asphalt section. For the tests conducted for a wide range of surface temperatures, from 6.1 ^{o}C in December to 27.2 ^{o}C in March, the GPM resulted in much better fits than the GWM. Table 8 shows that for all tests the SSE for the GPM was less than half of the SSE for the GWM. More importantly, the initial stiffness backcalculated using the GPM is within the ranges expected for the asphalt material, while the initial stiffness backcalculated for the GWM is closer to what could be expected for portland cement concrete and is greater than the typical asphalt stiffnesses. The findings of an earlier study support this argument as well. *Von Quintus and Simpson* [2002] used the elastic layered approach to backcalculate the elastic moduli of this pavement section at different months. These elastic moduli were in close agreement with the values backcalculated with GPM (listed in Table 8).

In contrast to the observation made for Case C, the GWM model did not result in a good fit for Case D when the asphalt temperature was low. The backcalculation for the data collected in January and in December resulted in significantly greater improvements with the GPM over the GWM model for these months compared to the other months. A possible explanation of this phenomenon is that Case D is located in substantially colder climate (Wyoming) than Case C (Nevada). It is quite possible that the Case D aggregate base layer was frozen during the testing. This made the GWM model even less applicable for description of the base/subgrade behavior. The fact that the backcalculation with the GPM model for Case D for cold surface temperature resulted in a high foundation shear modulus and very high mass of the movable foundation supports this explanation.

Another observation of the backcalculation results for Case D is that the backcalculation with the GPM for the highest surface temperature resulted in a lower foundation shear

modulus for this section and weightless subgrade. One possible explanation for this different trend could be that the foundation behaves differently when it undergoes a frost season. Another possibility would be the well-known effect of non-uniqueness of the backcalculation solutions for interpreting of the FWD data [*Stolle and Hein*, 1989]. To investigate this phenomenon, two alternative sets of the GPM parameters were generated (using a different seed value) and the deflection time histories generated using these parameters were compared with the measured deflection time histories. These parameters and the corresponding SSEs are presented in Table 9. One can observe that even though the three deflection basins resulted in very similar error values, the two alternative basins resulted in a higher foundation shear modulus and subgrade weight. Therefore, interpretation of the FWD deflection basins should not rely solely on the evaluation of the goodness of fit, but engineering judgment should also be used.

One general drawback of the mechanical models, such as Winkler and Pasternak models, to describe the slab-on-grade structures is that the analyses are highly dependent on the selected system parameters which cannot be measured in the laboratories. However, this time-efficient semi-analytical approach and the developed backcalculation scheme provides a reliable tool to overcome this issue.

4.9. Conclusions

In this study, a generalized Pasternak model (GPM) was considered to simulate the problem of a thin viscoelastic slab-on-grade subjected to short-duration dynamic loading. The generalized Pasternak model accounts for damping and inertia effects, as well as the shear contribution of the foundation. The governing differential equation for this problem was solved in the time domain to avoid the need for high-frequency noise filtration. The obtained semi-analytical solution was used as the forward analysis to compute the slab deflections given the model parameters. An efficient and reliable inverse solution was developed and verified to backcalculate the model parameters by matching the model predicted deflections with the field-measured deflections.

In order to illustrate the importance of the shear parameter in the foundation model, a Case study was performed on four pavement sections constructed with concrete, thicker and thinner asphalt layers, and the collected FWD time histories were analyzed. The results of the performed analyses are summarized below.

- The traditional elastic weightless Winkler and Pasternak foundation models cannot describe the behavior of the slab-on-grade system under short-period dynamic loading.
- Viscoelastic behavior and inertial effects of grade must be accounted for.
- The agreement between the observed and calculated responses showed that the proposed viscoelastic slab-on- generalized Pasternak model is capable of simulating the behavior of thin slabs with various mechanical properties (very thin asphalt layer in high test temperature versus thicker concrete slabs).
- The use of a generalized Pasternak foundation resulted in reasonable model parameters.
- When the rigidity of the plate was relatively high (as was observed for the Sections of the concrete pavement and the pavement with a thicker top asphalt layer at cold temperatures), the Pasternak shear parameter was found to be zero. This observation indicates that the generalized Winkler model can adequately simulate the behavior of stiff elastic plates on grade.

Overall, this study demonstrates that, with minor additional computational efforts, the use of generalized Pasternak model offers a significant improvement in accuracy compared to the traditional elastic weightless Winkler and Pasternak model. The more reasonable backcalculated model parameters have implications for design and analysis purposes. These parameters could also be used as inputs for estimating the deflection-induced fuel consumption and pavement life cycle assessment.

5

Dynamic Analysis of Viscoelastic Plate on a Generalized Vlasov Foundation: Forward and Inverse Solutions

5.1. Summary

This chapter describes the slab-on-grade structure as a viscoelastic plate resting on a generalized Vlasov foundation. The Vlasov subgrade model leads to the same mathematical formulation as the Pasternak model, but the advantage of the Vlasov formulation is the association of the mechanical model parameters with the physical properties of the foundation soil. In this study, the Vlasov formulation is extended to account for the viscoelastic behavior of the system. A backcalculation procedure for determination of the Vlasov model parameters was developed by minimizing the quantified discrepancy between the field-measured deflections using falling weight deflectometer (FWD) and the model-calculated deflections. This procedure uses multiple seeding values for the sought properties to overcome the potential issue of non-uniqueness. The seeding values for the moduli of slab and grade are randomly generated following a normal distribution around the backcalculated moduli obtained from a static backcalculation program, BAKFAA. An analysis of field data is performed to evaluate the ability of the proposed forward- and inverse-solutions to describe the response of slab-on-grade systems. The results show that the generalized Vlasov model can simulate the behavior of slab-on-grade systems for a wide range of slab and grade properties and under several climatic conditions.

5.2. Introduction

In previous chapters, the mechanical-based foundation models were introduced. The related studies were noted, and the generalized Winkler model (GWM) and the generalized Pasternak model (GPM) were presented. Several pavement sections were studied to demonstrate the improvements made using the GPM. One of the drawbacks of the GPM is that although each additional parameter used to extend the Winkler foundation represents a particular physical behavior of the grade, e.g., mass parameter represents the foundation inertia effects observed in the field, these parameters are not directly dependent on the physical properties of the foundation materials. This interpretation seems to be justified if the objective is only to analyze the overall response of the structure. An example for such application would be the deflection-induced energy consumption evaluations due to pavement-vehicle interaction [*Louhghalam et al.,* 2013].

In Vlasov's approach, a continuum media is considered and then simplified by introducing assumptions and applying boundary conditions in line with the expected physical behavior. Vlasov's method analyzed a structure consisting of an elastic plate and a linear elastic isotropic foundation using a variational approach [*Vlasov and Leontiev,* 1966]. He assumed that the horizontal displacements in the foundation are negligible. Also, to simplify the three-dimensional problem, the decrease or variation of the vertical displacement with depth was assumed constant, following a function, $\phi(z)$. Interestingly, this approach led to the same governing differential equation as in the Pasternak's model. Vlasov was able to describe the pavement surface deformation if the soil properties including elastic modulus, Poisson's ratio, depth to the rigid layer, and $\phi(z)$, were given. This approach was attractive because it benefitted from the physical interpretations introduced by the continuum formulation as well as the simplicity of a mechanical model. Detailed description of this formulation is presented later.

Vlasov model parameters are highly dependent on the assumed displacement profile, $\phi(z)$. Vlasov suggested that this shape function follows an exponential decay but did not give a precise value for the rate of decrease of the displacement with depth of the grade, γ; instead,

he recommended a range depending on the type of the soil [*Vallabhan and Das*, 1988]. *Jones and Xenophontos* [1977] strengthened the Vlasov model by approaching the problem of slab-on-an-elastic-grade through a different variational principle. The advantage of the modified formulation was that it yielded a rigorous theoretical basis for the shape of the vertical deformation profile. They concluded that the Pasternak parameters, *k* and *G*, are functions of load and shape of loading, soil properties, and, interestingly, the flexural rigidity of the plate.

Vallabhan and Das [1988] included γ as the third parameter involved in the model for a beam resting on elastic foundation. Because the three variables are interdependent and unique for a given problem of beam-on-an-elastic-foundation, they developed a simple iterative procedure to determine these parameters. This method was improved by solving the governing differential equation with making use of finite difference method [*Vallabhan and Das*, 1991]. The iterative procedure allowed for obtaining an automatic consistent value for γ. The results were then compared to the more exact finite element solution and good agreement was observed. Similar to the findings by *Jones & Xenophontos* [1977], *Vallabhan and Das* [1991] pointed out that the Pasternak parameters depend on the depth of the soil, loading distribution, stiffness of the soil, and also stiffness of the beam/slab. Therefore, these values are not unique for a certain type of soil.

Ayvaz et al. [1998] and *Daloglu et al.* [1999] investigated the effects of the subsoil depth and the plate dimensions on the dynamic response of plates resting on an elastic foundation subjected to both uniformly distributed load and concentrated load at the center of the plates. *Ayvaz and Ozgan* [2002] analyzed the effects of the subsoil depth, the beam length, their ratio, and the value of γ within the subsoil on the frequency parameters of beams on elastic foundations. *Daloglu and Ozgan* [2004] determined the affected subsoil depth from the load on the plate resting on elastic foundation using stress distribution within the subsoil that will occur depending on the loading and dimension of the plate. In a recent study, *Teodoru and Musat* [2010] compared the predictions of the Vlasov model with a 2D finite element analysis for a beam subjected to static pressure. They emphasized the superiority

of the Vlasov formulation over the classic Winkler foundation, and pointed out that the estimations made by the Vlasov model are relatively conservative but reasonably close to those from more sophisticated finite element solutions. Many other relevant studies can be found in the literature [*Turhan*, 1992; *Liang and Zhu*, 1995, 1998; *Vallabhan and Daloglu*, 1999, *Matsunaga*, 2000; *Celik and Omurtag*, 2005; *Ayvaz and Oguzhan*, 2008; *Worku*, 2010; *Worku and Degu*, 2010; *Ozgan and Daloglu*, 2009, 2014; *Ozgan*, 2012, 2013; *Dimitrovová*, 2016, 2017].

Regardless of the numerical and analytical improvements suggested for various applications, very few studies evaluated the validity of this foundation model using field and experimental observations. This is even more of an issue when the structure is subjected to a dynamic excitation. As noted in previous chapters, accounting for the foundation inertia forces and the damping effects is substantially important when dynamic analysis of the slab-on-grade is the topic of interest. Whence, the Vlasov model has to be modified accordingly to account for such effects.

In comparison with the mechanical models such as the generalized Pasternak model, one potential concern associated with the Vlasov formulation is the interdependence of the model parameters: k, G, and m. Because these parameters are functions of the material properties, the optimization schemes cannot freely alter these variables in the process of the parameter identification through multiple iterations. Such material-enforced constraints on the variables search domain may lead to a poor correlation between the model predictions and the experimental observations.

In this study, a viscoelastic plate resting on a generalized Vlasov foundation is considered. The generalized Vlasov model (GVM) accounts for the effects of inertia and damping of the soil. A forward-solution in the time-domain for an infinite plate resting on a Vlasov foundation and subjected to a short-duration impulse is developed and verified. Then, a gradient-based backcalculation scheme that takes advantage of the static backcalculation

results as guidelines for the seeding values, is introduced and validated. Finally, an analysis of the falling weight deflectometer (FWD) deflection data is performed to evaluate the ability of the proposed forward- and inverse-solutions to describe the response of slab-on-grade systems. The focus of this field study is to find answers to two main questions: 1) if the Vlasov formulation and the associated material-enforced limitations on the inverse-solution can result in an acceptable agreement between the model-calculated and field-measured responses, and 2) if the backcalculated material properties are reasonable.

5.3. Formulation

The Vlasov approach to foundation modeling, the assumptions used, and the modifications made to generalize this model for a viscoelastic slab-on-viscoelastic grade subjected to axisymmetric dynamic excitation are described here.

Vlasov Foundation

Consider a semi-infinite three-dimensional linear elastic soil medium with a finite depth, H, to an incompressible rigid layer. The soil medium has a modulus of elasticity, E_s, and a Poisson's ratio, ν_s, and is subjected to an arbitrary static pressure (Figure 22). The total strain energy in this system can be written as

$$\Pi = \Pi_s + V \tag{5-1}$$

where

Π_s = the strain energy stored in the soil, and
V = the potential energy of the external loads.

Based on the principles of continuum mechanics, we have

$$\Pi_s = \frac{1}{2}\int_0^H \int_{-\infty}^{+\infty} \int_{-\infty}^{+\infty} \sigma_{ij}\epsilon_{ij}\,dx\,dy\,dz \tag{5-2}$$

where i and j denote directions x, y, and z, and,

$$V = -\int_{\Omega} q(x,y)w(x,y,0)dxdy \tag{5-3}$$

where

σ	=	stress in the soil medium
ϵ	=	strain in the soil medium
w	=	the vertical displacement
q	=	the applied distributed loads, and
Ω	=	domain of the applied loads.

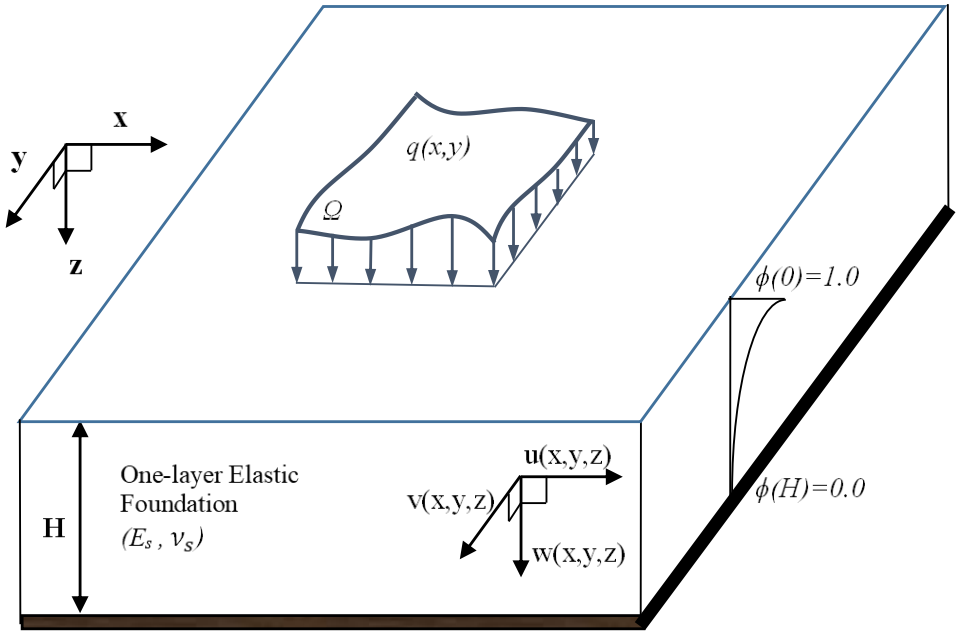

Figure 22. One-layer elastic foundation with finite depth subjected to an arbitrary static pressure

Since the horizontal displacements, $u(x,y,z)$ and $v(x,y,z)$, in the foundation are significantly smaller compared to the vertical displacement, $w(x,y,z)$, when subjected to a vertical load, and following *Vlasov and Leontiev* [1966], we can assume that horizontal displacements are negligible. To simplify this three-dimensional problem, the decrease or variation of the vertical displacement with depth is assumed constant, following a function,

$\phi(z)$, in the z-direction as illustrated in Figure 22. This function is defined so that $\phi(0)$ equals 1.0 and $\phi(H)$ is equal to 0.0. Therefore, the deformations in the foundation are [*Vlasov and Leontiev*, 1966]

$$u(x,y,z) = 0 \tag{5-4}$$

$$v(x,y,z) = 0$$

$$w(x,y,z) = w(x,y)\phi(z)$$

where

$w(x,y)$ = vertical displacement on the foundation surface, and
$\phi(z)$ = variation of vertical displacement in the z-direction.

Next, the strain in all directions can be computed as follows.

$$\epsilon_x = \frac{\partial u}{\partial x} = 0 \tag{5-5}$$

$$\epsilon_y = \frac{\partial v}{\partial y} = 0$$

$$\epsilon_z = \frac{\partial w}{\partial z} = \frac{\partial \phi}{\partial z} w(x,y)$$

$$\gamma_{xy} = \frac{\partial u}{\partial x} + \frac{\partial v}{\partial y} = 0$$

$$\gamma_{xz} = \frac{\partial u}{\partial z} + \frac{\partial w}{\partial x} = \frac{\partial w(x,y)}{\partial x}\phi(z)$$

$$\gamma_{yz} = \frac{\partial v}{\partial z} + \frac{\partial w}{\partial y} = \frac{\partial w(x,y)}{\partial y}\phi(z)$$

From the stress-strain constitutive relationship for a linearly elastic, isotropic, and homogenous medium we have

$$\sigma_{ij} = \lambda \epsilon_{kk} \delta_{ij} + \mu \epsilon_{ij} \tag{5-6}$$

where

$$\lambda = \frac{E_0 \nu_0}{1 - \nu_0^2}$$

$$\mu = \frac{E_0}{2(1 + \nu_0)}$$

$$E_0 = \frac{E_s}{1 - \nu_s^2}$$

$$\nu_0 = \frac{\nu_s}{1 - \nu_s}$$

E_s = elastic modulus of soil medium

ν_s = Poisson's ratio of soil medium

Plugging in the strain values using equation (5-5), the normal and shear stresses in the foundation can be expressed as

$$\sigma_x = \sigma_y = \frac{E_0 \nu_0}{1 - \nu_0^2} w(x,y) \frac{\partial \phi}{\partial z} \tag{5-7}$$

$$\sigma_z = \frac{E_0}{1 - \nu_0^2} w(x,y) \frac{\partial \phi}{\partial z}$$

$$\tau_{xz} = \frac{E_0}{2(1 + \nu_0)} \frac{\partial w(x,y)}{\partial x} \phi(z)$$

$$\tau_{yz} = \frac{E_0}{2(1 + \nu_0)} \frac{\partial w(x,y)}{\partial y} \phi(z)$$

$$\tau_{xy} = 0$$

Substituting the expressions for the strains, equation (5-5), and the stresses, equation (5-7), into equation (5-2) results in the simplified equation below for the stored strain energy in the soil [*Vlasov and Leontiev*, 1966].

$$\Pi_s = \frac{1}{2}\int_0^H \int_{-\infty}^{+\infty} \int_{-\infty}^{+\infty} \left(\frac{E_0}{1-\nu_0^2} (\frac{\partial \phi}{\partial z})^2 w^2(x,y) + \frac{E_0}{2(1+\nu_0\ )} \phi^2(z) (\nabla w(x,y))^2 \right) dxdydz \tag{5-8}$$

The introduction of the following constants

$$k = \frac{E_0}{1-\nu_0^2} \int_0^H (\frac{d\phi}{dz})^2\, dz \tag{5-9}$$

and

$$G = \frac{E_0}{2(1+\nu_0)} \int_0^H \phi(z)^2\, dz \tag{5-10}$$

reshapes equation (5-8) into the following expression:

$$\Pi_s = \frac{1}{2}\int_{\Omega} (kw^2(x,y) + G(\nabla w(x,y))^2) dxdy \tag{5-11}$$

Application of the variational principles to equation (5-1), and minimizing the total potential energy by taking variations in $w(x,y)$ and $\phi(z)$ lead to [*Vlasov and Leontiev*, 1966; *Turhan*, 1992]:

$$kw(x,y) - G\nabla^2 w(x,y) = q(x,y) \tag{5-12}$$

A variety of options are available for the proper shape of the function $\phi(z)$, but the following is most widely used in the literature as it was shown that it is able to capture the realistic behavior of the soil with a good accuracy [*Vlasov and Leontiev*, 1966]. In this study, this shape function is employed as well.

$$\phi(z) = \frac{sinh[\gamma(H-z)]}{sinh(\gamma H)} \tag{5-13}$$

As required by the Vlasov's assumptions (see Figure 5.1), this function takes a value of zero if $z = H$ and a value of one when $z = 0$ (i.e., at the surface of the foundation). γ is the coefficient determining the rate of decrease of the vertical displacement with depth of the foundation.

Elastic Plate Resting on a Vlasov Foundation Subjected to a Dynamic Axisymmetric Circular Load

Consider an infinite, homogeneous, isotropic, and linearly elastic Kirchhoff-Love plate resting on an elastic foundation. The differential equation for the response of such plate to a dynamic circular load is expressed below [*Vlasov and Leontiev*, 1966].

$$D\nabla^4 w(r,t) = p(r,t) - q(r,t) - m_p \frac{\partial^2 w(r,t)}{\partial t^2} \tag{5-14}$$

By virtue of the axial symmetry, the plate deflections, $w = w(r,t)$, are independent of the polar coordinate angle, θ, and depend solely on the distance r from the center of the circular pressure, and the time, *t*. The Laplacian of w becomes $\nabla^2 = \frac{1}{r}\frac{\partial}{\partial r} + \frac{\partial^2}{\partial r^2}$. The term $(-m_p \frac{\partial^2 w(r,t)}{\partial t^2})$ is related to the inertial forces acting upon the plate elements, where m_p is the unit mass of the plate, and $D = Eh^3/12(1-\nu^2)$ is the plate's instantaneous flexural stiffness. *E*, *h*, and *v* are instantaneous modulus of elasticity, thickness, and Poisson's ratio of the plate, respectively. $p(r,t)$ is the time-dependent applied pressure which can be presented as $p(r,t) = \frac{P}{\pi a^2} H(r-a)g(t)$ where *P* is the maximum total applied load, *a* is the radius of the circular contact area, $H(r)$ is the Heaviside function to indicate that the plate is unloaded for $r > a$, and $g(t)$ is an arbitrary function of time that represents the change of pressure with respect to time, *t*.

Using the similar principles of variational energy explained earlier and taking into account the inertia of the elastic foundation, the reaction of the elastic foundation to the applied dynamic pressure, $q(r,t)$, can be formulated as

$$kw(r,t) - G\nabla^2 w(r,t) + m_f \frac{\partial^2 w(r,t)}{\partial t^2} = q(x,y) \tag{5-15}$$

where m_f is the inertial mass of the elastic foundation that can be expressed as

$$m_f = m_s \int_0^H \phi(z)^2 \, dz \tag{5-16}$$

where m_s is the unit mass of the foundation soil [*Vlasov and Leontiev*, 1966].

Since the slab is modeled as Kirchhoff-Love plate, and assuming that full-bonding exists at the layers interface, the vertical deformations of the plate are equal to the surface deformations of the elastic foundation. Hence, the plate differential equation of the system, equation (5-14), can be re-written as

$$D\nabla^4 w(r,t) + kw(r,t) - G\nabla^2 w(r,t) + m\frac{\partial^2 w(r,t)}{\partial t^2} = p(r,t) \tag{5-17}$$

where $m = m_p + m_f$.

Viscoelastic Plate Resting on a Generalized Vlasov Foundation Subjected to a Dynamic Axisymmetric Circular Load

Let us assume that both the plate and the foundation are composed of isotropic homogenous linear viscoelastic material with a constant Poisson's ratio. The principles of viscoelasticity indicate that the stress-strain relationships in equation (5-6) for the foundation can be re-written as

$$\sigma_{ij}(t) = \frac{\lambda}{E_0} \int_{\tau=0}^{t} E_0(t-\tau)\, d\epsilon_{kk}(t)\delta_{ij} + \frac{\mu}{E_0} \int_{\tau=0}^{t} E_0(t-\tau)\, d\epsilon_{ij}(t) \tag{5-18}$$

where $E(t)$ is the uniaxial linear viscoelastic relaxation function. Having the definition of $E(t)$, it is a matter of a mathematical transformation to find the equivalent complex

modulus $E^*(\omega)$ for a given loading frequency [*Das*, 2014; *Varma*, 2015]. This value is used as a primary input for design purposes in the pavement industry. In this study, the focus is on the $E(t)$, as the computation is performed in the time domain. We know that $E(t)$ can be reformulated as

$$E(t) = E_0(\tilde{I} - \tilde{R}(t)) \tag{5-19}$$

in which $\tilde{R}(t)$ is the associated relaxation function, and $\tilde{I}$ is the identity operator. The same constitutive relationships hold true for the plate viscoelasticity. Thus, two relaxation functions are required to describe the system of a viscoelastic plate resting on a viscoelastic Vlasov foundation. Therefore, for a viscoelastic plate on a viscoelastic Vlasov foundation we have

$$\widetilde{D}\nabla^4 w(r,t) + \tilde{k}w(r,t) - \tilde{G}\nabla^2 w(r,t) + m\frac{\partial^2 w(r,t)}{\partial t^2} = p(r,t) \tag{5-20}$$

wherein

$$\widetilde{D} = D(\tilde{I} - \tilde{R}_p(t))$$

$$\tilde{k} = k\left(\tilde{I} - \tilde{R}_s(t)\right) = \frac{E_0\left(\tilde{I} - \tilde{R}_s(t)\right)}{1-\nu_0^2}\int_0^H \left(\frac{d\phi}{dz}\right)^2 dz$$

$$\tilde{G} = G\left(\tilde{I} - \tilde{R}_s(t)\right) = \frac{E_0\left(\tilde{I} - \tilde{R}_s(t)\right)}{2(1+\nu_0)}\int_0^H \phi(z)^2\, dz$$

Here, $\tilde{R}_p$ is the relaxation function of the plate; $\tilde{R}_s$ is the relaxation function of the soil which would be the same for both $\tilde{k}$ and $\tilde{G}$.

Various models are available for the relaxation function such as Maxwell, Kelvin-Voigt, standard linear solid, and generalized Maxwell model, or in the form of sigmoid, or Prony series can be mentioned among others [*Das*, 2014]. As illustrated in Figure 23 in this study the three-parameter standard linear solid (SLS) model was used to describe the viscoelastic behavior for both the plate and the foundation. This model is selected based on a preliminary study done by the author to find a simple viscoelastic model that can sufficiently describe the behavior of both the plate and the foundation. *Zhang et al.* [2014]

suggested the same viscoelastic model for simulating the soil medium. *Liang and Zhu* [1998] made use of the three-parameter viscoelastic model to emulate the HMA.

The stress-strain relationship (constitutive equation) of the SLS model indicates that the unitless relaxation functions for viscoelastic plate and viscoelastic foundation, $\tilde{R}_1$ and $\tilde{R}_2$, can be expressed as:

$$\tilde{R}_p\epsilon(t) = \frac{1}{\tau_p}\left(1 - \frac{E_{1p}}{\left(E_{1p} + E_{2p}\right)}\right)\int_0^t e^{\frac{(t-x)}{-\tau_p}}\epsilon(x)dx \tag{5-21}$$

$$\tilde{R}_s\epsilon(t) = \frac{1}{\tau_s}\left(1 - \frac{E_{1s}}{(E_{1s} + E_{2s})}\right)\int_0^t e^{\frac{(t-x)}{-\tau_s}}\epsilon(x)dx \tag{5-22}$$

where E_1 and E_2 are two stiffness parameters of the SLS model (see inset of Figure 23). Then, the instantaneous modulus of elasticity of the plate is $E = E_1 + E_2$. In addition, η (see Figure 23) is the material viscosity parameter, and therefore, $\tau = \eta/E_2$ is the associated relaxation time for the viscoelastic material. The detailed steps for deriving equations (5-21) and (5-22) can be found in Chapter 2.

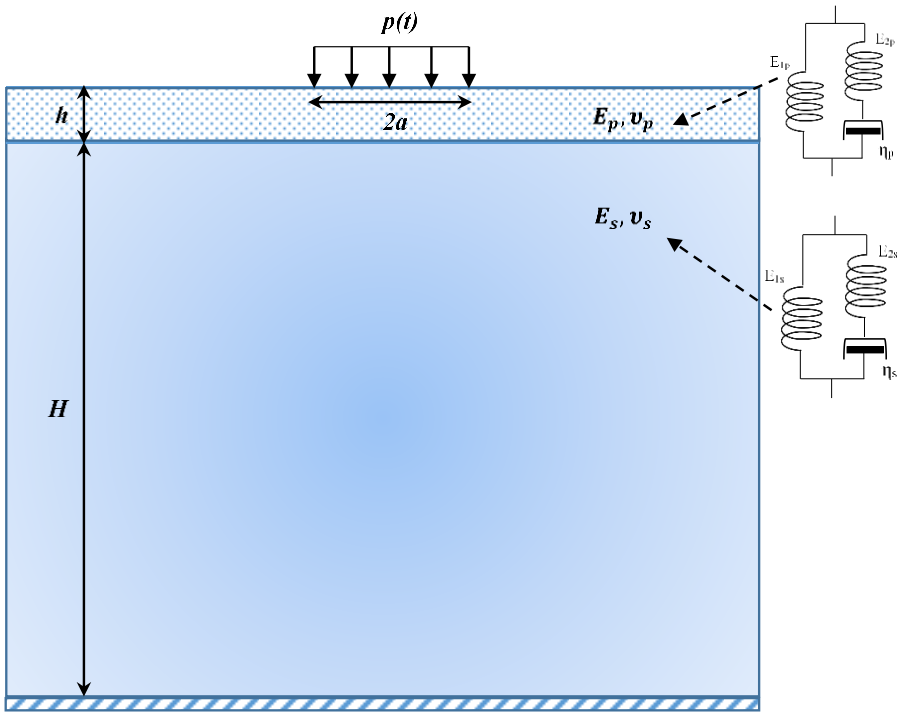

Figure 23. Viscoelastic plate resting on a generalized Vlasov foundation

To summarize, the inputs needed to describe the viscoelastic plate are: $E_p, E_{1p}, \tau_p, h, \nu_p, m_p$.

Similarly, the generalized Vlasov model requires the following properties: $E_s, E_{1s}, \tau_s, H, \gamma, \nu_s, m_s$.

5.4. Forward Analysis

Here, we approach the problem by transforming the physical parameters into a non-dimensional domain. The governing differential equation (5-20), can be re-written in a non-dimensional form:

$$\left(\tilde{I} - \tilde{R}_p\right)\nabla^4 w^* + \left(\tilde{I} - \tilde{R}_s\right)w^* - \left(\tilde{I} - \tilde{R}_s\right)G^*\nabla^2 w^* + m^*\frac{\partial^2 w^*}{\partial t^{*2}} = p^* \qquad (5\text{-}23)$$

The terms with asterisk represent the non-dimensional variables defined as $t^* = 2\pi\frac{t}{T}$; $w^* = w^*(s,t^*) = \frac{kl^2}{P}w(r,t)$; $p^* = p^*(s,t^*) = \frac{l^2}{P}p(r,t)$; $G^* = \frac{G}{kl^2}$; $m^* = (\frac{2\pi}{T})^2\frac{m}{k}$; where l is the radius of relative stiffness, defined as $l = \sqrt[4]{\frac{D}{k}}$; s is the nondimensional distance from the center of the applied load, defined as $s = \frac{r}{l}$; and *T* is the loading duration of the applied dynamic pressure.

The non-dimensional governing differential equation (5-23) is solved in three stages: I) the application of Hankel transform in space, II) finite difference method in time, and III) the application of inverse Hankel transform in space. In this approach, first, the zero order Hankel transform is applied with respect to the space variable, *s*. The zero order Hankel transform of a function, *f(s)*, is defined as:

$$(H_0 f)(\alpha) = \int_0^\infty s f(s) J_0(\alpha \cdot s) ds \tag{5-24}$$

where J_0 is the zero order Bessel function, and α is a parameter of the Hankel transform. An application of the zero Hankel transform to Equation (5-23) gives

$$\alpha^4\left(\tilde{I} - \tilde{R}_p\right) W^* + \left(\tilde{I} - \tilde{R}_s\right) W^* + \alpha^2\left(\tilde{I} - \tilde{R}_s\right) G^* W^* + m^* \frac{\partial^2 W^*}{\partial {t^*}^2} = \frac{J_1(\alpha a_l)}{\pi a_l \alpha} g(t^*) \tag{5-25}$$

where $W^* = W^*(\alpha, t^*)$ is the nondimensional Hankel transformed surface deflection, a_l = *a/l*, and J_1 is the Bessel function of order one.

The Hankel transformed system can then be numerically solved for $W^*(\alpha, t^*)$ by means of finite difference scheme. In this connection, the time scale is first discretized into evenly spaced intervals: $t_i^* = i\Delta t^* (i = 0..N)$. Next, the first and second derivatives in time at each time step are approximated using the central-difference formula of order $O(h^2)$.

$$\frac{\partial {W^*}_i}{\partial t^*} \approx \frac{{W^*}_{i+1} - {W^*}_{i-1}}{2\Delta t^*} \tag{5-26}$$

$$\frac{\partial^2 W_i^*}{\partial t^{*2}} \approx \frac{W_{i+1}^* - 2W_i^* + W_{i-1}^*}{\Delta t^{*2}} \tag{5-27}$$

A recursive form is derived at by substituting equations (5-26) and (5-27) into equation (5-25). After rearrangement we have:

$$\begin{aligned} W_{i+1}^* = \frac{1}{m^*}\big[&\alpha^4 \Delta t^{*2} S^*{}_{p_i} + (1 + \alpha^2 G^*)\Delta t^{*2} S^*{}_{s_i} \\ &+ \big(2m^* - (1 + \alpha^2 G^* + \alpha^4)\Delta t^{*2}\big) W_i^* - m^* W_{i-1}^* + \Delta t^{*2} F_i\big] \end{aligned} \tag{5-28}$$

wherein $F_i = \frac{J_1(\alpha a_l)}{\pi a_l \alpha} g(t_i^*)$; $S^*{}_{p_i}$ and $S^*{}_{s_i}$ are the memory terms holding the viscoelastic information of the plate and soil, respectively, from the beginning. From equations (5-21) and (5-22), the definition of these terms can be derived using the trapezoidal rule as stated below.

$$\begin{aligned} S^*{}_i = \widetilde{R} W_i^* = \frac{E_2}{\tau^* E} \sum_{j=1}^{i} \Bigg[\Bigg(&exp\left(\frac{t_i^* - t_j^*}{-\tau^*}\right) W_j^* \\ &+ exp\left(\frac{t_i^* - t_{j-1}^*}{-\tau^*}\right) W_{j-1}^* \Bigg) \left(\frac{t_j^* - t_{j-1}^*}{2}\right) \Bigg] \end{aligned} \tag{5-29}$$

The assumption that the system is at rest at time $t^* = 0$, introduces the following two initial conditions which are equivalent to annulling any initial plate displacement or velocity. This allows for solving the recursive equation (5-29).

$$W^*(\alpha, 0) = 0 \tag{5-30}$$

$$\frac{\partial W^*(\alpha, t^*)}{\partial t^*}\Big|_{t^*=0} = 0 \tag{5-31}$$

Next, the obtained $W^*(\alpha, t^*)$ for each value of α is transferred back to the nondimensional space using the inverse zero order Hankel transform, defined as:

$$w^*(s, t^*) = \int_0^\infty W^*(\alpha, t^*) J_0(\alpha s) \alpha d\alpha \tag{5-32}$$

Finally, the obtained nondimensional values, $w^*(s,t^*)$, are converted back into dimensional term, $w(r,t)$, using the following equation:

$$w(r,t) = \frac{P}{kl^2} w^*(s,t^*) \tag{5-33}$$

As mentioned in previous chapters, performing this analysis in the time domain eliminates the potential problems associated with the use of frequency domain [*Uzan*, 1994a; *Chatti*, 2004; *Zaabar et al.*, 2014].

Stability of Solution

The mentioned numerical approach entails a source of numerical instability due to the discretization in time, which impacts the inverse zero order Hankel transform that follows equation (5-32). More specifically, because Δt is finite, the solution to the plate differential equation becomes numerically unstable, and the scheme diverges for α values larger than some critical value α_{cr}. At $\alpha = \alpha_{cr}$ the solution oscillates between positive and negative values, i.e., the value of the response, w, jumps from positive to negative in between calculation steps. These oscillations are magnified for $\alpha > \alpha_{cr}$.

As means of quantifying this situation, the oscillating condition can be formulated as: $-W_{i+1}^* = W_i^* = -W_{i-1}^*$ with W_i^* representing some arbitrary oscillation magnitude at time t_i^*. When this condition is imposed on the recursive equation (5-28), the following equation is formed from which α_{cr} may be computed:

$$\begin{aligned} W_i^*\left[4m^* - (1 + \alpha_{cr}^2 G^* + \alpha_{cr}^4)\Delta t^{*2}\right] + \Delta t^{*2} F_i \\ + \Delta t^{*2}\left[\alpha_{cr}^4 {S^*}_{p_i} + (1 + \alpha_{cr}^2 G^*){S^*}_{s_i}\right] = 0 \end{aligned} \tag{5-34}$$

In this equation, the first, second, and third terms are associated to the elastic properties, external excitation, and viscous properties of the loaded structure. This shows that α_{cr} depends on the system properties, the history, as well as the external loading. As an example of a simpler case, consider the calculation for an elastic system beyond which $F_i =$

0, i.e., after the applied pressure is removed. Since the second and third terms in equation (5-34) are zero, a closed-form expression for α_{cr} transpires:

$$\alpha_{cr}^{e} = \frac{1}{2\Delta t^{*2}}\left(\sqrt{(G^{*}-4)\Delta t^{*4} + 16m^{*}\Delta t^{*2}} - G^{*}\Delta t^{*2}\right) \tag{5-35}$$

For a given choice of Δt^{*} this equation identifies the upper (finite) integration value for performing the inverse zero order Hankel transform, i.e., from zero to α_{cr}^{e} (superscript e denotes the elastic condition) instead of zero to infinity. Obviously, as expected, α_{cr}^{e} approaches infinity when Δt^{*} approaches zero. Also, by requiring a positive value in the parentheses in equation (5-34), this expression gives guidance to the selection of Δt:

$$4m \gg k\Delta t^{2} \rightarrow \Delta t \ll \sqrt{\frac{4m}{k}} \tag{5-36}$$

Solving for α_{cr} for a general case in equation (5-34) demonstrates that $\alpha_{cr} > \alpha_{cr}^{e}$. Nonetheless, the proposed calculation of α_{cr} provides the stability condition required for this numerical approach.

Verification

The forward analysis was implemented into a Fortran program, and the explained stability requirements were included. In order to verify the numerical analysis, it is compared with an analytical solution for an elastic system subjected to a circular sinusoidal pressure. Consider the Hankel transformed equation (5-25) with no relaxation operator, as the plate-foundation system is assumed elastic; also, let us define the time variation of the applied load as $g(t) = \frac{1}{2}(1-\cos(t))$ for $0 < t < T$ and $g(t) = 0$ for $t > T$. Equation (5-25) then becomes:

$$\alpha^{4}W^{*} + W^{*} + \alpha^{2}G^{*}W^{*} + m^{*}\frac{\partial^{2}W^{*}}{\partial t^{*2}} = \frac{J_{1}(\alpha a_{l})}{\pi a_{l}\alpha}g(t^{*}) \tag{5-37}$$

This equation can be solved mathematically, which leads to a solution containing the first-order Bessel function, J_1, and two unknown coefficients. Imposing the initial conditions for the at-rest state, as noted in equations (5-30) and (5-31), leads to a closed-form solution for the period $0 < t < T$. For the post-loading period, $t > T$, the continuity of the plate suggests the following two initial conditions:

$$W^*_{unload}(\alpha, T^{*+}) = W^*_{load}(\alpha, T^{*-}) \tag{5-38}$$

$$\frac{\partial W^*_{unload}(\alpha, t^*)}{\partial t^*}|_{t^*=T^{*+}} = \frac{\partial W^*_{load}(\alpha, t^*)}{\partial t^*}|_{t^*=T^{*-}} \tag{5-39}$$

Thus, another closed-form solution is obtained for the post-loading state (free vibration) of the plate. These equations were solved using the Mathematica program. In the interest of brevity and due to the length of these mathematical solutions, they are not included in the text.

Next, the obtained $W^*(\alpha, t^*)$ for each value of α is transferred back to the nondimensional, and then dimensional space following equations (5-32) and (5-33). This semi-analytical solution is compared here with the numerical solution proposed for the viscoelastic system subjected to an arbitrary dynamic circular load.

The slab-on-grade system simulated here has the following properties:

Plate properties: $E_p = 30.0\ GPa, \nu_p = 0.15, SG_p = 2.20, h = 0.18\ m,\ m_p = 396 \frac{Kg}{m^2}$ (SG stands for specific gravity of the material)

Foundation properties: $E_s = 100.0\ MPa, \nu_s = 0.35, SG_s = 1.70, H = 3.0\ m$

Loading Configuration: $P = 60\ KN, T = 0.03\ s, a = 0.15\ m.$

A comparison of the numerical and closed-form solutions for the same foundation with four γ-value is presented in Figure 24. The profiles shown are the deflections of the plate at $r = 0.0\ m$, i.e., at the center of the loading. The corresponding foundation parameters for the selected γ-values are listed here to demonstrate the sensitivity of the system response to this Vlasov parameter.

$$\gamma = 0.25 \rightarrow k = 53.84 \frac{KPa}{mm}, G = 34.47\ MPa, \frac{m_f}{m_p} = 4.00, l = 0.73\ m$$

$$\gamma = 1.00 \rightarrow k = 83.04 \frac{KPa}{mm}, G = 18.06\ MPa, \frac{m_f}{m_p} = 2.09, l = 0.65\ m$$

$$\gamma = 2.00 \rightarrow k = 160.52 \frac{KPa}{mm}, G = 9.26\ MPa, \frac{m_f}{m_p} = 1.07, l = 0.55\ m$$

$$\gamma = 4.00 \rightarrow k = 320.99 \frac{KPa}{mm}, G = 4.63\ MPa, \frac{m_f}{m_p} = 0.54, l = 0.46\ m$$

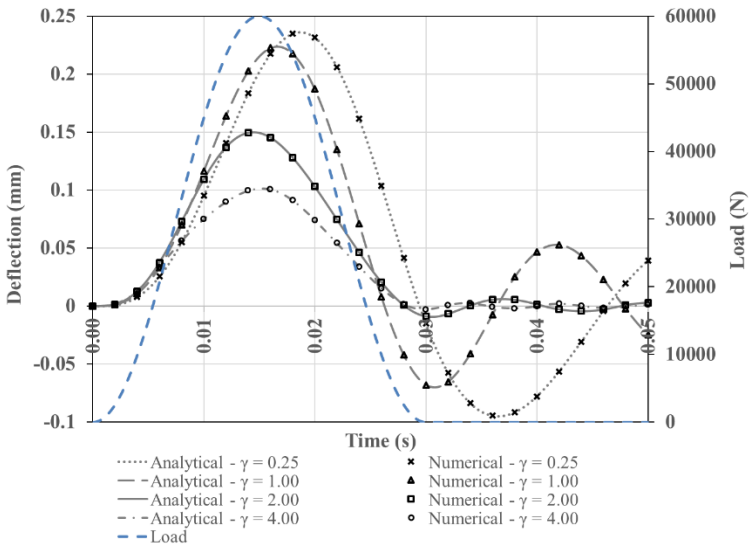

Figure 24. Verification of the numerical solution for an elastic plate on elastic vlasov foundation with different γ

The perfect match between the numerical and the semi-analytical solutions, shown in Figure 24, validates the accuracy of this numerical approach for the elastic system.

To verify that the viscoelastic behavior of the plate is properly implemented, the same slab-on-grade system used for verification of the numerical solution (Figure 24) is simulated here. In this simulation, the foundation is assumed elastic with $\gamma = 0.25$; the plate is viscoelastic with the following properties: $E_{1p} = 3\ GPa, E_{2p} = 27\ GPa$, while the relaxation time of the plate, τ_p, varies. The responses of the system to the same sinusoidal impact load employed in Figure 24 were generated for various values of relaxation time (Figure 25).

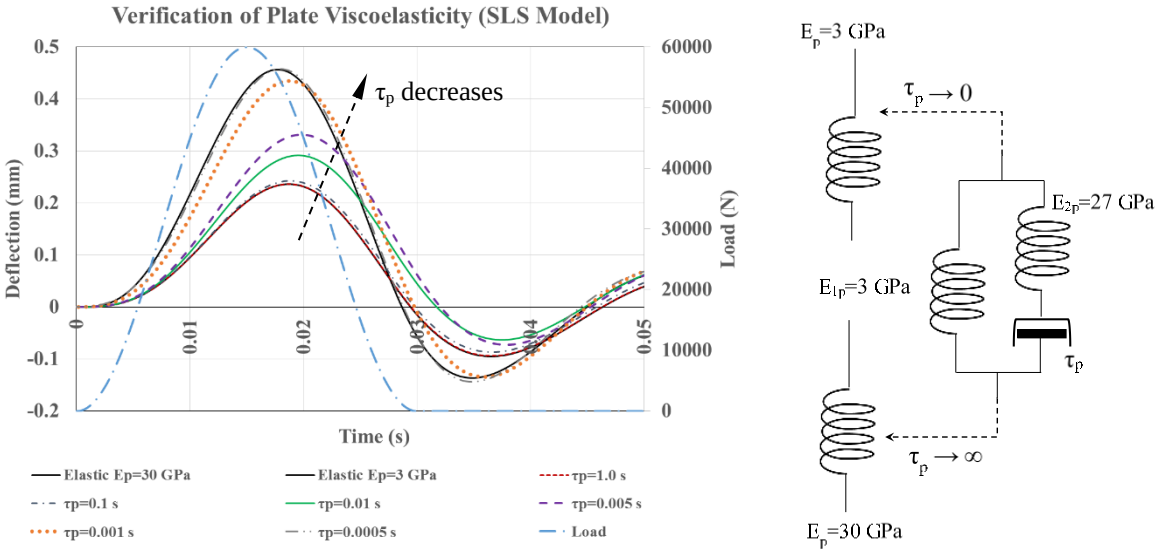

Figure 25. Comparison of the response for elastic plates with response for viscoelastic plates with various viscosities subjected to a dynamic load

The extreme case responses are related to the elastic behavior with $E_p = E_{1p} = 3\ GPa$ when τ_p approaches zero, and the elastic behavior with $E_p = E_{1p} + E_{2p} = 30\ GPa$ when τ_p approaches infinity. The surface deflections for the two elastic limit cases were computed using the obtained semi-analytical solutions. Figure 25 shows that, in line with the expectation, the numerical solutions for the slab-on-grade systems incorporating viscoelastic slabs were enclosed by the solutions for the elastic limit cases.

Similar investigation must be done regarding the viscoelastic modeling of the foundation. Again, the same slab-on-grade system and impact load are used here as in Figure 24. The plate is assumed elastic with $E_p = 30\ GPa$; for the viscoelastic foundation $\gamma = 0.25, E_{1s} = 30\ MPa, E_{2s} = 70\ MPa$, while the foundation relaxation time, τ_s, varies. As can be seen in Figure 26, the behavior of the viscoelastic foundation is encased by the two elastic extremes, which is in line with our expectation.

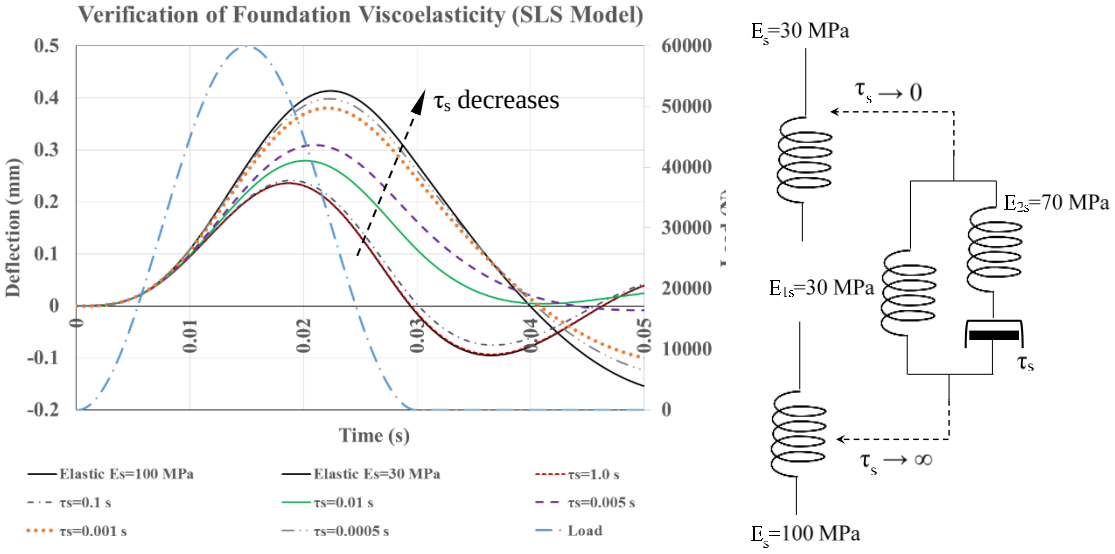

Figure 26. Comparison of the response for elastic foundation with response for viscoelastic foundation with various viscosities subjected to a dynamic load

In short, the observations made in Figure 25 and Figure 26 verify the proper implementation of the relaxation operators, $\tilde{R}_p$ and $\tilde{R}_s$, in the numerical solution for the viscoelastic plate-on-generalized Vlasov foundation.

5.5. Inverse Analysis (Backcalculation)

With adequate interpretation of the responses to the applied dynamic loads of the FWD device two objectives can be achieved: 1) evaluating the ability of the generalized Vlasov

model to describe the behavior of a slab-on-grade system, and 2) finding the sought proper inputs for a desired slab-on-grade structure.

In the inverse problem at hand, the loading mechanism and its characteristics are provided by the FWD test device. The inputs for the structure are $h, \nu_p, m_p, \nu_s, m_s$. The Poisson's ratios can be taken into account as additional variables; however, assuming that the value of the Poisson's ratio is known and constant does not result in serious errors [*Uzan*, 1994a; *Von Quintus and Simpson*, 2002] while the advantage is the reduction of the computational efforts. The FWD provides the loading plate radius, *a*, the loading duration, *T*, the location of the sensors, and the time histories of the applied pressure and surface deflections at the location of each sensor, all of which are required for the backcalculation. Therefore, the sought parameters are $E_p, E_{1p}, \tau_p, E_s, E_{1s}, \tau_s, H,$ and γ. The flow chart for the computation procedure is presented in Figure 27 which explains the inverse steps required to find these parameters.

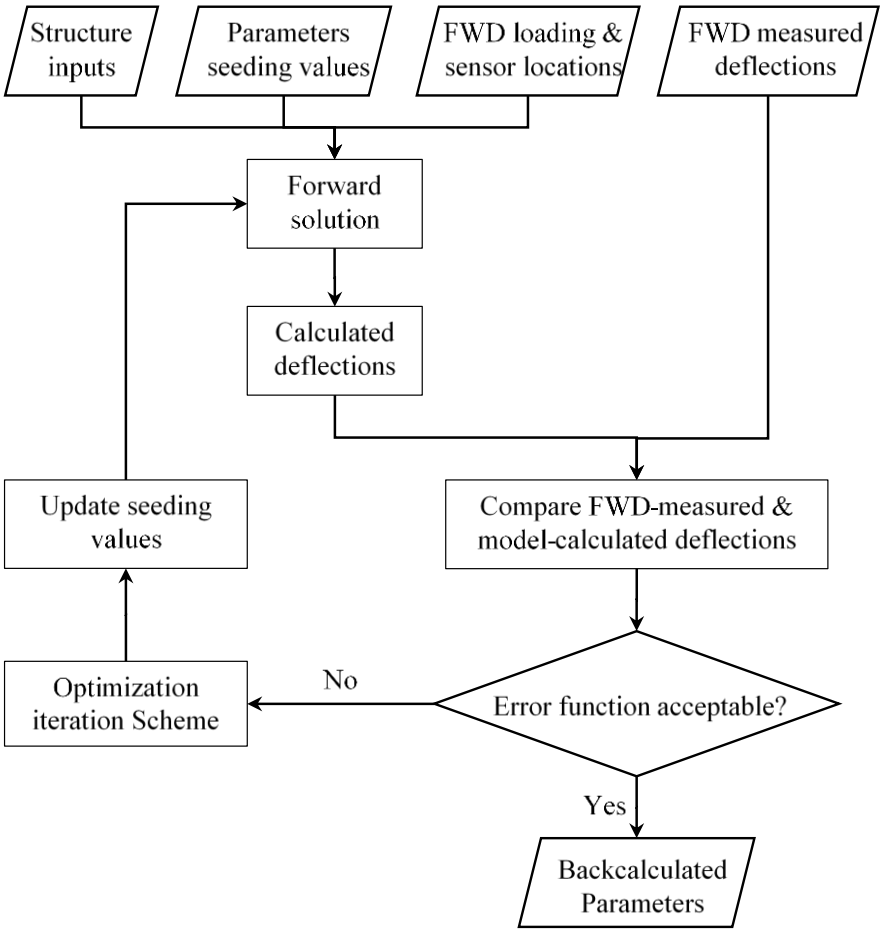

Figure 27. Flow chart for inverse solution (backcalculation)

The parameter identification procedure involves the minimization of an objective function that represents the error between the calculated and measured responses through iteration. The error function used in this study is defined as the normalized sum of squared errors (SSE) normalized by the maximum recorded deflection:

$$SSE = \sum_{i=1}^{n}\sum_{j=1}^{m}\left(\frac{w_{ij}^{M} - w_{ij}^{C}}{w_{max}^{M}}\right)^2 \tag{5-40}$$

where n is the number of sensors, m is the number of time steps, w_{max}^{M} is the maximum measured deflection in the FWD deflection history, and w_{ij}^{M} and w_{ij}^{C} are the FWD-measured and model-calculated deflection for sensor i at time j, respectively. Further

analysis of equation (5-36) indicates that the time step smaller than 0.00015 s would be sufficient for stability requirements for typical pavements. FWDs usually record values in step size equal to 0.0001s and 0.0002s. If required by the user, a splitting function is implemented in the program to reduce the time step of the FWD measurements, and to interpolate the measurements for smaller time steps.

As noted in Figure 27, an optimization procedure is required to indicate the updated seeding values, and recalculate the system responses and the corresponding error. This procedure repeats and the parameters are updated until the numerical error becomes acceptable. In essence, the precision of a backcalculation analysis is sensitive to type and coverage of the pavement response analysis, and the selected error function. Nevertheless, the efficiency is affected by the optimization methodology employed in the inverse analysis. Therefore, in order to enhance the performance of the backcalculation procedure, it is vital to use an optimization technique that overcomes the inherent problem of local minimums while also being fast and precise [*Goktepe et al.*, 2006]. Previous researchers have made use of different techniques such as linear least squares, gradient descent, Newton-Raphson, and Gauss-Newton methods, as well as pattern searching method, and genetic algorithm [*Von Quintus et al.*, 2015].

The optimization scheme employed in this study uses the well-established quasi-Newton method [*Dennis and Schnabel*, 1996] and an active set strategy [*Gill and Murray*, 1976] to solve a minimization problem subject to simple bounds on the variables [*IMSL*, 1994]. Also, the logarithmic scale is applied to the parameters $E_p, E_{1p}, \tau_p, E_s, E_{1s},$ and τ_s for improving the numerical stability.

Selection of Seeding Values

To address a problem of multiple local minimums of the error function, multiple heuristically selected seeding values are used in this backcalculation scheme. The approach for selection of seeding value made the use of a static backcalculation technique. In this study, we employ the backcalculation software developed by Federal Aviation Agency

(FAA) named BAKFAA [*BAKFAA*, 2012]. In this software, the forward solution is based on the layered elastic principles, in which the system is treated as a stratum of multiple isotropic homogenous elastic layers. The software provides two options for the interface condition of the layers: I) fully bonded, and II) unbonded. Each layer has its particular elastic modulus, E, Poisson's ratio, ν, and thickness, h. In this study, in virtue of resemblance between the two models, i.e., the slab-on-grade and the layered elastic models, the sections analyzed by BAKFAA are set to be composed of two layers: I) the plate (or the surface layer), and II) the infinite subgrade. The boundary condition between the two layers is assumed fully bonded.

Deflection basin is a term used for the peaks of the deflection profiles recorded by each sensor plotted against the radial distance of the sensor location with respect to the center of FWD loading plate. Since the static backcalculation is used in the BAKFAA, only the deflection basins are required as inputs from the FWD measurements. The elastic moduli of the two layers can be statically backcalculated, given the ν and h. Next, the achieved statically backcalculated moduli are used to generate the seeding values for E_p and E_s for the dynamic backcalculation. For further clarification, this methodology is explained through the following example.

Consider the two arbitrary pavement sections in Table 10 with similar subgrade and different surface layers comprised of hot mix asphalt (HMA) and Portland cement concrete (PCC). The PCC section is assumed elastic while the HMA section is assumed viscoelastic, i.e., values are assigned to E_{1p}/E_p and τ_p in the SLS model. Using the validated forward analyses explained earlier, the responses of these pavement sections to a synthetic sinusoidal FWD load with a peak load of 60 KN and a duration of 0.03 s are computed. In this example, FWD sensors are located at typical distances of 0.0, 0.2, 0.3, 0.45, 0.6, 0.9, and 1.5 m away from the center of loading. These synthetic data were then employed to backcalculate the layers moduli using the BAKFAA. The results of this static backcalculation are listed in Table 10. Figure 28 compares the synthetic and the BAKFAA-backcalculated deflections basins for these two arbitrary pavement sections.

Table 10. Pavement properties for the arbitrary HMA and PCC sections, and backcalculated pavement properties using BAKFAA

Case	Foundation Parameters					Plate Parameters			
	E_s	γ	H	E_{1s}/E_s	τ_s	E_p	E_{1p}/E_p	τ_p	ν_p
	MPa	-	m	-	s	GPa	-	ms	-
PCC-Synthetic	100.0	1.00	3.00	0.30	0.003	30.00	-	-	0.15
HMA-Synthetic	100.0	1.00	3.00	0.30	0.003	6.00	0.30	2.00	0.35
PCC-BAKFAA	89.1	-	-	-	-	27.05	-	-	0.15
HMA-BAKFAA	63.1	-	-	-	-	2.20	-	-	0.35

- Note: for both pavements, $h = 0.18\,m, \nu_s = 0.35, SG_p = 2.20, SG_s = 1.70$

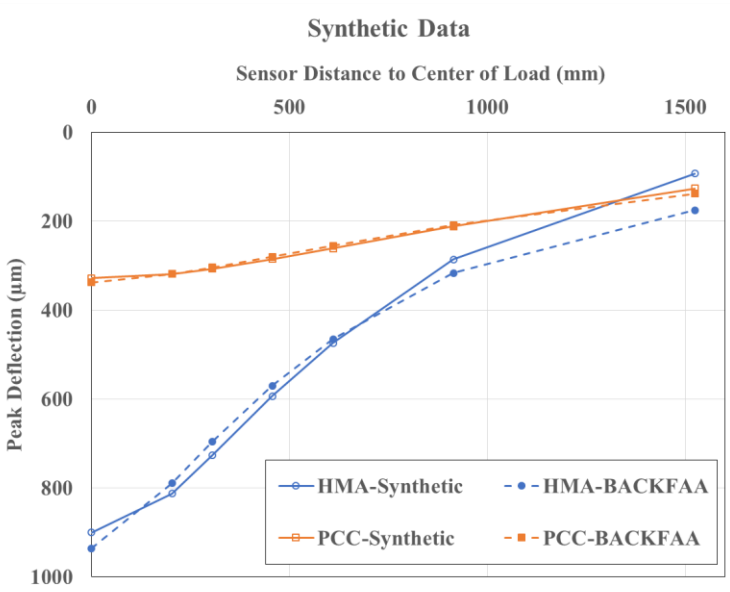

Figure 28. Synthetic deflection basins generated with the dynamic forward-solution versus statically-backcalculated deflection basins

The static backcalculation resulted in the elastic moduli for both HMA and PCC pavements reasonably close to the input values of the dynamic forward analyses. Conducting the same comparison on a variety of synthetic deflection basins led to similar observations. Therefore, the static backcalculation may be used as a guideline to achieve a starting point closer to the objective, instead of relying on a completely random number. In the backcalculation procedure developed here, the seeding values for the moduli follow a normal distribution with the mean equal to the modulus backcalculated by BAKFAA, and a variance specified by the user.

Relationships between Vlasov and Pasternak Foundation Model Parameters

The sought properties in the Vlasov foundation are: $E_s, E_{1s}, \tau_s, H,$ and γ. Based on equation (5-20), these variables manifest their influence in the differential equation of the slab-on-grade as $k, G, m_f, \tilde{R}_s$. The relationship between these parameters are examined here.

Consider the following two integrations, and their closed-form solutions.

$$\chi(\gamma, H) = \int_0^H \phi'^2(z)dz = \frac{\gamma}{4} csch^2(\gamma H)[2\gamma H + sinh(2\gamma H)] \quad (5\text{-}41)$$

$$\Psi(\gamma, H) = \int_0^H \phi^2(z)dz = \frac{1}{2\gamma}[coth(\gamma H) - \gamma H csch^2(\gamma H)] \quad (5\text{-}42)$$

Equation (5-20) indicates that $k = k(E_s, \upsilon_s, \chi)$, $G = G(E_s, \upsilon_s, \Psi)$, and $m_f = m_f(m_s, \Psi)$. Since χ and Ψ are dependent on γ and H, let us first take a look at the variation of $\phi(z)$ with the change in γ and H. Figure 29 demonstrates that when γ approaches zero $\phi(z) = 1 - \frac{z}{H}$, which describes a linear decrease of displacement with depth. Also, based on the comparison of these graphs for various depths to rigid layer, H, one can conclude that for each value of γ, there exists a value of H beyond which the shape and magnitude of $\phi(z)$ do not change. For instance, when $\gamma = 1.50$, for any $H > 2.37\ m$, $\phi(z)$ is exactly the same regardless of the value of H.

This observation suggests that for any γ there exists a value of H beyond which the two functions χ and Ψ do not vary, as depicted in Figure 30. Therefore, it is important to constrain the H for each selected γ to avoid the seeding value for H falling in the plateau region in the process of minimization as any change in H does not result in the change in the error function. This must be done to avoid the optimization scheme making the wrong assumption that the error function is insensitive to H.

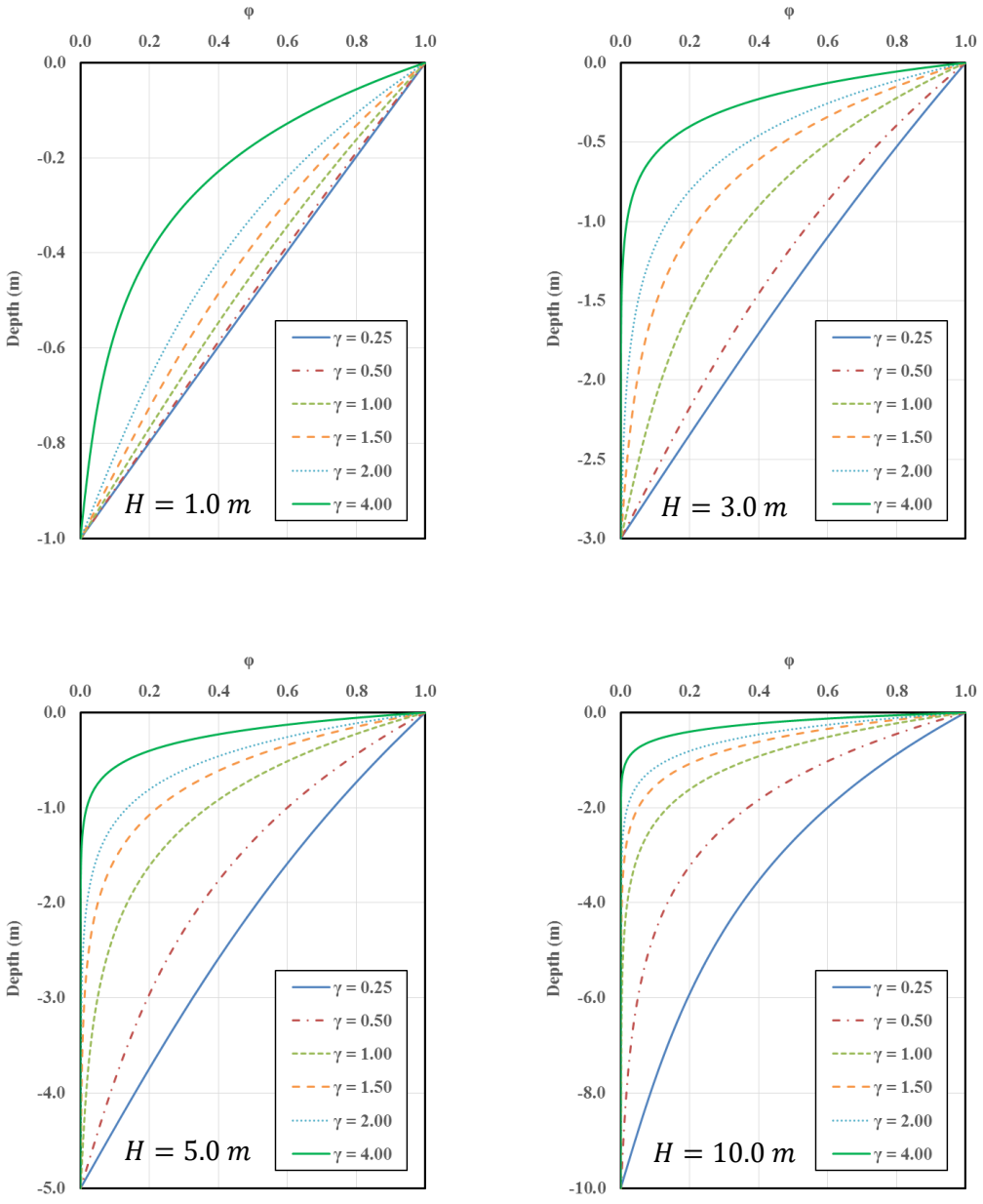

Figure 29. Variation of $\boldsymbol{\phi}$ with respect to $\boldsymbol{\gamma}$ for different depth to rigid layers

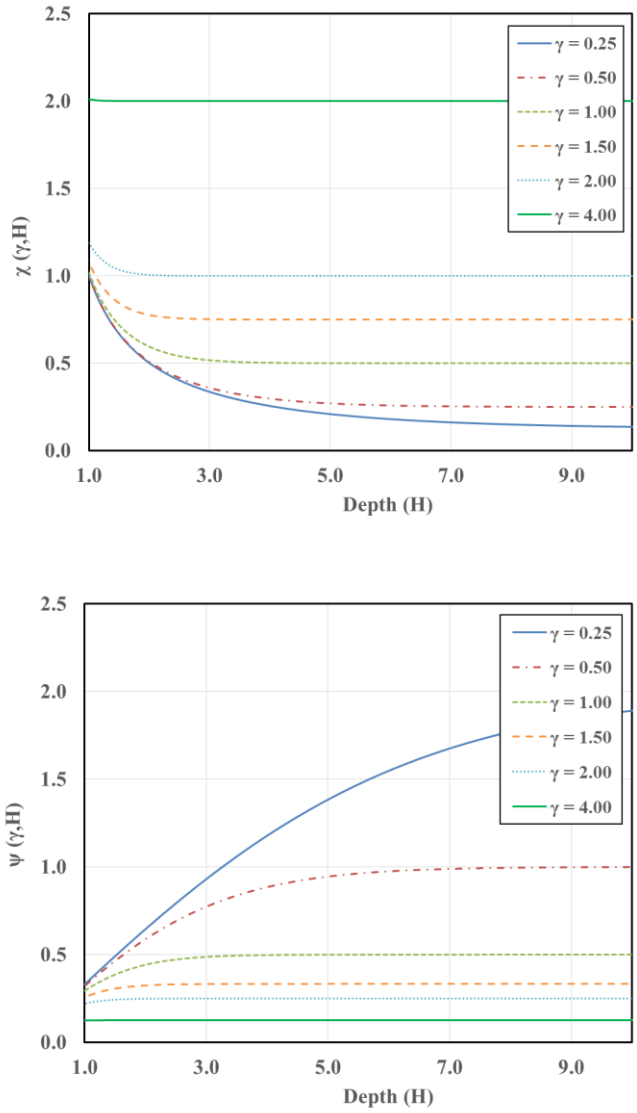

Figure 30. Variation of $\boldsymbol{\chi}$ and $\boldsymbol{\Psi}$ with respect to $\boldsymbol{H}$ for different $\boldsymbol{\gamma}$

Another interesting observation can be made on the relationship between functions χ and Ψ. Figure 31 illustrates this relationship for various values of γ and H. As can be seen, when the deformation dissipates quickly, i.e., $\gamma \to \infty$, the value of χ increases, while the approach of γ to zero leads to larger values of Ψ. Moreover, this plot indicates that χ and Ψ are nonlinearly disproportional, i.e., large values of χ and Ψ do not happen simultaneously.

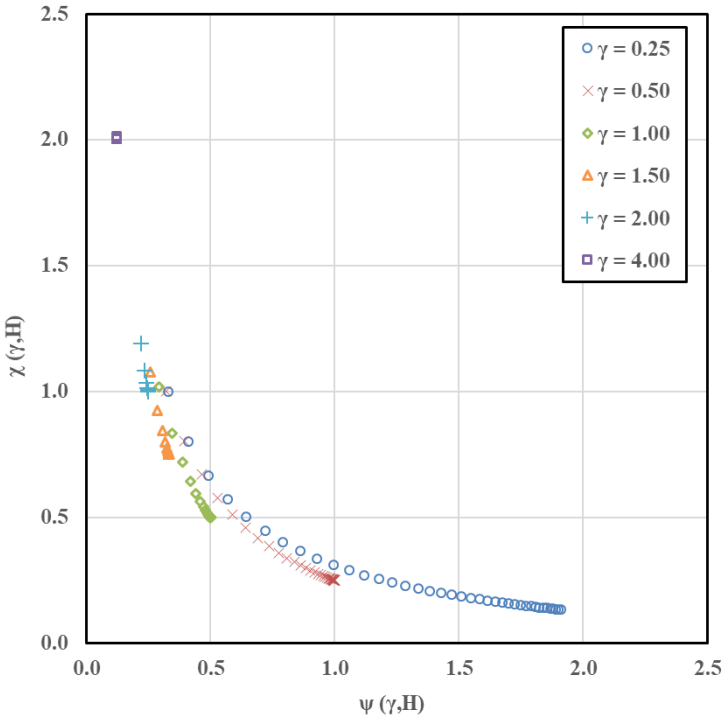

Figure 31. Relationship between $\boldsymbol{\chi}$ and $\boldsymbol{\Psi}$ for a factorial of $\boldsymbol{H}$ and $\boldsymbol{\gamma}$

Because of the explained correlation between of χ and Ψ, the model parameters k, G and m_f have similar relationship for any given E_s and υ_s. This statement is transformed into a plot in Figure 32 in which a factorial of γ and H is used to generate the points on the plot. We can see that the domain in which the optimization searches to find the solution for k and G is limited compared to that of the Pasternak model in which k, G and m_f are independent model parameters. We can also infer that when the foundation takes a high value of k, the two parameters G and m_f take smaller values and vice versa.

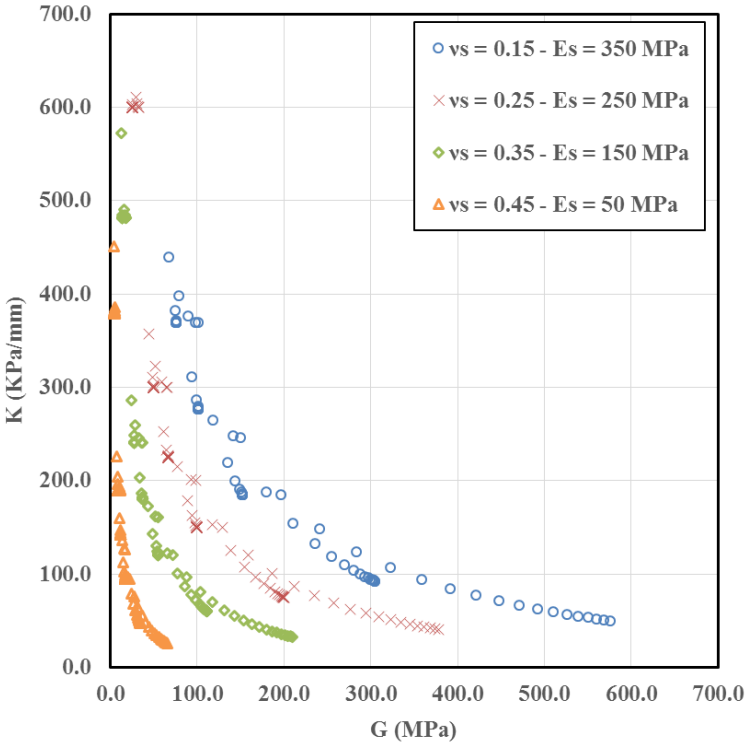

Figure 32. Example of a search domain for Vlasov foundation parameters: $\boldsymbol{k}$ and $\boldsymbol{G}$

Validation

In this study, laboratory testing of pavement materials was not performed to validate the dynamic backcalculation results due to the following reasons: I) it is not feasible to ensure that the laboratory testing conditions are similar to the in-situ situations including the loading frequency and material confined conditions used during field FWD testing; II) the sample preparation from field involves coring and sawing which are destructive for test roads and costly. Therefore, rather than using the laboratory validation, a theoretical validation procedure is used.

The theoretical validation is conducted by considering nonexistent pavement sections that can represent a variety of pavements including HMA and PCC layers with various stiffnesses and thicknesses resting on foundations with various properties. The responses of these sections to a time-varying FWD load are computed using the proposed forward solution, and named as “synthetic data”. Next, the backcalculation routine is performed on

the synthetic data to find the sought model parameters. The true parameters are then compared with the backcalculated parameters to evaluate the accuracy of the backcalculation procedure.

Unknown Depth to Rigid Layer

Consider the two synthetic pavement sections introduced in Table 10. The backcalculation is performed on the synthetic data for these two sections. First, the ability of the employed optimization technique is evaluated by displaying the convergence of the error function in Figure 33. We can see that for the selected random seedings in these examples, the error function converges to very small values in about 100 iterations. The steps witnessed in this graph are related to the iterations at which the optimization procedure makes decision on the search direction. Of course, other optimization techniques can be used to reduce the number of iterations, but because of the extremely efficient forward solution employed in this procedure, the computational cost of this backcalculation technique is acceptable. If needed, with the use of the parallel processing technology and the other available backcalculation techniques, the computational cost can be reduced.

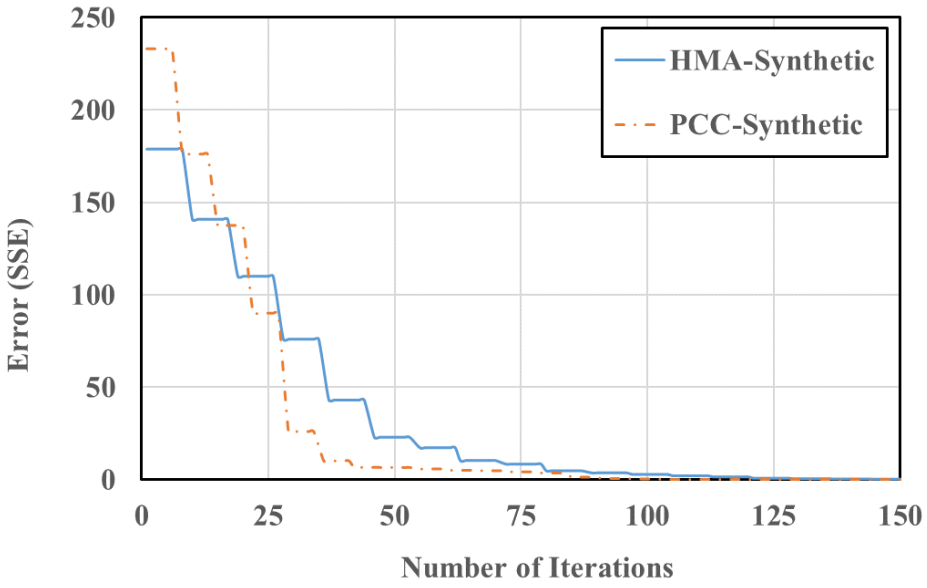

Figure 33. Convergence of the error function

The results of the backcalculation for these two sections are listed in Table 11. The analyses resulted in very good fits for both PCC and HMA. Smaller error values are obtained for PCC because it involves less variables (since the plate is assumed elastic). Regardless of the success of the backcalculation in finding multiple solutions that match the true deflections for both pavement sections, the backcalculated parameters do not match the true parameters one-to-one.

This can be attributed to the fact that different combinations of γ, H, E_s, and soil viscoelastic properties, E_{1s}/E_s and τ_s, can lead to very similar pavement behaviors. To better demonstrate this issue, the model parameters, K and G, are plotted for an elastic foundation in Figure 34. As highlighted with the red dashed lines, there exists an overlap between the calculated model parameters when the soil modulus, E_s, changes; hence, similar pavement behavior. This is a non-uniqueness issue present in this problem due to the confounding effect of these soil properties. For instance, in the case of the PCC section in Table 11, even though for all solutions fairly similar PCC elastic moduli are predicted, the foundation properties are different. The issue of non-uniqueness is intensified further for the HMA section as the plate is viscoelastic, which introduces more variables to the problem.

Table 11. Backcalculated pavement properties for the arbitrary HMA and PCC sections (unknown depth to rigid layer)

Case	Sol.	Foundation Parameters					Plate Parameters			SSE
		E_s	γ	H	E_{1s}/E_s	τ_s	E_p	E_{1p}/E_p	τ_p	
		MPa	-	m	-	ms	GPa	-	ms	
PCC	True	100.0	1.00	3.00	0.30	3.00	30.00	-	-	-
	#1	84.8	0.50	1.59	0.29	2.92	30.53	-	-	0.00
	#2	98.6	1.00	3.33	0.31	3.12	30.29	-	-	0.01
	#3	84.9	0.25	1.59	0.30	3.08	29.36	-	-	0.03
	#4	83.3	0.25	1.46	0.28	2.76	30.04	-	-	0.03
HMA	True	100.0	1.00	3.00	0.30	3.00	6.00	0.30	2.00	-
	#1	101.4	1.00	3.33	0.30	3.04	7.38	0.25	1.37	0.01
	#2	101.7	1.25	2.76	0.26	2.28	6.54	0.26	1.74	0.09
	#3	102.9	1.25	2.35	0.25	2.22	8.02	0.18	1.31	0.15
	#4	109.3	1.25	2.43	0.24	1.93	5.83	0.34	3.22	0.17

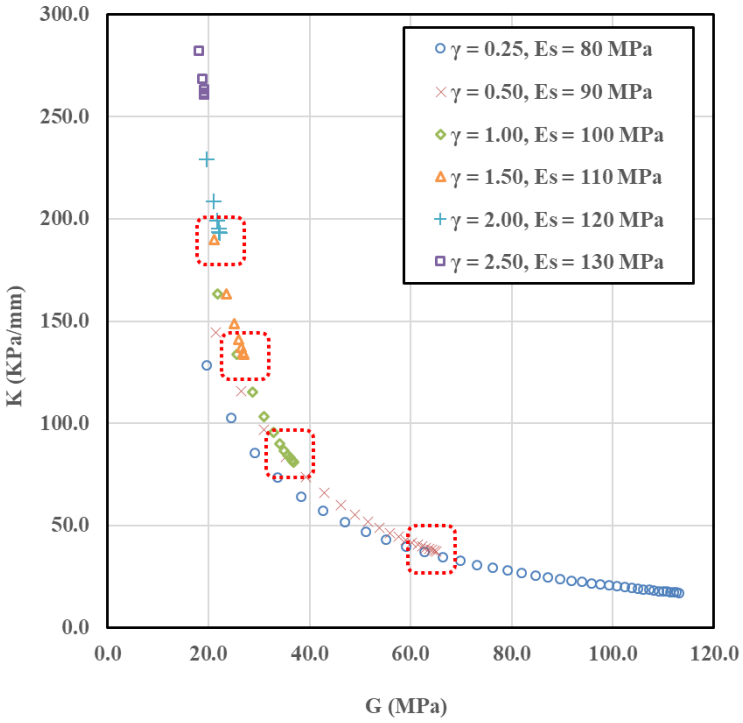

Figure 34. Issue of non-uniqueness with unknown depth to rigid layer

To alleviate this issue, one approach is to limit the number of unknown parameters [*Grenier et al.*, 2009]. In the next section, it is assumed that the depth to the rigid layer, *H*, is known. Similar approach was taken by *Liang and Zhu* [1995]. This assumption is used because usually in the field some information is available in this regard. For example, sample cores are drilled at multiple locations to find the average depth to shallow bedrock (rigid layer).

Known Depth to Rigid Layer

Here, the depth to the rigid layer is introduced to the program as an input and not as a variable. The results of the inverse analyses performed on the synthetic sections for multiple seeding values are summarized in Table 12. Despite having different seeding values for each solution, the optimization scheme was successful in converging to the true solution for both sections. This alleviates the non-uniqueness issue due to the reduction of the number of inter-dependent parameters.

Table 12. Backcalculated pavement properties for the arbitrary HMA and PCC Sections (known depth to rigid layer)

Case	Sol.	Foundation Parameters					Plate Parameters			SSE
		E_s	γ	H	E_{1s}/E_s	τ_s	E_p	E_{1p}/E_p	τ_p	
		MPa	-	m	-	ms	GPa	-	ms	
PCC	True	100.0	1.00	3.00	0.30	3.00	30.00	-	-	-
	#1	100.7	1.00	3.00	0.30	2.99	29.44	-	-	0.01
	#2	97.0	1.07	3.00	0.29	2.85	30.99	-	-	0.04
	#3	97.0	1.12	3.00	0.28	2.63	31.90	-	-	0.06
HMA	True	100.0	1.00	3.00	0.30	3.00	6.00	0.30	2.00	-
	#1	100.3	1.01	3.00	0.30	2.93	6.01	0.33	2.89	0.02
	#2	95.0	1.11	3.00	0.30	3.01	6.83	0.31	1.35	0.06
	#3	101.9	0.91	3.00	0.31	3.15	5.53	0.42	3.42	0.16

Figure 35 presents the comparison of the synthetic and backcalculated deflections to visualize how small the listed error values are. Deflection profiles with smaller magnitude correspond to the sensors located farther away from the center of loading. It can be seen that the profiles match almost perfectly. Few other notes to point out about the general behavior of elastic and viscoelastic plates resting on similar foundations are:

- There is a time delay between the happenstance of the peak load and the peak deformations for both sections.
- The time delay between the occurrence of the peak of the center deflections and the peak of the farthest deflections is larger for viscoelastic plate (HMA) compared to the elastic plate (PCC).
- The change in the peak deformations between the center and the farthest location is larger for viscoelastic plate compared to the elastic plate.

To further display the convergence of the error function using the explained backcalculation procedure as well as the process of approaching the true pavement properties, an example is offered in Figure 36. Figure 36a shows the decrease of the error value with the iteration steps. In this example, the discrepancy between the true and backcalculated responses is larger for the seeding value generated for HMA section (solution #1 for HMA section in Table 12) as compared to that of the PCC section (solution

#1 for PCC section in Table 12). Although there is a considerable difference in terms of the initial error values for these randomly-generated seedings, the employed technique was able to minimize the error function.

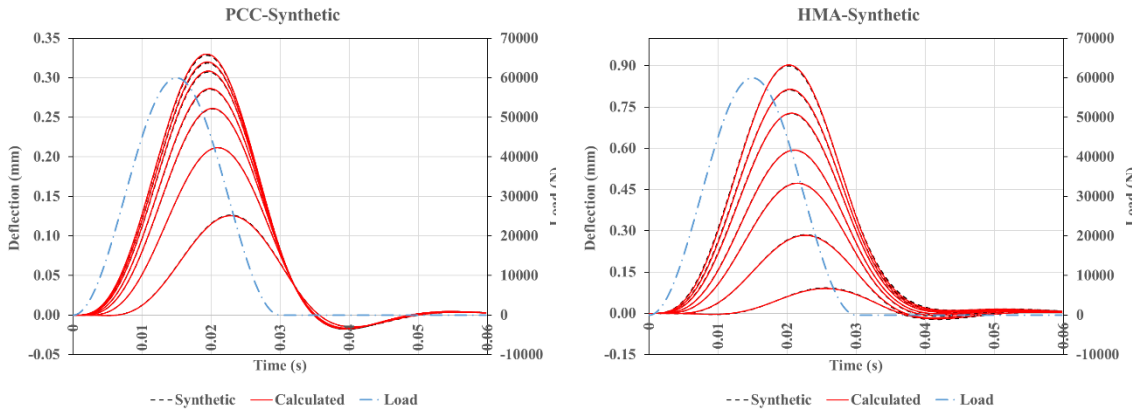

Figure 35. Measured and calculated FWD deflection profiles for synthetic data

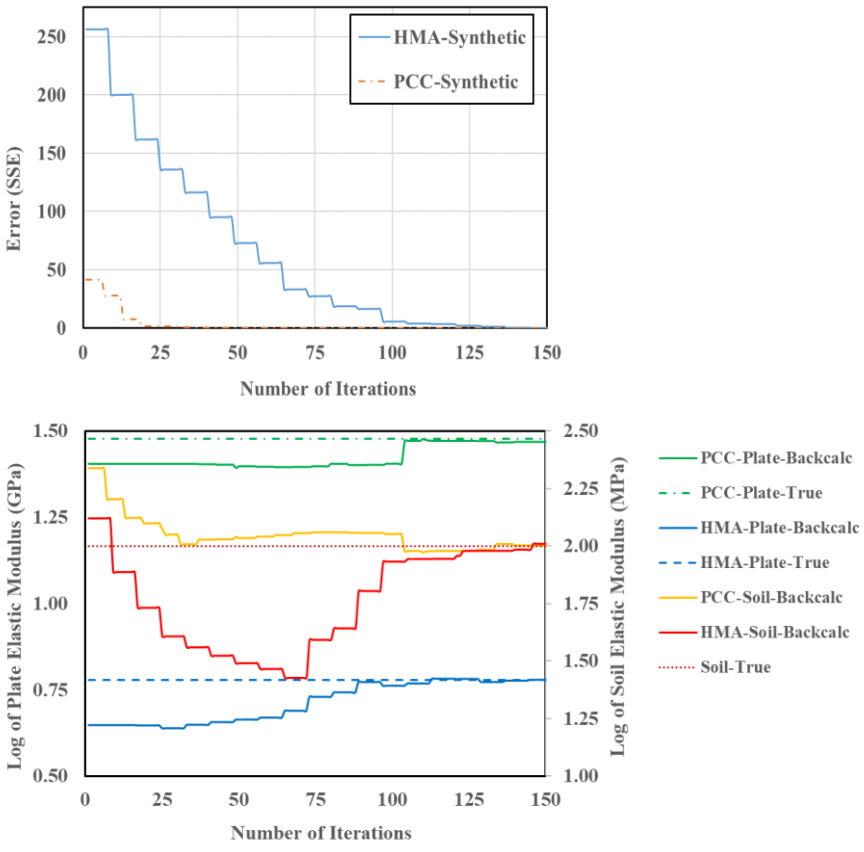

Figure 36. Backcalculation of synthetic HMA and PCC sections: (a) error vs number of iterations, and (b) plate and foundation moduli vs number of iterations

Figure 36b shows how the optimization technique takes the randomly-generated moduli of the plate and foundation and finds the true values for both PCC and HMA sections. Note that other than the values plotted here, other parameters are involved in the backcalculation, such as the γ and the viscoelasticity terms for the plate and foundation, which explains why for some cases the moduli do not approach the true values directly and might initially distant themselves from or oscillate around the solution.

As the next step, the ability of the developed inverse solution is tested for a larger sample. Total of sixteen arbitrary pavement sections are considered here. In this sample of 16 pavement sections, eight simulate rigid pavements with a PCC (elastic) surface layer and the other eight simulate flexible pavements with an HMA (viscoelastic) surface layer. A wide range of properties and geometries are assigned to these pavement sections to represent the typical existing roadways.

Table 13 summarizes the statistics of engineering error (mean and standard variance) in terms of the percent difference between the true and backcalculated values for these 16 cases. A very close agreement is obtained between the true and backcalculated values with mean percent differences of less than 5% for most parameters. This confirms the capability of the employed backcalculation scheme (quasi-Newton method along with multiple seeding values) of solving this optimization problem.

Table 13. Accuracy of the backcalculation technique for the synthetic data

Case	Statistical Value	Foundation Parameters				Plate Parameters			SSE
		γ	E_s	E_{1s}/E_s	τ_s	E_p	E_{1p}/E_p	τ_p	
PCC	Mean (%)	4.91	2.84	1.82	0.58	2.58	-	-	0.012
	σ[1](%)	7.04	2.87	2.48	1.17	2.24	-	-	0.013
HMA	Mean (%)	4.85	5.12	2.09	0.81	3.95	6.09	3.66	0.193
	σ(%)	4.47	5.23	3.25	0.83	3.18	6.50	2.18	0.404

[1] σ is the standard deviation of the sample

5.6. Case Studies

To examine the ability of the generalized Vlasov model to predict the behavior of slab-on-grade systems, FWD measurements collected for four pavements located on the Minnesota Road Research Facility, also known as MnROAD [*MnROAD*, 2017], as well as three pavements under the Long-Term Pavement Performance (LTPP) program [*FHWA*, 2017] were considered. The layer description of the selected pavement sections is listed in Table 14. The selected pavement sections are categorized as follows:

- A1 and A2: neighboring PCC sections located on cells 36 and 38 in MnROAD with a fairly similar surface and a thin base layer but different soil types for subgrade consisting of sand and silty-clay, respectively.
- B1 and B2: neighboring HMA sections located on cells 25 and 26 in MnROAD with a fairly similar surface with no base layer and different soil type for subgrade consisting of sand and silty-clay, respectively.
- C1, C2 and C3: located on the highway I-80 in Nevada with PCC, thin HMA, and thick HMA, respectively, as surface layers resting on fairly similar underlying layers consisting of base, subbase, and subgrade.

Sections B1 and B2 are placed directly on subgrade while A1 and A2 have an additional thin base layer protecting the subgrade. Considering the two different materials used for subgrade, the objective is to investigate if the proposed generalized Vlasov model can identify the difference between subgrades with different comprising material. The model would also be evaluated for its ability to describe the behavior of both elastic and viscoelastic surface layers (slab/plate).

Sections C1, C2, and C3 are included in this study to check if this slab-on-grade model can be used to describe multi-layer grades. Similar to the MnROAD sections, this set of pavements are suitable candidates to conduct a comparison between the predictions of the model for different types of surface layers.

Another objective here is to conduct a seasonal study on pavements in extremely different climatic conditions. The state of Minnesota is one of the coldest regions in US, in which the roadways undergo harsh seasonal variations with very cold temperatures and frost-thaw cycles; in contrast, the average temperature in the state of Nevada is considerably higher and pavements do not experience frequent freezing conditions. The FWD data used here are related to multiple site visits conducted during the years 1994, 1995, and 2000 for sections A1 & A2, B1 & B2, and C3, respectively. Because the FWD is not a continuous test device, the test data for the same stop were used to have roughly similar test location in each visit to better facilitate the comparison. For pavement sections C1 and C2 only one site visit was carried out during the year 2000.

Table 14. Detailed information on the selected pavement sections

Case	Loc.	Top Layer				Base Layer		Subbase Layer		Subgrade		
		Type	h mm	SG -	m_p Kg/m^2	Type	h mm	Type	h mm	Type	v	SG -
A1	MN	PCC	163	2.25	367	CA[1]	127	-	-	Sand	0.35	1.85
A2	MN	PCC	163	2.25	367	CA	127	-	-	Silty - Clay	0.40	1.70
B1	MN	HMA	132	2.20	290	-	-	-	-	Sand	0.35	1.85
B2	MN	HMA	150	2.20	330	-	-	-	-	Silty - Clay	0.40	1.70
C1	NV	PCC	234	2.22	520	CA	150	A[2] LTS[3]	551 305	Sand	0.35	1.85
C2	NV	HMA	109	2.23	244	CA	297	A LTS	544 305	Sand	0.35	1.85
C3	NV	HMA	183	2.23	409	CA	216	A LTS	579 305	Sand	0.35	1.85

[1] Crushed Aggregate
[2] Aggregate
[3] Lime Treated Soil

For the pavement sections considered in this study, no rigid layer is present in the depth less than 5 meters [*Berd*, 1997; *MnROAD*, 2017; *FHWA*, 2017]. In conventional layered elastic pavement models, such as implemented in the Mechanistic Empirical Pavement Design Guide (MEPDG), if no shallow bedrock is present, the depth of 192 inches (4.88 m) is assigned to the subgrade thickness. This is done mainly because the typical vehicular loads do not impact the soil stratum deeper than the mentioned depth. Accordingly, in this study, the depth to the rigid layer is assumed constant and equal to 5 meters for all sections. It is of crucial importance to mention this is entirely an assumption made with the objective of showcasing the abilities and limitations of the proposed approach. Accurate information about the depth to the rigid layer could improve the accuracy of the computations.

In addition, the Poisson's ratio of the plate, ν_p, and the foundation soil, ν_s, are assumed known and introduced to the analysis as inputs. The laboratory tests performed on the soil samples collected from the site as well as the literature [*MnROAD*, 2017; *FHWA*, 2017] provide the information needed to assign proper values. Here, in the forward and inverse analysis, the Poisson's ratio of the plate was assumed to be constant and equal to 0.15 for concrete. For asphalt sections, depending on the test temperature, a reasonable value of 0.20 to 0.40 was assigned using the laboratory tested values reported in the literature [*Von Quintus and Simpson*, 2002]. The surface layer temperatures at the time of FWD testing are listed in Table 16. It is worth noting that in order to minimize the effects of pavement joints and edges, the FWD data collected at the center of the slab and away from the pavement edges (interior loading) were taken into consideration.

5.7. Results

FWD deflection data collected in August of 1995 for the concrete pavement section Case A1 were used to evaluate the importance of various components of the generalized Vlasov model for describing pavement behavior under short term dynamic loading. The following four versions of the model were considered (see equation (5-20)):

- Elastic weightless Vlasov model (EWV), in which $\tilde{R}_s = \tilde{I}$, and $m_f = 0$,

- Elastic Vlasov model with foundation inertia (EIV), in which $\tilde{R}_s = \tilde{I}$,
- Viscoelastic weightless Vlasov model (VWV), in which $m_f = 0$.
- Generalized Vlasov model (GVM), which accounts for both inertia and viscoelastic behavior.

Figure 37 shows the fit between the measured deflections at the location of the FWD sensors and the corresponding model-calculated deflections for the PCC section, A1. The assumption of weightless elastic foundation leads to significant underestimation of the time lag between peak load and deflection peaks. Moreover, the deflection peaks for the inner and outer sensors occur almost simultaneously, which is in contrast with the measurements (Figure 37a). With the addition of the foundation inertia, m_f, one can observe significant improvement in time lag predictions, but the oscillation of deflections in the post-loading period is exaggerated (Figure 37b). When the foundation is assumed weightless but damping is accounted for, as shown in Figure 37c, there is an improved agreement between measured and simulated responses. However, the predicted responses diminish to zero without changing sign, which clearly contradicts the measured responses that take place after the end of the load impulse.

The use of the generalized Vlasov model yielded the best fit among the models considered here (Figure 37d). No issues associated with time lag or deflection oscillation are observed. Table 5.6 summarizes the backcalculation solutions for the introduced models. The considerable visual enhancement of the fit and the much smaller error values (see

Table 15) obtained by the simultaneous addition of the foundation inertia and viscous effects underlines the importance of using the generalized Vlasov model for slab-on-grades subjected to short-duration loading.

The generalized Vlasov model was used to analyze the FWD data for the remaining sections introduced in Table 14. Table 16 presents the backcalculated pavement properties and the associated error values.

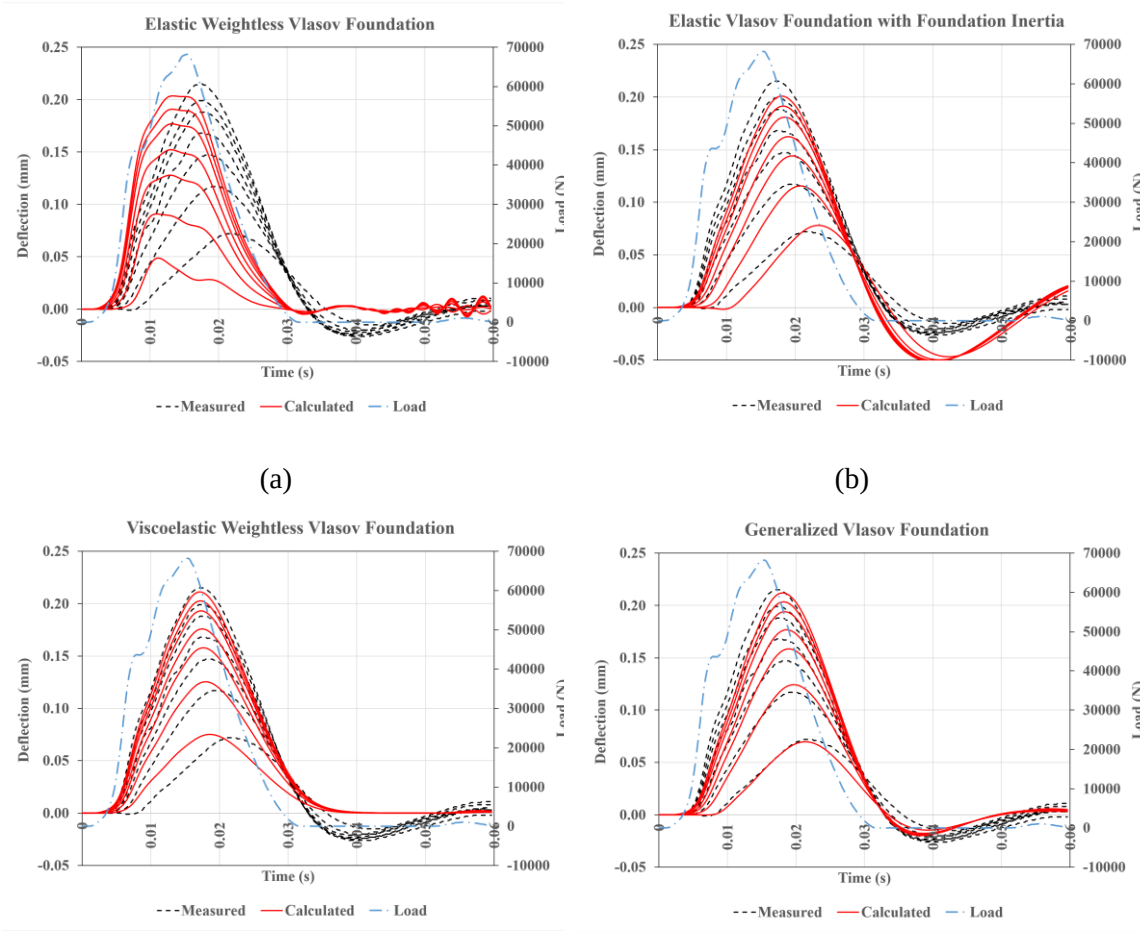

Figure 37. Measured and calculated FWD deflection profiles for concrete section (Case A1) in the month of August modeled with (a) elastic weightless Vlasov foundation, (b) elastic Vlasov foundation with foundation Inertia (c) viscoelastic weightless Vlasov foundation, and (d) generalized Vlasov foundation

Table 15. Backcalculated pavement parameters for various Vlasov models

Model	Foundation Parameters					Plate Parameters				Error (SSE)
	E_s	γ	E_{1s}/E_s	τ_s	m_F	E_p	E_{1p}/E_p	τ_p	ν_p	
	MPa	-	-	ms	kg/m^2	GPa	-	ms	-	-
EWV	151.7	0.61	-	-	-	23.79	-	-	0.15	98.13
EIV	157.8	0.12	-	-	2984	22.91	-	-	0.15	24.56
VWV	631.0	0.11	0.14	0.71	-	44.04	-	-	0.15	12.92
GVM	379.9	0.57	0.28	1.42	1438	45.05	-	-	0.15	5.04

Table 16. Backcalculated pavement properties for Cases A, B, and C using generalized Vlasov model

Case	Test Date	Air Temp.	Grade Properties							Slab Properties				Error (SSE)
			E_s	γ	E_{1s}/E_s	τ_s	K	G	m_f	E_p	E_{1p}/E_p	τ_p	ν_p	
		˚C	MPa	-	-	ms				GPa	-	ms	-	-
A1	3/13/1995	-0.6	246.7	4.26	0.12	0.75	844	10.7	217	48.43	1.00	-	0.15	5.51
	4/17/1995	8.9	631.0	0.63	0.17	0.74	329	181.2	1435	44.25	1.00	-	0.15	5.51
	5/18/1995	15.6	291.0	0.81	0.21	1.12	189	66.6	1143	47.57	1.00	-	0.15	6.01
	6/20/1995	21.1	358.6	0.45	0.34	1.90	147	134.8	1878	45.66	1.00	-	0.15	6.77
	8/18/1995	21.7	379.9	0.57	0.28	1.42	182	119.0	1438	45.05	1.00	-	0.15	5.04
A2	3/13/1995	-0.6	42.8	5.27	0.25	2.81	241	1.4	161	38.80	1.00	-	0.15	2.34
	4/17/1995	8.9	206.8	1.35	0.08	0.50	298	27.4	631	33.66	1.00	-	0.15	3.68
	5/18/1995	15.6	74.1	3.73	0.14	1.15	137	1.6	228	35.40	1.00	-	0.15	5.04
	6/20/1995	21.1	158.5	0.98	0.16	1.11	167	28.8	865	32.78	1.00	-	0.15	3.04
	8/18/1995	21.7	216.9	1.20	0.10	0.71	278	32.4	711	33.82	1.00	-	0.15	2.80
B1	2/18/1994	-5.6	760.4	1.41	0.27	5.58	859	100.0	657	13.64	1.00	-	0.15	7.59
	4/20/1994	10.0	298.7	1.62	0.16	1.11	387	34.2	572	8.70	1.00	-	0.25	4.54
	6/22/1994	21.7	213.0	1.05	0.40	2.44	180	37.6	881	0.83	0.00	6.03	0.30	5.18
	9/21/1994	15.6	232.0	0.85	0.33	1.96	158	50.5	1087	1.54	0.14	8.91	0.25	5.20
	10/25/1994	7.2	388.5	1.59	0.10	0.64	494	45.4	583	9.62	1.00	-	0.22	4.66
B2	2/18/1994	-5.6	2260.4	0.10	0.18	3.53	970	1302.2	2742	12.94	1.00	-	0.15	43.49
	4/20/1994	10.0	211.1	1.08	0.17	1.84	244	35.0	788	8.01	1.00	-	0.25	4.24
	6/22/1994	21.7	106.0	1.10	0.38	2.96	126	17.1	769	0.87	0.00	5.65	0.30	1.65
	9/21/1994	15.6	166.1	1.00	0.31	2.24	178	29.7	852	1.24	0.00	9.59	0.25	1.26
	10/25/1994	7.2	226.3	1.35	0.15	1.56	328	29.8	628	10.84	1.00	-	0.22	4.13
C1	6/13/2000	40.1	285.7	1.67	0.13	1.02	383	31.7	553	19.42	1.00	-	0.15	2.08
C2	6/21/2000	50.0	308.9	1.14	0.38	3.59	282	50.3	813	0.59	0.00	5.01	0.35	4.66
C3	2/2/2000	1.4	381.4	0.41	0.34	3.21	148	152.7	2000	24.98	1.00	-	0.15	7.98
	3/24/2000	16.5	497.0	0.57	0.25	2.12	237	156.7	1575	18.29	1.00	-	0.25	6.75
	5/9/2000	18.2	442.4	0.51	0.31	2.70	195	151.8	2742	10.10	0.89	27.54	0.30	5.67
	8/3/2000	34.9	446.7	0.69	0.32	2.64	251	118.4	1324	4.16	0.30	7.76	0.35	4.56
	9/28/2000	23.7	351.5	0.40	0.39	3.86	275	156.1	1457	6.79	0.63	10.47	0.30	6.45
	11/7/2000	3.9	440.9	0.50	0.29	2.35	192	153.5	1739	22.58	1.00	-	0.18	7.50

Figure 38 compares the deflection basins recorded at the same location (stop 2) tested at multiple months during the year 1995 for PCC sections, A1 and A2. The plot legend indicates the "test section-month of testing-air temperature in ˚C-FWD peak load in KN". Under a fairly similar load and the same climatic condition, Case A2 exhibits larger deformations. This could be due to the weaker soil, slab, or both. Also, the change in the displacement is greater in Case A2 with silty-clay subgrade as this type of soil is more susceptible to frost-thaw cycles.

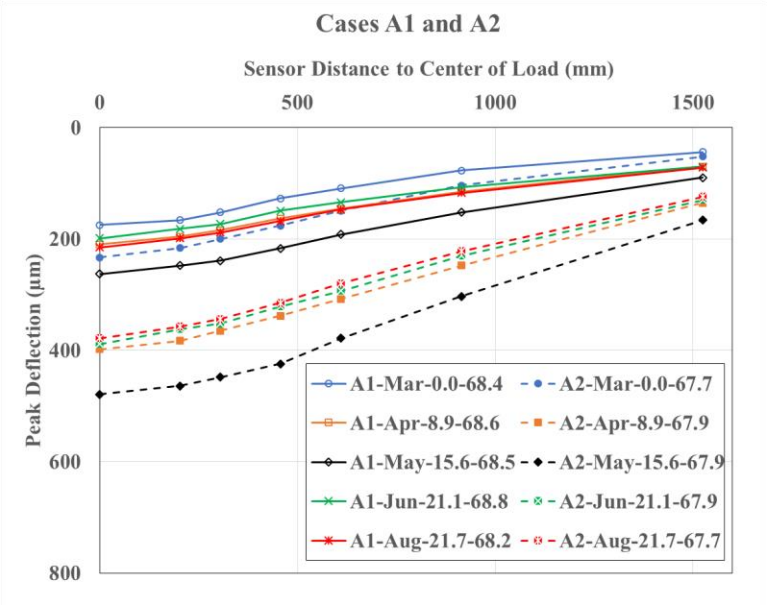

Figure 38. FWD deflection basins for MnROAD concrete pavement sections (Cases A1 & A2)

Figure 39 and Figure 40 present the FWD-measured versus the model-calculated deflections for cases A1 and A2 in various months using the backcalculated model parameters listed in Table 16. As indicated in these plots, despite the considerably different behavior at different months for both PCC pavements (elastic slab-on-grade), there is a good agreement between the model predictions and the field measurements. This observation is confirmed by the SSE value listed in Table 16.

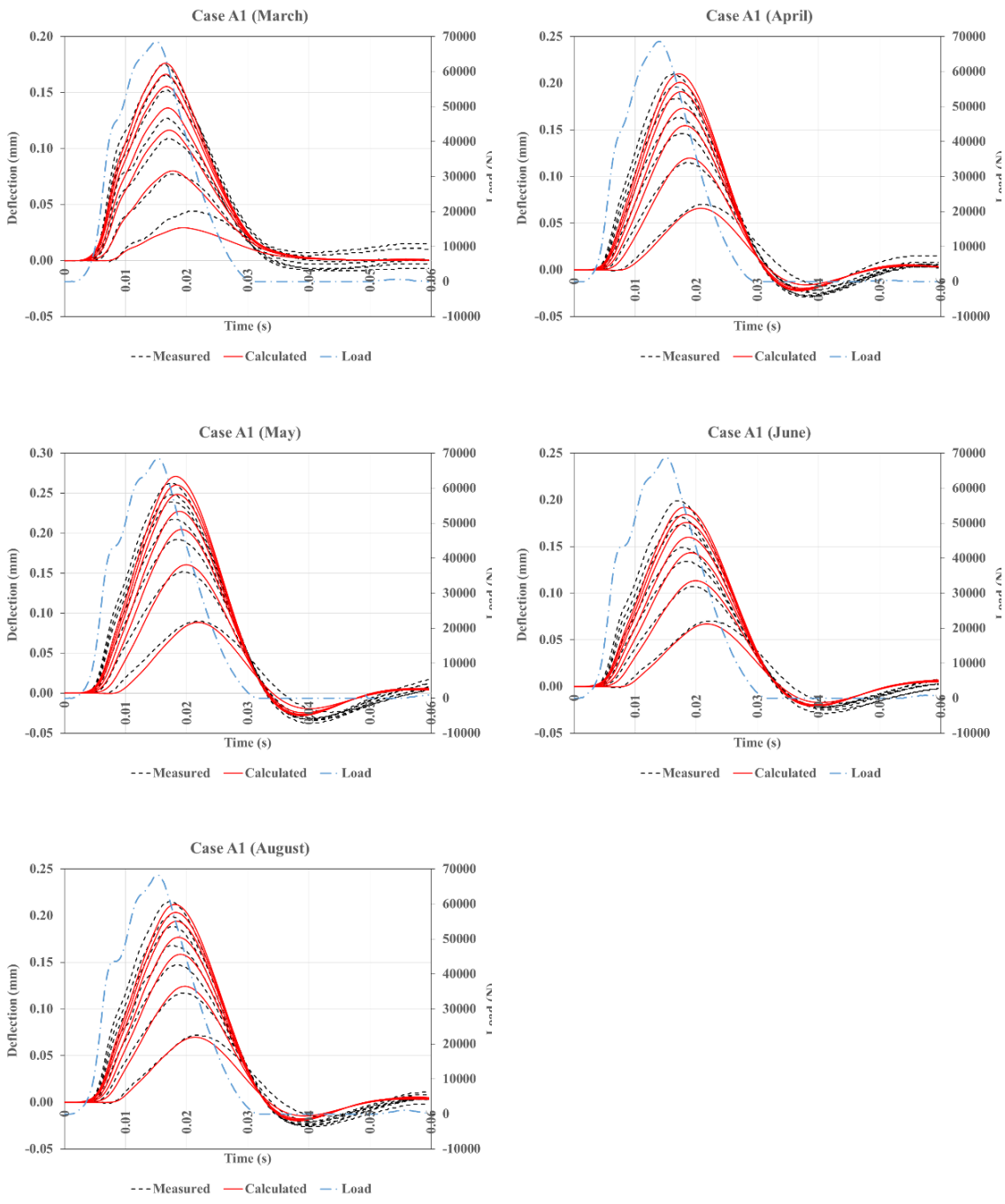

Figure 39. Measured and calculated FWD deflection profiles for MnROAD concrete pavement section with sandy foundation (Case A1)

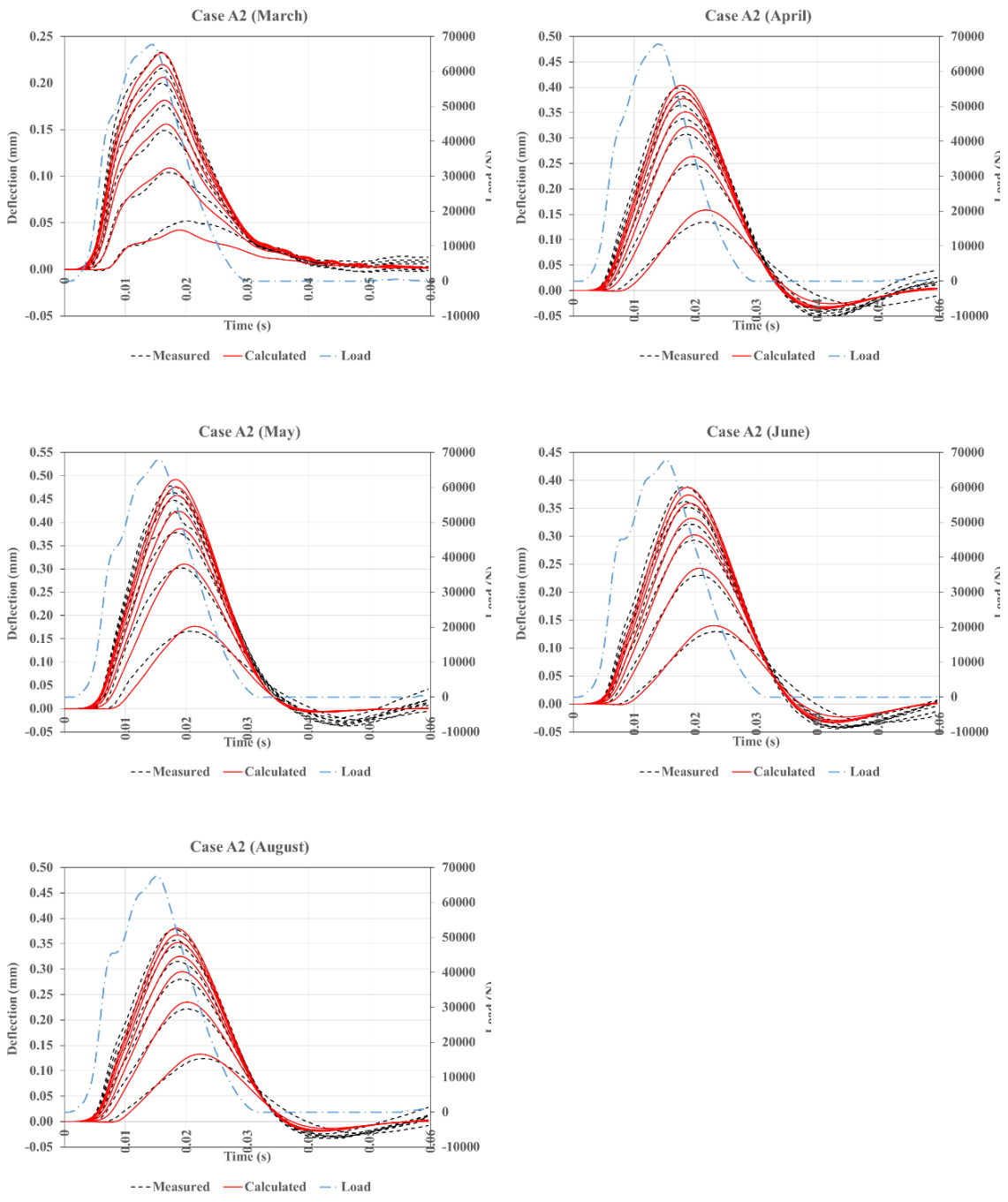

Figure 40. Measured and calculated FWD deflection profiles for MnROAD concrete pavement section with silty-clayey foundation (Case A2)

Similar information is presented here for the HMA sections located at MnROAD, Cases B1 and B2. As indicated in Figure 41, the deflection basins collected at several months of the year 1994, follow the same trend as for the PCC sections A1 and A2, meaning that the change of the deflections for the section with silty-clay subgrade, B2, is larger than for the section with sand subgrade. The silty-clay soil is more prone to frost-thaw cycles, especially in this particular case where the HMA layer is constructed directly on top of the subgrade with no non-frost susceptible base layer. It is worthwhile to mention that the displacement of the pavement when the subgrade is fully frozen, the month of February, is considerably smaller than the measurements taken during the other months.

The visual comparison of the deflection basins for PCC and HMA in Figure 38 and Figure 41 demonstrates the difference of the basin shape and its correlation with the viscous properties of the slab, i.e., the more viscous the slab, the larger the gap between the central and the farthest sensor; as radiating away from the load center, the effect of excitation induced to the viscoelastic slab diminishes more quickly.

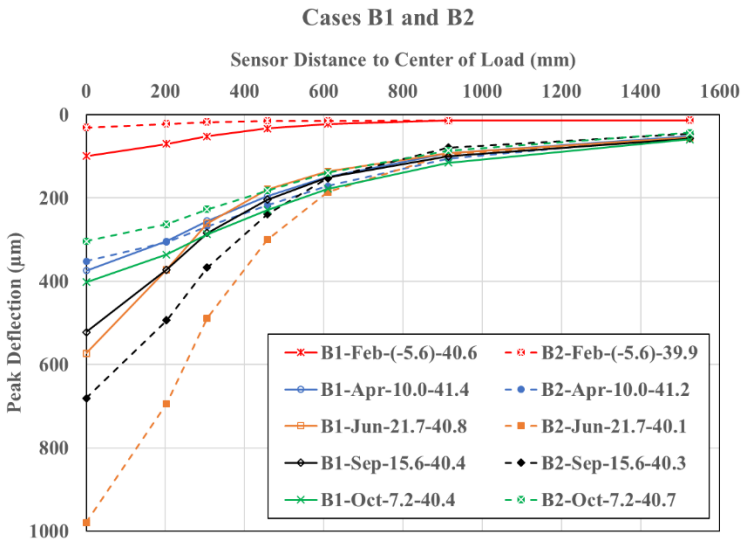

Figure 41. FWD deflection basins for MnROAD asphalt pavement sections (Cases B1 & B2)

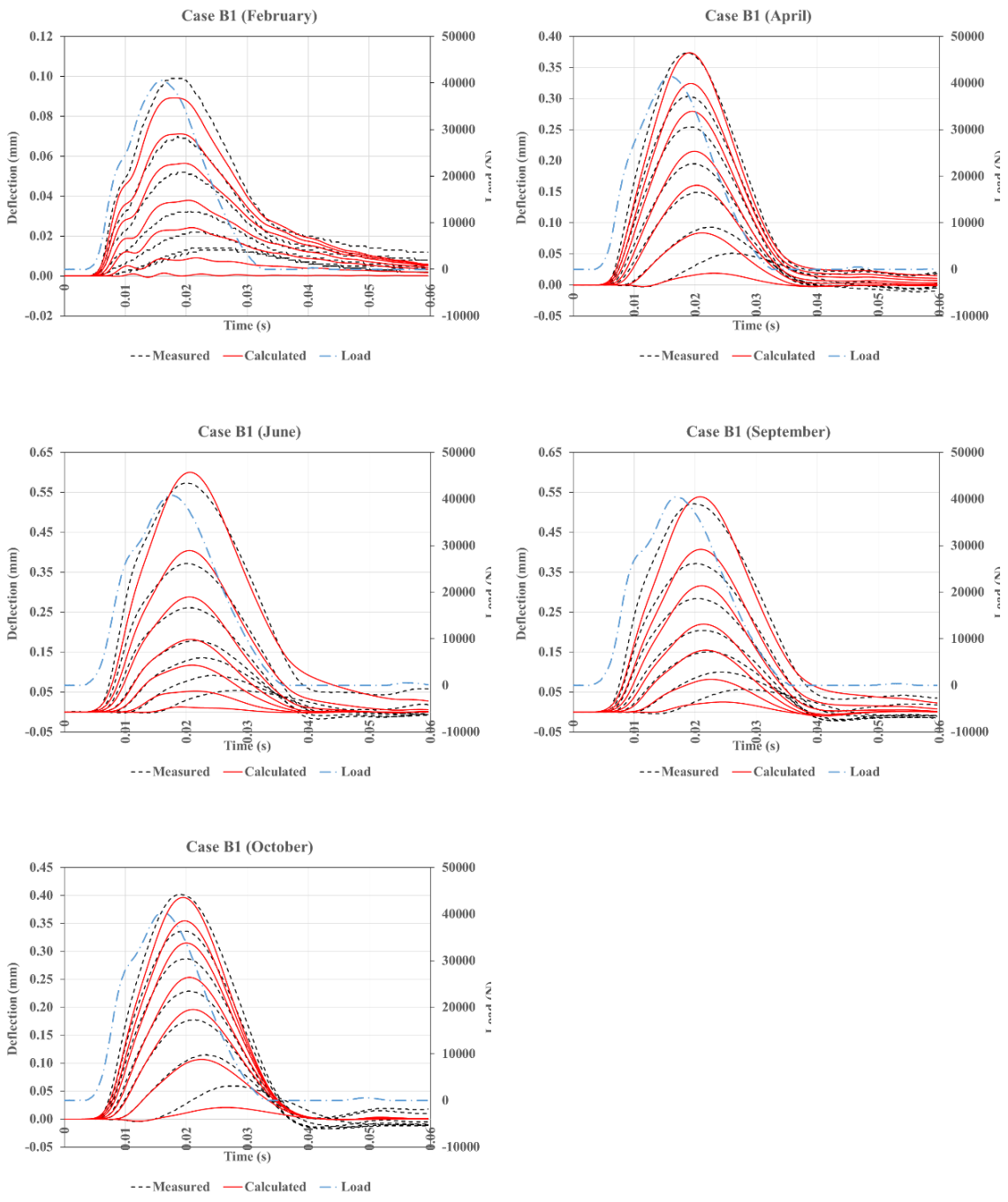

Figure 42. Measured and calculated FWD deflection profiles for MnROAD asphalt pavement section with sandy foundation (Case B1)

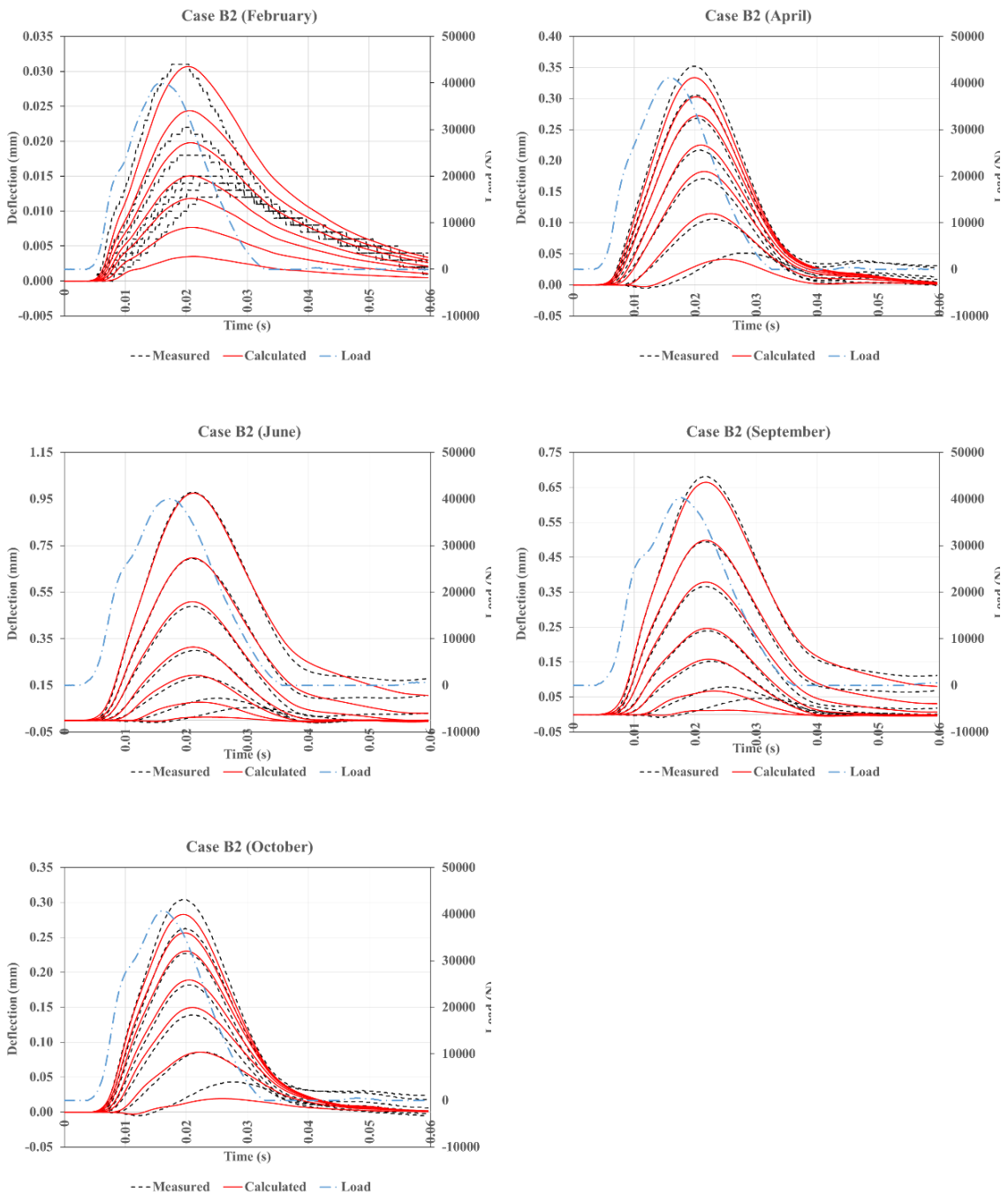

Figure 43. Measured and calculated FWD deflection profiles for MnROAD asphalt pavement section with silty-clayey foundation (Case B2)

Figure 42 and Figure 43 compare the deflections generated by the model using the backcalculated parameters, listed in Table 16, with the FWD measurements for multiple months for asphalt pavement sections B1 and B2 (viscoelastic slab-on-grade). Apart from the test during the month of February, a good fit for this pavement section is achieved, as confirmed by much smaller error values, regardless of the test temperature or season, and the various surface deformation profiles.

The deflection basins for the sections C1, C2 and C3 are plotted in Figure 44. The visual comparison with the previous cases indicate that the seasonal variation in the state of Nevada is not as significant of an issue compared to the state of Minnesota. Also, in line with our expectation, the section with thinner HMA layer, C2, was deformed the largest despite undergoing a smaller excitation. Interestingly, the concrete section deformed more than the pavement with thicker HMA layer during the cold seasons, C3.

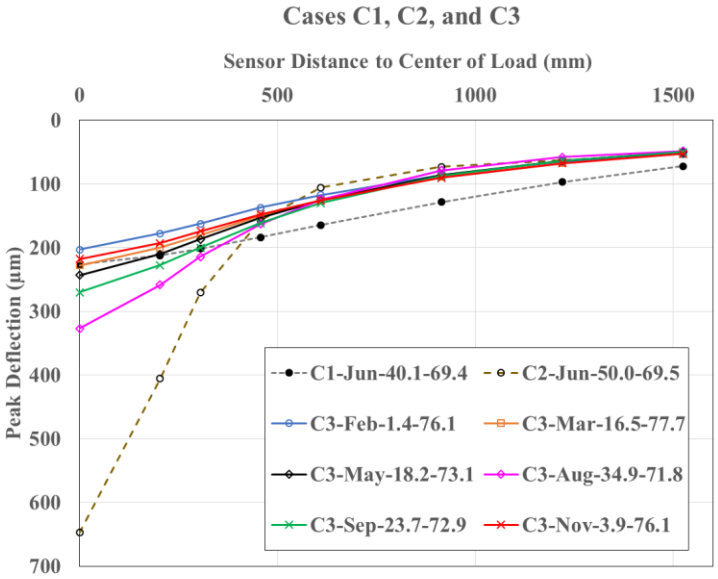

Figure 44. FWD deflection basins for LTPP pavement sections located in Nevada (Cases C1, C2 & C3)

Figure 45 depicts the comparison between the measured and calculated deflection profiles for Cases C1 and C2. Figure 46 generates similar graphs for Case C3 for multiple visits at the year 2000. The good fit obtained for these different pavements with multi-layered grades proposes that the generalized Vlasov model may be applicable for such structures as well.

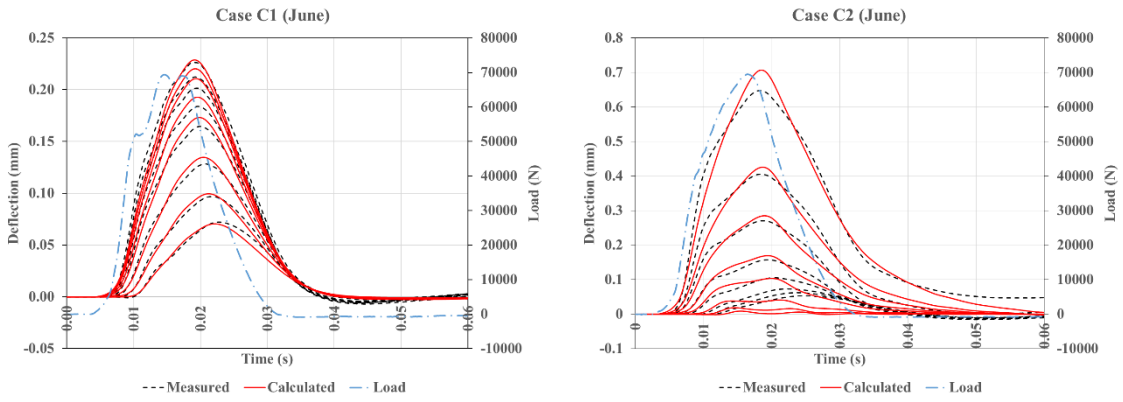

(a) (b)

Figure 45. Measured and calculated FWD deflection profiles for LTPP pavement sections: (a) Case C1, and (b) Case C2

The visual comparisons carried out between the model-predicted and field-measured system responses allude to the fact that the proposed generalized Vlasov model is capable of capturing the behavior of elastic and viscoelastic slab-on-grade systems with a range of properties and climatic conditions. The discussion presented hereafter aims at finding an answer for the other concern associated with any inverse analysis with the objective of fitting a certain behavior: whether the obtained fitting parameters are reasonable and in line with the documented expectations? In other words, whether the proposed generalized Vlasov model can be used as a reliable tool for assessing the structural properties of pavements?

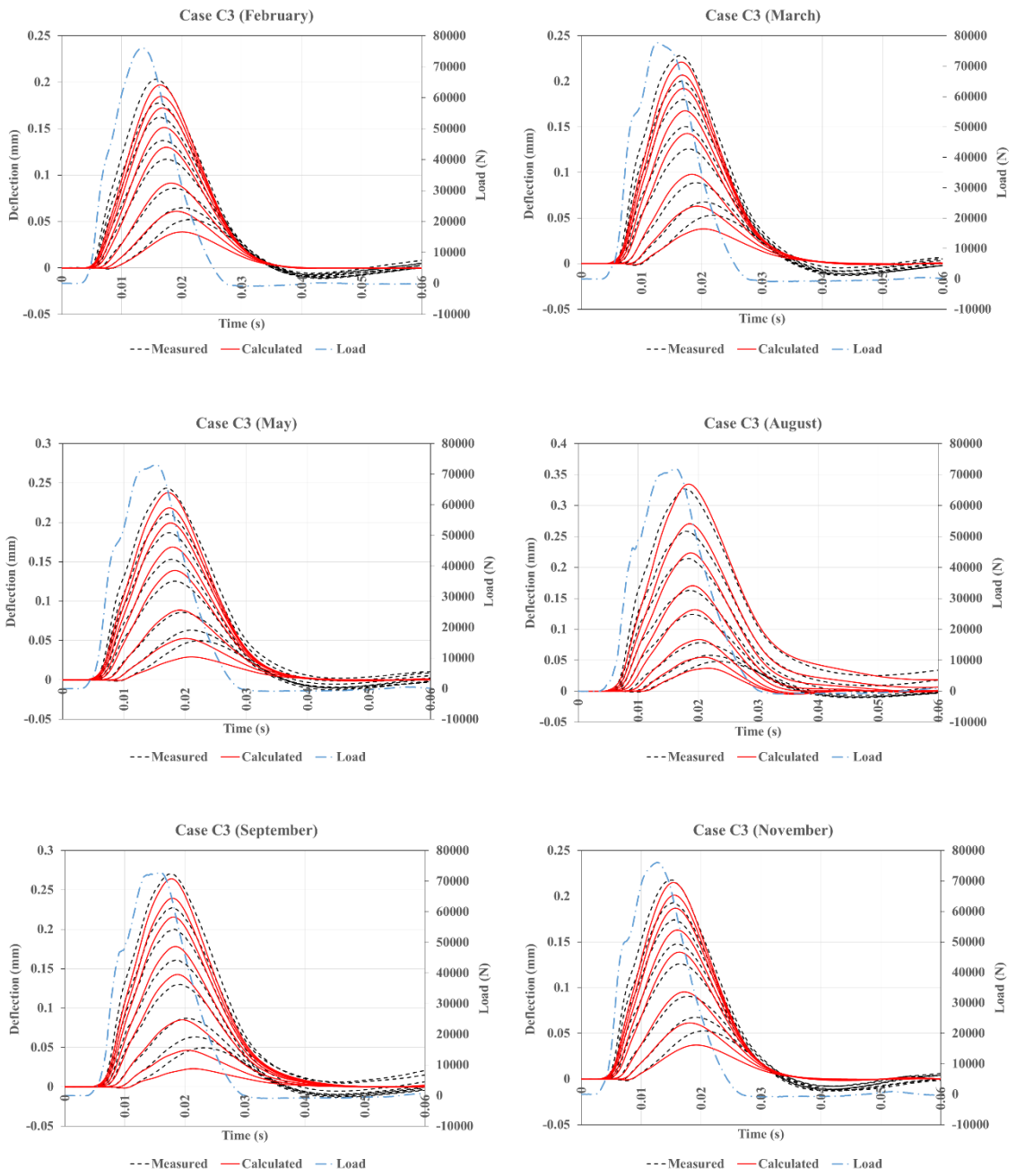

Figure 46. Measured and calculated FWD deflection profiles for LTPP asphalt pavement section (Case C3)

5.8. Discussion

Top Layer (Plate) Properties

Cases A1 and A2

These two pavements have a PCC surface layer. As expected, regardless of the seasonal variation and the different types of soil properties, the backcalculation identified the elastic behavior of the plates, as indicated by the backcalculated E_{1p}/E_p ratio equal to 1. The backcalculated moduli for both PCC sections led to reasonable values for concrete and did not vary considerably during different seasons, which is in line with our expectation. The analysis was performed on the same stop in each visit, so the expectation was to observe similar moduli for the slab throughout a year as the properties of concrete are invariant to temperature change. The laboratory results for the "static" modulus of elasticity test performed on pavement cores at ages between 28 to 360 days are listed Table 17, and compared with the backcalculated dynamic moduli.

Table 17. Laboratory versus backcalculated concrete elastic moduli

Case	Type	# of tests	Min	Max	Mean	σ	ν_p
		-	GPa	GPa	GPa	GPa	-
A1	Laboratory	6	25.61	36.67	32.22	4.98	0.25
	Backcalculated	5	44.25	48.43	46.19	1.75	0.15
A2	Laboratory	5	30.39	31.65	30.94	0.55	0.23
	Backcalculated	5	33.66	38.80	35.85	2.28	0.15

The difference between the mean of the laboratory tested moduli is not large (32.22 vs 30.94 GPa); conversely, there is a difference in magnitude for the average backcalculated moduli (46.19 vs 35.85 GPa). Also, there is a clear gap between the laboratory and backcalculated values. This could be attributed to the following reasons:

- The thickness of the concrete layer plays an important role in the magnitude of the elastic modulus; if the concrete layer is thicker than the assumed value in the analysis, the backcalculated modulus will be larger than the real modulus at the test location. For example, if the real thickness is 10% greater than the assumed thickness, the backcalculated modulus will be 33% greater than the real modulus. Since in the pavement construction, variation of the layer thickness is very common, it is possible that at the test location for section A1, the thickness of the layer was larger than the reported average in Table 14, which is the assumed value in the analysis.
- Since the FWD test is a discrete test, there is a possibility that the concrete stiffness at the test location for section A1 belonged to the higher end of the stiffness range.
- The laboratory measured Poisson's ratios (0.25 and 0.23) are different from the assumed values (0.15). Using analogous Poisson's ratios reduces the backcalculated moduli (4-5%).
- Laboratory tests were performed on intact pavement sections while the FWD data utilized here were collected during the year 1995. At the time of testing, the pavements had experienced two freeze-thaw cycles. Pavement section A2 is constructed on a silty-clay subgrade, which is the most prone soil mixture to frosting [*Corps of Engineers*, 1984]. This might have distressed the pavement top layer by causing micro cracks in the concrete matrix, which explains why section A1 exhibits larger moduli compared to section A2.

Nevertheless, the backcalculation results for the elastic slab-on-grade seem reasonable and in line with our expectations. It also indicates that relying solely on the laboratory tests in providing inputs for design and analysis of slab-on-grade systems may be erroneous.

Cases B1 and B2

Viscoelastic behavior is an intrinsic characteristic of asphaltic materials. Temperature and rate of loading significantly influence HMA. Therefore, the behavior of HMA layer could be different at different temperatures throughout a year [*Booshehrian et al.*, 2012]. The backcalculated moduli for the HMA sections, B1 and B2, were intimately linked to the test temperature/season. During the colder months in the state of Minnesota (Feb, Apr, and late Oct) both HMA courses behaved elastically, while during the warmer periods the surface layers became more viscous with much lower stiffness (more compliant). A glance at Figure 41 and examining the shape of the deflection basins confirm that these HMA sections behave elastically during the mentioned cold months. It is of value to point out that the HMA followed a Maxwell model, i.e., E_{1p}/E_p is equal to zero, at the hottest periods of the year.

Sections B1 and B2 are comprised of similar materials including aggregate and asphalt binder (the Superpave binder grade was PG 58-28). Whence, one may anticipate similar properties for both asphalt courses. The similarity of the backcalculated slab properties could be anticipated. Both the obtained elastic moduli and the relaxation times for these HMA sections are in agreement with the reported typical values in the literature [*Akbarian*, 2015].

Cases C1, C2, and C3

According to the proposed analysis, for the PCC section, Case C1, similar to Cases A1 and A2, an elastic behavior is anticipated. The obtained elastic modulus of 19.42 GPa seems low for concrete. However, the results of the modulus of elasticity test conducted on the samples taken from this pavement during the years 1995 and 1996 confirm such low stiffness. The average laboratory-reported modulus is 19.13 GPa with a standard deviation of 2.04 GPa. Considering that the FWD tests were performed in the year 2000 (few years after opening to traffic) and the possible presence of micro cracks justifies the low backcalculated modulus.

Among the FWD recordings studied here, the highest test temperature (50 ˚C) is related to the thin HMA section, Case C2. The dynamic backcalculation led to assigning the most compliant behavior to this HMA layer. Similar to Cases B1 and B2, the asphalt material at high temperature can be described as a Maxwell spring-dashpot model.

The thicker HMA section, Case C3, was tested several times during the year 2000. In line with the temperature-dependent properties reported for Cases B1 and B2, this HMA layer follows the elastic-viscoelastic-elastic behavior simultaneous with the occurrence of cold-warm-cold seasons. Interestingly, the asphalt elastic modulus at the coldest test temperature (1.4 ˚C) is higher than that of the concrete section on the same highway, Case C1 (compare 24.98 to 19.42 GPa). The deflection basins plotted in Figure 44 showed smaller displacement for Case C3 at the coldest months compared to Case C1. One can anticipate a stiffer slab, or grade, or both for Case C3.

Thus far, the generalized Vlasov model and the proposed numerical analysis has shown the capability of assigning reasonable values to the surface layer. The discussion on the properties of the foundation is followed here.

Foundation Properties – Seasonal Study

Cases A1 and A2

The resilient modulus, M_R, is a material property used in pavement engineering that describes the deformation of materials comprising a pavement structure subjected to repetitive loads similar to those imposed by vehicles. A loading protocol is followed where the confining pressure and the repetitive deviator stress are varied to simulate different states of stress [*Tanyu et al.*, 2003]. For more information on the test configuration see [*Yau and Von Quintus*, 2002].

Since the pavements of interest are located in Minnesota, specific attention is paid to the effect of moisture and freeze/thaw cycle on the M_R of unbound materials and consequently on the elastic modulus. The freeze/thaw cycles and their associated negative impacts on the pavement performance are thoroughly described in *Corps of Engineers* [1984]. It has been shown that the material property, resilient modulus, is intimately linked with the moisture content as described here:

- All other conditions being equal, the higher the moisture content, the lower the modulus; this can be explained by two separate physical phenomena: I) moisture can affect the state of stress through suction or pore water pressure, and II) moisture of the soil may impact the soil structure by destructing the cementation between the soil particles [*MEPDG*, 2004].
- At freezing temperature, on the other hand, the water in the soil freezes and the resilient modulus rises to values 20 to 120 times greater than the value of the unfrozen modulus. The process of freezing can be accompanied by formation of ice lenses that creates zones of greatly reduced strength in the pavement when thawing occurs [*MEPDG*, 2004].

- A reduction factor relative to the unfrozen modulus is recommended for the thawing cycle based on the frost-susceptibility of soil, which is determined depending on the percent passing the No. 200 sieve and the plasticity index (PI). A reduction between 0.55-0.85 is suggested for coarse-grained soil. This issue is more detrimental in fine-grained and expansive soils, such as clayey soil, thus, the recommended reduction factor ranges between 0.40-0.60 [*MEPDG*, 2004]. The lowest reduction factor must be applied to silty-clayey soil [*Corps of Engineers*, 1984].
- Next, the material experiences recovery of the lost modulus immediately after thawing until it reaches the unfrozen modulus. The recovery period could take between 90 and 180 days for coarse-grained (sand/gravel) and for fine-grained (silt/clay) subgrades [*MEPDG*, 2004].

In evaluation of the backcalculated pavement properties, having more information about the in-situ properties of these pavements, especially the temperature and the frost depth (if any), at the time of testing could be beneficial. Figure 47 sheds light on the topic of frost-thaw cycle in Minnesota by presenting the frost depth variation during the years 1994 and 1995 (the years at which the FWD data were collected for MnDOT sections) for two LTPP sections located in a similar general area in the state of Minnesota. This information was recorded under the seasonal monitoring program (SMP) by boring holes in the pavements.

In Figure 47, the continuous line is the temperature, the dashed line is the water freezing temperature, and the blue area demonstrates the frost layer and its variation with respect to the pavement surface (depth equal to zero represents the pavement). A short description of these LTPP sections is provided in each graph. Detailed information can be found in *FHWA* [2017]. These two sections are selected because of the resemblance with the MnDOT sections, i.e., no subbase layer with both coarse- and fine-grained subgrades.

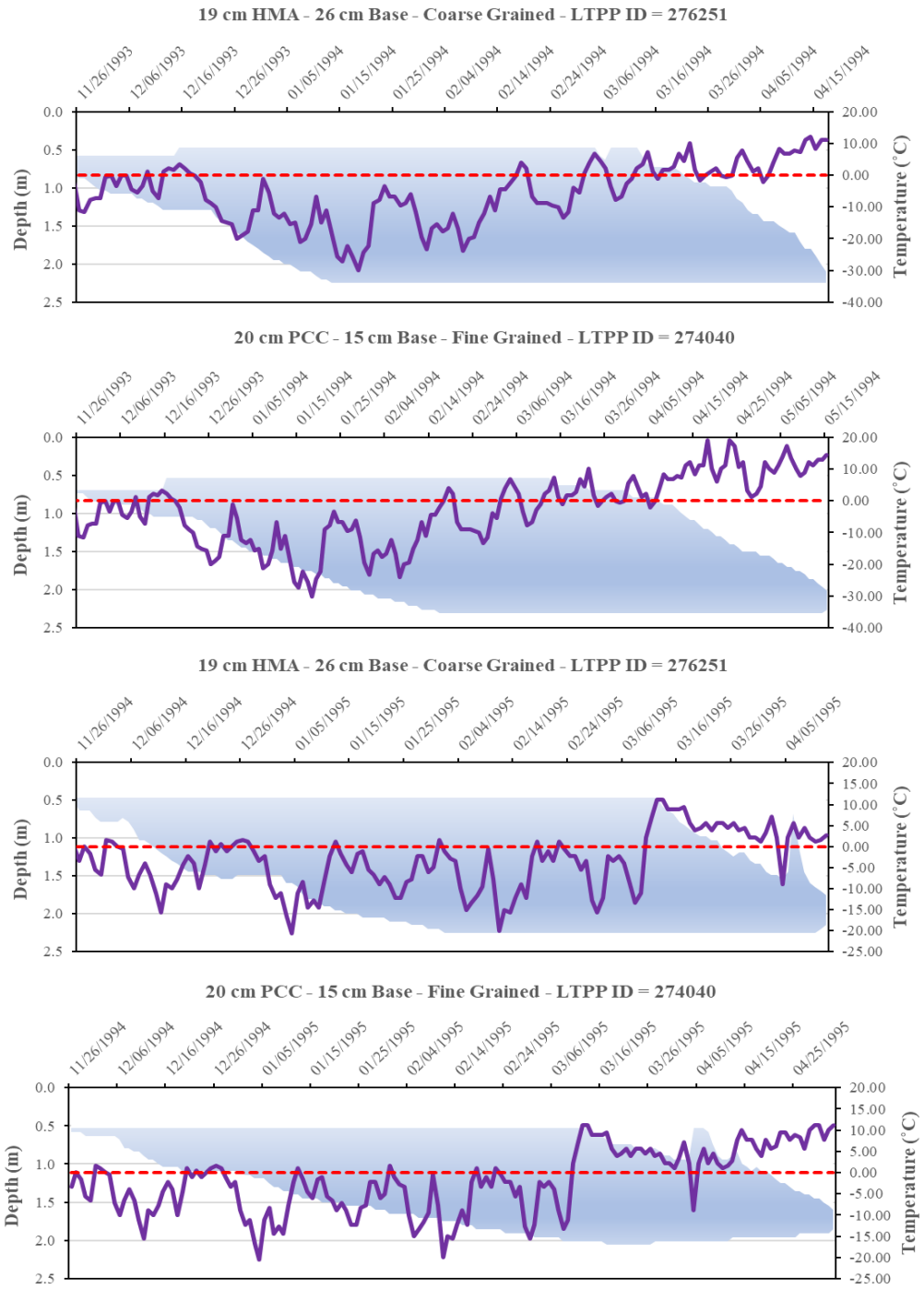

Figure 47. In-situ frost depth measurements for LTPP sections with coarse- and fine-grained subgrades located in Minnesota during the years 1994 and 1995

The following points can be inferred from Figure 47 for the years 1994 and 1995:

- Frost is initiated in late November when the underlying ground water turns into ice due to consistent subzero ambient temperature.
- Frost is formed from the top of the grade and penetrates through the depth of the foundation.
- Both for the coarse- and fine-grained subgrades, the maximum depth of the frost is about 2.3 m.
- Thawing starts to occur in both years in the first half of March when the average ambient temperature rises above the freezing temperature.
- Similar to the formation of the ice, thawing happens from the top of the frost as the temperature of the top layers rises with the ambient temperature.
- During the month of April, the thickness of the frost layer drops to roughly the half of the maximum depth.
- Thawing approaches its end in late April and early May.
- As expected, the coarse-grained subgrade thaws faster relative to the fine-grained subgrade.

The backcalculated soil properties are listed in Table 16. Due to the frost-thaw cycle experienced by sections A1 and A2, there is a clear variation in the soil properties, especially E_s and γ; nevertheless, the variation trend, e.g. moduli ascent or descent, for both soil types seems fairly identical.

In March (03/13/1995), the smallest E_s was attributed to both soil types, which was associated with the highest γ, smallest m_f and G, and high K. The test was performed in mid-March in the year 1995; exactly around that period, the thawing process started due to the consistent above-zero temperature (Figure 47). The thawing negatively impacted the quality of the top soil, while a thick layer of frosted soil was still present (about 1.5 m depth). The large γ-values (4.26 and 5.27) indicate that the vertical displacement dissipates very quickly in the top 0.5 m of the grade (see Figure 29 and Figure 30). On the other hand,

the small value of the foundation inertial mass means that the applied FWD load was not able to mobilize the foundation. The shape of the deflection profiles in Figure 39 and Figure 40, i.e., the lack of oscillation in the tail, indicates a small inertial mass as well.

The overall evaluation of these values suggests that the thick frost layer did not experience significant deformations under the FWD loading, so the model detected the presence of this relatively rigid layer, and attributed the moduli only to the top thawed and weak portion of the foundation.

In the second half of April (04/17/1995), the frost layer thawed to half of its maximum thickness; the large m_f for both subgrades demonstrates that a large portion of the underlying soil is mobilized under the dynamic FWD load. This suggests that the rigidity of the thinner frost layer is not sufficient to behave as a rigid layer. As a result, the modified Vlasov model attributes an overall E_s to the combination of thawed base and thin frost layer, which led to the high elasticity moduli. This speculation is supported by the smaller γ, which shows that the induced vertical strain on the pavement surface penetrates through the assumed depth of the grade (5 m).

In second half of May (05/18/1995), thawing was completed; thus, as noted before, the grade experienced its weakest state. The backcalculation analysis assigned low stiffness to the soil for both sections, which confirms this phenomenon.

In the following months (June and August of 1995), both sections went through the recovery period during which the subgrade became more resilient. This is manifested in the higher backcalculated E_s. It is worthwhile to mention that the drop of the moduli for Case A1 with sandy soil with respect to the unfrozen state (in August) is equal to

$\frac{291.0\ MPa}{379.9\ MPa} = 0.77$; this ratio for Case A2 with silty-clayey soil is equal to $\frac{74.1\ MPa}{216.9\ MPa} = 0.34$. Interestingly, the in-situ backcalculated reduction factors obtained here agree with the previously-mentioned suggested reduction factors used for design and evaluation of pavements (0.55-0.85 for sandy soil, and 0.4-0.6 for silty-clayey soil).

Cases B1 and B2

These two pavements are fabricated with fairly similar subgrade material as A1 and A2. The HMA layers were constructed directly on subgrades (no base layer).

As shown in Figure 41, in the month of February, the deflections are smaller compared to the next measurements in the month of April (99 μm vs 374 μm for B1, and 31 μm vs 352 μm for B2) which could be attributed to multiple reasons:

- Due to absence of base and subbase layers, and since the subgrade was fully frozen at -5.6 ˚C, the frozen soil behaved as an extremely stiff layer.
- There is no guarantee that the FWD device performs accurately at harsh subzero temperatures (here -5.6 ˚C).
- Due to very small recorded displacements, the ratio of systematic error (noise) to real measurements inherent in any test device increases, which in turn impacts the accuracy of measurements negatively.

Assuming that the collected data is reliable, the backcalculation was performed on the data collected in February. An acceptable fit was obtained for Case B1, while the fit for Case B2 was very poor. The obtained E_s were very large, in particular for the silty-clayey subgrade. The ratio of the frozen in-situ elastic modulus to the unfrozen state (in October) is equal to $\frac{760.4\ MPa}{388.5\ MPa} = 1.96$ for the sandy subgrade, and $\frac{2260.4\ MPa}{226.3\ MPa} = 10.00$ for the silty-

clayey subgrade. Very large foundation inertial mass was obtained through the backcalculation, in particular for the silty-clayey soil. This observation may be explained by mentioning that the stiff frosted layer, if mobilized, moves as a unit, which results in large values of m_f. Silty-clayey soil is a more frost-susceptible material, which could explain why the change of the modulus is more pronounced.

For the test data recorded in the next months (April, June, September, and October), a trend similar to what was described for the PCC sections (A1 and A2) was observed. In other words, a drop in the modulus due to thawing was followed by the recovery period.

Case C3

This section is located in Nevada. The cores taken in the year 2000 through the SMP program verified that no frosting took place due to the considerably higher average temperature. Therefore, other than the soil moisture variation due to the change of the underground water level, no major source of climatic impact exists. Whence, the expectation is to see fairly similar backcalculated soil properties. The values listed in Table 16 confirm this statement, as the elastic and viscoelastic properties of the soil as well as the γ-value did not encounter notable changes.

Foundation Properties – Comparison

Soil Elastic Modulus vs Resilient Modulus

With the exception of Case B1, the resilient modulus test results with different confining pressures are available for the sections studied here. The tests were performed as part of the MnROAD and LTPP investigations. For the Cases C1, C2, and C3 (LTPP sections), the resilient moduli for the lime-treated soil as part of the subbase were not available. The

results are tabulated in Table 18, and compared with the backcalculated instantaneous elastic modulus of the unfrozen soil.

Many researchers have tried to find a correlation between the resilient modulus and the elastic modulus of the desired pavement layer. A range of 1.5-4.0 has been reported for the ratio of elastic modulus to resilient modulus [*Tanyu et al.*, 2003]. The discussion is still ongoing and no consensus has been reached yet. The roots for this difference are still unknown but may be described by the following reasons [*Xu*, 2014]:

- The difference between the test conditions such as the small specimen tested in the lab as compared with the in-situ conditions.
- The difference between the several confining pressures applied in the lab and the in-situ pressure at the time of testing.
- Variable axial load applied in the lab does not necessarily simulate the actual dynamic loading exerted by FWD device.
- The FWD test is performed on a different date with an environmental condition unique to the time of testing such as moisture, freezing, etc.

The seasonal effects noted earlier, as well as the vague understanding about the soil elastic modulus, especially in the harsh climatic conditions, puts more emphasis on the key role that a proper non-destructive test and associated inverse analysis can play in the design and evaluation of pavements and other slab-on-grade structures.

For Cases A1 and A2, the sandy subgrade is stiffer than the silty-clayey subgrade with a ratio of 1.88 and 1.75 for M_R and E_s, respectively, which shows that the elastic modulus follows a similar ratio. Also, the ratio of E_s/M_R is equal to 2.92 and 3.14 for sandy and

silty-clayey soils. This value for B2 is equal to 2.29. This ratio is within the range of 1.50-4.00 recommended in the literature [*Tanyu et al.*, 2003].

For the multi-layer sections (Cases C1, C2, and C3), it is not rational to compare the elastic modulus with the resilient modulus of each layer, or only the subgrade, or the average of the layers (especially because there is no M_R assigned to the lime-treated soil subbase). Even though the subgrade for these sections has the stiffness similar to that of silty-clayey subgrades (Cases A2 and B2), the contribution of the relatively thick layers of base and subbase led to a greater overall stiffness of the foundation. This explains the larger backcalculated elastic modulus for these multi-layered pavement sections.

Table 18. Resilient modulus for pavement layers vs soil backcalculated elastic modulus

Case	Layer	# of tests	Min	Max	Median	Mean	σ	E_s
		-	MPa	MPa	MPa	MPa	MPa	MPa
A1	Subgrade	90	49	220	138	130	47	379.9
A2	Subgrade	135	22	138	66	69	33	216.9
B1	Subgrade	NA[1]	NA	NA	NA	NA	NA	388.5
B2	Subgrade	90	40	180	99	99	33	226.3
C1	Base	45	72	292	175	168	59	285.7
	Subbase	NA	NA	NA	NA	NA	NA	
	Subgrade	15	58	99	72	75	13	
C2	Base	90	55	297	170	167	61	308.9
	Subbase	45	105	335	221	218	63	
	Subgrade	60	32	99	58	58	16	
C3	Base	45	55	297	169	167	63	426.7
	Subbase	45	105	335	221	218	63	
	Subgrade	45	32	76	52	52	12	

[1]NA: Not available

Static vs Dynamic Backcalculation

The results of the dynamic backcalculation were compared with the results of the conventional static backcalculation. The static backcalculation software used in this study, BAKFAA, is formulated based on the layered elastic theory [*BAKFAA*, 2012]. This approach assigns an elastic modulus to each layer, ignoring the viscoelastic properties of the comprising materials, and analyzes the pavement response to the peak FWD load. Since this software is one of the established static backcalculation schemes available, the comparison of the BAKFAA-backcalculated in-situ elastic moduli with the proposed dynamic moduli could be beneficial.

For the multi-layered pavements (Cases C1, C2, and C3), the backcalculation was initially performed using BAKFAA by including all the layers, their individual Poisson's ratios, and thicknesses. Because of the similarities of the Poisson's ratios, the backcalculated moduli for each layer varied around a certain number, and in some cases, unreasonably large or small moduli were assigned to a particular layer. To avoid such issues and to facilitate the comparison with the dynamic analyses based on the Vlasov approach, the BAKFAA was performed assuming that all pavement sections in this study are constructed directly over the subgrade with no base or subbase layers. This approach attributes one elastic modulus to multiple layers that represent the overall behavior of the soil stratum. The results of the static and dynamic backcalculation are presented in Table 19.

For Case B2 in February, a very poor fit was achieved using BAKFAA. Because of the very small recorded displacements in this month, the software computed an extremely large and unreasonable elastic modulus for the asphalt layer. For Cases A1 and A2 in March, BAKFAA attributed large soil modulus relative to the other months, which is related to the presence of thick frost layer in that month. As mentioned earlier, the dynamic analysis was

able to detect the relatively rigid frost layer, and to calculate the modulus for the top soil layer in the thawing condition; that is why the trend is not the same for those observations. For all the other FWD tests, an acceptable fit was obtained.

Table 19. Comparison of backcalculated pavement parameters using static (BAKFAA) versus the proposed dynamic inverse analysis

Case	Test Date	Air Temp.	Static		Dynamic			
			E_s	E_p	E_s	E_{s1}	E_p	E_{p1}
		˚C	MPa	GPa	MPa	MPa	GPa	GPa
A1	3/13/1995	-0.6	287.0	29.63	246.7	29.6	48.43	48.43
	4/17/1995	8.9	196.4	42.25	631.0	107.3	44.25	44.25
	5/18/1995	15.6	145.8	38.51	291.0	61.1	47.57	47.57
	6/20/1995	21.1	209.7	47.07	358.6	121.9	45.66	45.66
	8/18/1995	21.7	193.9	41.59	379.9	106.4	45.05	45.05
A2	3/13/1995	-0.6	211.8	24.26	42.8	10.7	38.80	38.80
	4/17/1995	8.9	89.3	27.98	206.8	16.5	33.66	33.66
	5/18/1995	15.6	72.1	24.08	74.1	10.4	35.40	35.40
	6/20/1995	21.1	95.1	26.99	158.5	25.4	32.78	32.78
	8/18/1995	21.7	99.5	26.77	216.9	21.7	33.82	33.82
B1	2/18/1994	-5.6	766.8	7.38	760.4	205.3	13.64	13.64
	4/20/1994	10.0	140.2	5.25	298.7	47.8	8.70	8.70
	6/22/1994	21.7	146.5	0.92	213.0	85.2	0.83	0.00
	9/21/1994	15.6	131.7	1.75	232.0	76.6	1.54	0.22
	10/25/1994	7.2	114.6	6.22	388.5	38.9	9.62	9.62
B2	2/18/1994	-5.6	1092.9	203.52	2260.4	406.9	12.94	12.94
	4/20/1994	10.0	120.3	5.93	211.1	35.9	8.01	8.01
	6/22/1994	21.7	81.7	0.47	106.0	40.3	0.87	0.00
	9/21/1994	15.6	110.3	0.81	166.1	51.5	1.24	0.00
	10/25/1994	7.2	145.4	6.40	226.3	33.9	10.84	10.84
C1	6/13/2000	40.1	173.4	16.66	285.7	37.1	19.42	19.42
C2	6/21/2000	50.0	254.9	1.32	308.9	117.4	0.59	0.00
C3	2/2/2000	1.4	300.9	21.40	381.4	129.7	24.98	24.98
	3/24/2000	16.5	291.8	15.85	497.0	124.3	18.29	18.29
	5/9/2000	18.2	280.7	11.24	442.4	137.1	10.10	8.99
	8/3/2000	34.9	280.2	4.17	446.7	142.9	4.16	1.25
	9/28/2000	23.7	273.5	8.60	351.5	137.1	6.79	4.28
	11/7/2000	3.9	283.2	18.90	440.9	127.9	22.58	22.58

Other than the months during which frosting occurred, generally the elastic modulus of the soil follows the same trend (increase or decrease) as the dynamic instantaneous modulus. The same is true for the HMA top layers. For instance, both backcalculation methods indicated that the asphaltic top layers for Cases B1 and B2 have very similar properties at each test temperature. For the PCC pavements (A1 and A2), BAKFAA computed more or less similar modulus during different seasons, which is in line with the expectation. However, the dynamic modulus was generally greater than the elastic modulus.

For the asphalt top layers and the soil stratum, the three-parameter viscoelastic model is assigned to account for the time-depending behavior of these layers under dynamic loading. The relaxation function selected in this study reduces the moduli from the instantaneous modulus, E, at $t = 0$ to the long-term modulus, E_1, when t approaches infinity, as shown in Figure 25 and Figure 26. Therefore, it is reasonable to expect an elastic modulus, computed by the static backcalculation, somewhere in between these two extremes. As can be observed from Table 20, the majority of the statically backcalcuated subgrade elastic moduli have values between the two bounds indicated by the corresponding backcalculated subgrade relaxation functions from the generalized Vlasov model. The same holds true for the top asphalt layers. For most cases, the elastic modulus of the top layer lies in the range provided by the dynamic analysis.

Generalized Pasternak Model vs Generalized Vlasov Model

The Vlasov and Pasternak models yield the same governing differential equation for plate-foundation interaction, but the generalized Vlasov model introduces additional restrictions on the model parameters. Naturally, it may reduce goodness of fit between the measured and predicted FWD deflection profiles. This concern was discussed earlier in detail and

depicted in Figure 30, Figure 31 and Figure 32. To investigate this more in detail, a comparison between the fits obtained using the generalized Pasternak model (GPM) presented in Chapter 4 and the generalized Vlasov model (GVM) was conducted using the LTPP sections located in Nevada (Cases C1, C2, and C3). The backcalculated slab properties and the associated error values (SSE) are tabulated here in Table 20 for both GPM and GVM.

Table 20. Comparison of backcalculated slab properties and errors using GVM versus GPM

Model	Case	Test Date	Air Temp.	Slab Properties				Error (SSE)
				E_p	E_{1p}/E_p	τ_p	v_p	
			˚C	GPa	-	ms	-	-
GVM	C1	6/13/2000	40.1	19.42	1.00	-	0.15	2.08
	C2	6/21/2000	50.0	0.59	0.00	5.01	0.35	4.66
	C3	2/2/2000	1.4	24.98	1.00	-	0.15	7.98
		3/24/2000	16.5	18.29	1.00	-	0.25	6.75
		5/9/2000	18.2	10.10	0.89	27.54	0.30	5.67
		8/3/2000	34.9	4.16	0.30	7.76	0.35	4.56
		9/28/2000	23.7	6.79	0.63	10.47	0.30	6.45
		11/7/2000	3.9	22.58	1.00	-	0.18	7.50
GPM	C1	6/13/2000	40.1	18.14	1.00	-	0.15	2.42
	C2	6/21/2000	50.0	1.02	0.00	10.42	0.35	7.85
	C3	2/2/2000	1.4	27.06	1.00	-	0.15	6.95
		3/24/2000	16.5	17.54	0.92	41.13	0.25	7.04
		5/9/2000	18.2	14.43	0.84	34.40	0.30	5.97
		8/3/2000	34.9	5.26	0.00	7.97	0.35	4.79
		9/28/2000	23.7	9.70	0.46	13.63	0.30	6.12
		11/7/2000	3.9	23.99	1.00	-	0.18	7.10

Based on the error values, SSE, there is no significant difference between these two backcalculation methods. In some cases, the error value was even reduced when using the GVM. This is due to the fact that, in the GVM, the viscoelastic behavior of the foundation is simulated with three-parameter SLS model, while in the GPM, the two parameters, *k* and

c, represent the elastic and viscous behavior of the foundation, respectively. The enhancement of the fit due to the addition of this parameter counteracts the restrictions put on the parameter search. Despite having different foundation models, the backcalculated slab properties seem similar. Figure 48 shows the deflection profiles generated with these two models for testing in May 2000 for section C3. It confirms that these two models yield very similar deflection basins, so they both can be used to simulate the behavior of the viscoelastic slab-on-grade structures.

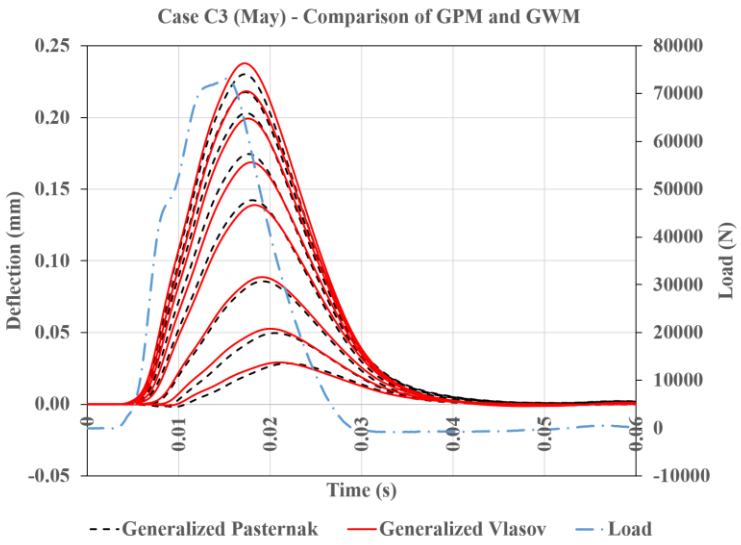

Figure 48. Comparison of the deflection profiles generated with generalized Pasternak and generalized Vlasov models for Case C3 in May 2000

Overall, it was shown that the generalized Vlasov model is able to provide useful information about the physical properties of the foundation without losing the accuracy of the fit between the model predictions and the field observations.

5.9. Conclusions

In this study, a generalized Vlasov model was considered to simulate the problem of a thin viscoelastic slab-on-grade subjected to short-duration dynamic loading. This was done to overcome one of the drawbacks of the mechanical foundation models, such as the generalized Pasternak model, by making a connection between the model parameters and the physical properties of the comprising soil materials. The generalized Vlasov model accounts for damping and inertia effects of the foundation. The governing differential equation for this problem was solved in the time domain, and verified by making a comparison with the analytical solution for a known sinusoidal load. An efficient and reliable inverse solution was developed and verified to backcalculate the pavement properties by matching the model predicted deflections with the field-measured deflections. The inverse solution uses multiple seeding values for the sought properties to overcome the potential issue of non-uniqueness. The seeding values for the moduli of slab and grade are randomly generated following a normal distribution around the backcalculated moduli obtained from a static backcalculation, BAKFAA.

Finally, a comprehensive field study was conducted to evaluate the ability of the proposed forward- and inverse-solutions to describe the response of slab-on-grade systems. This was done by analyzing the measured response of several pavement sections to the dynamic circular load of the falling weight deflectometer (FWD) test device. The selected pavement sections are located in the state of Minnesota and Nevada to represent very different climatic conditions. The results of the performed analyses are summarized below.

- The traditional elastic weightless Vlasov foundation model cannot describe the behavior of the slab-on-grade system under short-period dynamic loading. Accounting for the damping and inertia effects of the soil enhances the correlation between the model predictions and field observations.

- The agreement between the observed and calculated responses showed that the proposed viscoelastic slab-on-generalized Vlasov model is capable of simulating the behavior of thin slabs with various mechanical properties (very thin asphalt layer in high test temperature versus thicker concrete slabs).
- The analyses indicated that the material constraints imposed on the model parameters, as opposed to the unconstrained model parameters in the generalized Pasternak model, did not negatively impact the model correlations with the field observations.
- The use of the generalized Vlasov foundation reinforced the analysis with the ability to characterize the soil in addition to the top slab. This was supported by the reasonable properties of both HMA and PCC top layers, as well as the realistic characteristics of various grade types, e.g., sandy and silty-clayey soil.

Overall, this study demonstrates that the modified Vlasov model is able to describe the dynamic behavior of slab-on-grades. For more accurate evaluations, the exact depth to the rigid layer must be introduced as an input. The connection made between the model parameters and the material properties allows for the accurate evaluation of the existing structures. Because of the simplistic yet robust finite difference approach employed here, it constitutes a practical tool for utilization in design and analysis of slab-on-grade structures. The reasonable backcalculated pavement properties could also be used as inputs for estimating the deflection-induced fuel consumption and pavement life cycle assessment.

6

Concluding Remarks and Future Perspectives

6.1. Concluding Remarks

In this effort, the problem of slab-on-grade subjected to short-duration dynamic load was studied. The structure was described as a thin and infinite viscoelastic Kirchhoff-Love plate resting on a foundation. A gradient-based optimization scheme was employed in conjunction with a forward-solution in the time domain to develop a fast and reliable dynamic backcalculation. The shortcomings of the traditional foundation models, such as the Winkler, Pasternak and Vlasov models, in capturing the dynamic behavior of the system were highlighted, and required modifications were made. This was accomplished by making comparisons between the model predictions and the field data collected by falling weight deflectometer (FWD). The main results of this work can be summarized as follows:

- The traditional elastic weightless Winkler, Pasternak, and Vlasov foundation models cannot capture the behavior of the slab-on-grade system under short-duration dynamic loading of FWD.
- The generalized Winkler model was introduced. A field study, performed on both asphalt and concrete pavements, indicated that accounting for the soil inertia and damping effects is fundamental for dynamic analysis of foundations.

- The deflection-induced pavement-vehicle interaction analysis (PVI) was modified according to the generalized Winkler model to make the calculation of the pavement surface deflection more accurate. This offered a reasonable approach that established a link between the in-situ structural performance of the pavement to the fuel consumption of moving vehicles. It was demonstrated that a significant portion of the energy dissipation occurs in the soil stratum, which suggests that ignoring this effect may lead to underestimation of the energy dissipation, especially for concrete pavements. The simplicity of the described model and the availability of FWD device and measurements makes the proposed methodology an attractive tool for performing network scale analyses and, potentially, for designing more sustainable roads.
- Despite the improvements made to the Winkler model, the fit found for the asphalt pavement was not as good as that of the concrete pavement. This issue was addressed by making use of the generalized Pasternak model, which accounts for the shear resistance of the soil medium, as well as inertia and damping forces. This improved the fit and resulted in more reasonable backcalculated parameters.
- One of the issues associated with the generalized Pasternak model is that the mechanical elements used in the model are not directly dependent on the physical properties of the comprising materials, even though each represents a particular physical behavior of the grade. To address this limitation, the Vlasov approach was employed and modified to accommodate damping and inertia effects. The development of the generalized Vlasov model reinforced the analysis with the ability to characterize the soil in addition to the top slab.

These investigations culminated in the development of a fast and efficient quantitative tool to assess the structural properties of slab-on-grades. Furthermore, this thesis has implications for pavement design and analysis. In the AASHTO M-E procedure for flexible

pavements, the viscoelasticity of the system is accounted for through the HMA complex modulus only. At the same time, the subgrade is assumed to behave as an elastic body. This study indicates that viscoelastic properties of the subgrade may affect the responses of flexible pavements, which has implications for pavement design. This highlights the need for further investigation of this phenomenon.

6.2. Future Research

Some of the future research directions can be outlined here:

- The so-called PVI analysis could be modified according to the generalized Vlasov model to develop a more powerful tool. Since the analysis is fairly quick, a network level study could be carried out to demonstrate the macro-scale impact of the excess fuel consumption and greenhouse gas emissions.
- It would be more realistic to describe the asphalt surface as a compressible layer. This may potentially enhance the fit for the HMA layers tested at high ambient temperature, especially for the deflection profiles recorded by outer sensors.
- Since the numerical analysis provides us with the dynamic asphalt modulus, it can be used to obtain the in-situ asphalt master curve which is one of the primary MEPDG design inputs for design of asphalt pavements. However, it is argued that the simplistic viscoelastic models such as Maxwell model, Kelvin model, and standard linear solid model would not be able to well capture the master curve of complex moduli of asphaltic material at a full-range of reduced frequency. The generalized Maxwell model, generalized Kelvin model, Huet-Sayegh model, and sigmoidal function could capture the master curve of dynamic modulus at a wide range of reduced frequency. This could also improve the fit as the more generalized viscoelastic model better represents the viscoelastic characteristics.

- The applicability of the mentioned models for a wider range of pavement systems, such as sections supported with a cement-treated base, should be further investigated.
- The reported results for the generalized Vlasov model during the frost seasons offered promise that the backcalculation analysis could detect the presence of a rigid layer. Further study must be conducted to support this speculation.
- Vlasov offered an approach to formulate a two-layered foundation. This approach could be used (or extended) to account for the base and subbase. This allows for assigning different properties to the base/subbase versus the subgrade.
- A relationship between the resilient moduli and the backcalculated dynamic moduli can be achieved by making the laboratory and in-situ test conditions more analogous, e.g., use the confining pressure that emulates the pressure experience by the soil induced by the FWD impulse load. A methodology can be developed to assign an equivalent resilient modulus for multi-layered foundations.
- Finally, the findings of this study offer promise for advancing the dynamic analysis for other applications. For instance, the emerging non-destructive technologies such as rolling weight deflectometer (RWD) could be benefitted with the guidelines highlighted in this study.

References

Akbarian, M. (2015). Quantitative sustainability assessment of pavement-vehicle interaction: from bench-top experiments to integrated road network analysis. Doctoral dissertation, Massachusetts Institute of Technology.

Allen, R.G., Walter, I. A., Elliott, R., Howell, T., and Itenfisu, D. (2005). ASCE's standardized reference evapotranspiration equation, ASCE-EWRI Task Committee Report.

Al-Khoury, R., Scarpas, A., Kasbergen, C., and Blaauwendraad, J. (2001a). Spectral element technique for efficient parameter identification of layered media. I. Forward calculation. International Journal of Solids and Structures, 38(9), 1605-1623.

Al-Khoury, R., Kasbergen, C., Scarpas, A., and Blaauwendraad, J. (2001b). Spectral element technique for efficient parameter identification of layered media: Part II: Inverse calculation. International Journal of Solids and Structures, 38(48), 8753-8772.

Al-Khoury, R., Scarpas, A., Kasbergen, C., and Blaauwendraad, J. (2002). Spectral element technique for efficient parameter identification of layered media. Part III: viscoelastic aspects. International Journal of Solids and Structures, 39(8), 2189-2201.

ARA Inc. (2003). Guide for Mechanistic-Empirical Design of New and Rehabilitated Pavement Structures, Appendix QQ: Structural Response Models for Rigid Pavements. Report submitted to NCHRP and Transportation Research Board of the National Research Council. http://onlinepubs.trb.org/onlinepubs/archive/mepdg/2appendices_qq.pdf [Accessed Feb 2017]

Ardekani, S. A., and Sumitsawan, P. (2010). Effect of pavement type on fuel consumption and emissions in city driving, RMC Research and Education Foundation. http://www.rmc-foundation.org/images/UTA%20Fuel%20Consumption-Emissions%20Study%20Final%203-10.pdf

Ataman, M., and Szcześniak, W. (2014). Dynamic Stability of an Infinite Non-Homogenous Euler's Beam Resting on a Three-Parameter Inertial Foundation, Subjected to a Moving Distributed Load. Procedia Engineering, 91, 75-80.

Auersch, L. (1996). Dynamic plate-soil interaction—finite and infinite, flexible and rigid plates on homogeneous, layered or Winkler soil. Soil Dynamics and Earthquake Engineering, 15(1), 51-59.

Avramidis, I. E., and Morfidis, K. (2006). Bending of beams on three-parameter elastic foundation. International Journal of Solids and Structures, 43(2), pp. 357-375.

Ayvaz, Y., Daloglu, A., and Dogangün, A. (1998). Application of a modified Vlasov model to earthquake analysis of plates resting on elastic foundations. Journal of sound and vibration, 212(3), 499-509.

Ayvaz, Y., and Özgan, K. (2002). Application of modified Vlasov model to free vibration analysis of beams resting on elastic foundations. Journal of sound and vibration, 255(1), 111-127.

Ayvaz, Y., and Oguzhan, C. B. (2008). Free vibration analysis of plates resting on elastic foundations using modified Vlasov model. Structural Engineering and Mechanics, 28(6), 635-658.

BAKFAA (2012), Static Backcalculation Software, U.S. Department of Transportation, Federal Aviation Administration, Version 2.0. http://www.airporttech.tc.faa.gov/Download/Airport-Pavement-Papers-Publications-Detail/dt/Detail/ItemID/35/BAKFAA-version-20,-released-May-2012.

Basu, D., and Kameswara Rao N. S. V. (2013). Analytical Solutions for Euler–Bernoulli Beam on Visco-Elastic Foundation Subjected to Moving Load. International Journal for Numerical and Analytical Methods in Geomechanics, 37(8), 945-960.

Berd, R. (1997). Calculating Maximum Frost Depths at MnROAD Winters 1993-94, 1994-95 and 1995-96. Minnesota Department of Transportation, Report No. MN/RC – 97/21.

Booshehrian, A., Mogawer, W. S., and Bonaquist, R. (2012). How to construct an asphalt binder master curve and assess the degree of blending between RAP and virgin binders, Journal of Materials in Civil Engineering 2012, 25(12), 1813-1821.

Çalım, F. F. (2009). Dynamic analysis of beams on viscoelastic foundation. European Journal of Mechanics-A/Solids, 28(3), 469-476.

Celik, M., and Omurtag, M. H. (2005). Determination of the Vlasov foundation parameters-quadratic variation of elasticity modulus-using FE analysis. Structural Engineering and Mechanics, 19(6), 619-637.

Chatti, K., and Kim, T. (2001). Simple dynamic backcalculation procedure for falling weight deflectometer testing of rigid pavements. Transportation Research Record: Journal of the Transportation Research Board, (1764), 30-38.

Chatti, K. (2004). Use of dynamic analysis for interpreting pavement response in falling weight deflectometer testing. Materials evaluation, 62(7), 764-774.

Chatti, K., and Zaaber, I. (2012). Estimating the effects of pavement condition on vehicle operating costs. NCHRP Report 720. Transportation Research Board of the National Academies, Washington, D.C.

Chatti, K., Kutay, M. E., Lajnef, N., Zaabar, I., Varma, S., and Lee, H. S. (2017). Enhanced Analysis of Falling Weight Deflectometer Data for Use With Mechanistic-Empirical Flexible Pavement Design and Analysis and Recommendations for Improvements to Falling Weight Deflectometers (No. FHWA-HRT-15-063).

Christensen, R. (1982). Theory of viscoelasticity: An introduction, Academic Press, New York.

Chupin, O., Piau, J. M., and Chabot, A. (2013). Evaluation of the structure-induced rolling resistance (SRR) for pavements including viscoelastic material layers. Materials and structures, 46(4), 683-696.

Colasanti, R. J., and Horvath, J. S. (2010). Practical subgrade model for improved soil-structure interaction analysis: software implementation. Practice Periodical on Structural Design and Construction, 15(4), 278-286.

Coleri, E., Harvey, J. T., Zaabar, I., Louhghalam, A., and Chatti, K. (2016). Model Development, Field Section Characterization, and Model Comparison for Excess Vehicle Fuel Use Attributed to Pavement Structural Response. Transportation Research Record: Journal of the Transportation Research Board, 2589, 40-50.

Corps of Engineers (1984), Pavement Criteria for Seasonal Frost Conditions, U.S. Army Corps of Engineers, Washington, D.C., Engineer Manual No. 1110-3-138.

Daloglu, A., Do angün, A. and Ayvaz, Y. (1999). Dynamic analysis of foundation plates using a consistent Vlasov model. Journal of Sound and Vibration, 224(5), 941-951.

Daloglu, A. T., and Ozgan, K. (2004). The effective depth of soil stratum for plates resting on elastic foundation. Structural Engineering and Mechanics, 18(2), 263..

Das, A. (2014). Analysis of pavement structures. CRC Press, Taylor & Francis Group, LLC., ISBN: 978-1-4665-5856-4.

Dennis Jr, J. E., and Schnabel, R. B. (1996). Numerical methods for unconstrained optimization and nonlinear equations. Society for Industrial and Applied Mathematics.

Dong, Q. X., Hachiya, Y., Takahashi, O., Tsubokawa, Y., and Matsui, K. (2002). An efficient backcalculation algorithm of time domain for large-scale pavement structures using Ritz vectors. Finite elements in analysis and design, 38(12), 1131-1150.

Elseifi, M., Abdel-Khalek, A. M., and Dasari, K. (2012). Implementation of rolling wheel deflectometer (RWD) in PMS and pavement preservation. FHWA/11.492. Baton Rouge, LA: Louisiana Transportation Research Center.

Ferreira, A. J. M, Roque, C. M. C, Neves, A. M. A., Jorge, R. M. N. and Soares C. M. M. (2010). Analysis of Plates on Pasternak Foundations by Radial Basis Functions. Computational Mechanics, 46(6), 791-803.

FHWA (2017). U.S. Department of Transportation. LTPP: Long-Term Pavement Performance Program. http://www.infopave.com/ Accessed 2017.

Filonenko-Borodich, M. M. (1940). Some Approximate Theories of The Elastic Foundation. Uchenyie Zapiski Moskovskogo Gosudarstuennogo Universiteta Mechanika, 40, 3-18.

Fwa, T. F., Shi, X. P., and Tan, S. A. (1996). Use of Pasternak Foundation Model in Concrete Pavement Analysis. Journal of transportation engineering, 122(4), 323-328.

Foinquinos, R., Roesset, J. M., and Stokoe, K. H. (1993). FWD-DYN, a Computer Program for Forward Analysis and Inversion of Falling Weight Deflection Data (No. TX-94-1970-1F). Center for Transportation Research, Bureau of Engineering Research, the University of Texas at Austin.

Gill, P. E., and Murray, W. (1976). Minimization subject to bounds on the variables. National Physical Laboratory, Division of Numerical Analysis and Computing.

Goktepe, A. B., Agar, E. and Lav., A. H. (2006). Advances in backcalculating the mechanical properties of flexible pavements. Advances in engineering software, 37(7), 421-431.

Grenier, S., Konrad, J. M. and LeBœuf, D. (2009). Dynamic simulation of falling weight deflectometer tests on flexible pavements using the spectral element method: forward calculations. Canadian Journal of Civil Engineering, 36(6), 944-956.

Gschösser, F., and Wallbaum, H. (2013). Life cycle assessment of representative swiss road pavements for national roads with an accompanying life cycle cost analysis. Environmental science & technology, 47(15), 8453-8461.

Guzina, B., and Osburn, R. (2002). Effective tool for enhancing elastostatic pavement diagnosis. Transportation Research Record: Journal of the Transportation Research Board, (1806), 30-37.

Hadidi, R., and Gucunski, N. (2010). Comparative study of static and dynamic falling weight deflectometer back-calculations using probabilistic approach. Journal of Transportation Engineering, 136(3), 196-204.

Hasheminejad, S. M., Gheshlaghi, B. (2012). Three-dimensional Elastodynamic Solution for an Arbitrary Thick FGM Rectangular Plate Resting on a Two Parameter Viscoelastic Foundation. Composite Structures, 94(9), 2746-2755.

Hetenyi, M. (1950). A General Solution for The Bending of Beams on an Elastic Foundation of Arbitrary Continuity. Journal of Applied Physics 1950, 21(1), 55-58.

Horvath, J. S. and Colasanti, R. J. (2011). Practical subgrade model for improved soil-structure interaction analysis: model development. International Journal of Geomechanics, 11(1), 59-64.

Howard, I. and Warren K. (2008). Investigation of thin flexible pavement response between traffic and the falling weight deflectometer (FWD). International Journal of Geotechnical Engineering, 2(4), 329-341.

Huang, Y. H. (1993). Pavement analysis and design. New Jersey: Prentice Hall Inc.

IMSL, Inc. (1994). IMSL MATH/LIBRARY.: Fortran subroutines for mathematical applications. Vol. 2. Visual Numerics, Incorporated, 1994

Irwin, L. H., Yang, W. S., and Stubstad, R. N. (1989). Deflection reading accuracy and layer thickness accuracy in backcalculation of pavement layer moduli. In Nondestructive Testing of Pavements and Backcalculation of Moduli. ASTM International.

Jones, R., and Xenophontos, J. (1977). The Vlasov foundation model. International Journal of Mechanical Sciences, 19(6), 317-323.

Kang Y. V. (1998). Multi-frequency backcalculation of pavement layer moduli. J Transp Eng ASCE, 124(1):73–81.

Kargarnovin, M. H., Younesian, D. (2004). Dynamics of Timoshenko Beams on Pasternak Foundation Under Moving Load. Mechanics Research Communications, 31(6), 713-723.

Kerr, A. D. (1965). A study of a new foundation model. Acta Mechanica, 1(2), 135-147.

Khazanovich, L. (1994). Structural Analysis of Multi-layered Concrete Pavement Systems. Doctoral Dissertation, University of Illinois at Urbana-Champaign.

Khazanovich, L. (2000). Dynamic analysis of FWD test results for rigid pavements. In Nondestructive Testing of Pavements and Backcalculation of Moduli: Third Volume. ASTM International.

Killingsworth, B., and Von Quintus H. (1997). Backcalculation of Layer Moduli of LTPP General Pavement Study (GPS) Sites. US. Department of Transportation, Federal Highway Administration, No. FHWA-RD-97-086.

Kim, Y., and Kim, Y. (1998). Prediction of layer moduli from falling weight deflectometer and surface wave measurements using artificial neural network. Transportation Research Record: Journal of the Transportation Research Board, 1639, 53-61.

Kim, D. K., and Yun, C. B. (2000). Time-domain soil–structure interaction analysis in two-dimensional medium based on analytical frequency-dependent infinite elements. International Journal for Numerical Methods in Engineering, 47(7), 1241-1261.

Kuo, C. M., and Tsai, T. Y. (2014). Significance of subgrade damping on structural evaluation of pavements. Road Materials and Pavement Design, 15(2), 455-464.

Kuo, C. M., Lin, C. C., Huang, C. H., and Lai, Y. C. (2016). Issues in simulating falling weight deflectometer test on concrete pavements. KSCE Journal of Civil Engineering, 20(2), 702.

Kutay, M., Chatti, K., and Lei, L. (2011). Backcalculation of dynamic modulus mastercurve from falling weight deflectometer surface deflections. Transportation Research Record: Journal of the Transportation Research Board, 2227, 87-96.

Lee, H. S. (2014). Viscowave–a new solution for viscoelastic wave propagation of layered structures subjected to an impact load. International Journal of Pavement Engineering, 15(6), 542-557.

Liang, R. Y., and Zhu, J. X. (1995). Dynamic analysis of infinite beam on modified vlasov subgrade. Journal of transportation engineering, 121(5), 434-442.

Louhghalam, A., Akbarian, M., and Ulm, F. J. (2013). Flügge's conjecture: dissipation-versus deflection-induced pavement–vehicle interactions. Journal of Engineering Mechanics, 140(8), 04014053.

Louhghalam, A., Akbarian, M., and Ulm, F. J. (2014a). Scaling relationships of dissipation-induced pavement-vehicle interactions. Transportation Research Record: Journal of the Transportation Research Board, 2457, 95-104.

Louhghalam, A., Akbarian, M., and Ulm, F. J. (2014b). Pavement Infrastructures Footprint: The Impact of Pavement Properties on Vehicle Fuel Consumption. Computational Modelling of Concrete Structures: Proceedings of EURO-C 2014, 2, 1051-1058.

Louhghalam, A., Tootkaboni, M., and Ulm, F. J. (2015a). Roughness-induced vehicle energy dissipation: Statistical analysis and scaling. Journal of Engineering Mechanics, 141(11), 04015046.

Louhghalam, A., Akbarian, M., & Ulm, F. J. (2015b). Roughness-Induced Pavement–Vehicle Interactions: Key Parameters and Impact on Vehicle Fuel Consumption. Transportation Research Record: Journal of the Transportation Research Board, (2525), 62-70.

Lytton, R. L. (1989). Backcalculation of layer moduli, state of the art. NDT of pavements and backcalculation of moduli, AJ Bush and GY Baladi, Eds, 1, 7-38.

Maheshwari, P., and Khatri, S. (2010). Nonlinear response of footings on granular bed-stone column-reinforced poor soil, International Journal of Geotechnical Engineering 4(4), 435-443.

Maheshwari, P., and Khatri, S. (2012). Generalized model for footings on geosynthetic-reinforced granular fill-stone column improved soft soil system. International Journal of Geotechnical Engineering, 6(4), 403-414.

Maheshwari, P. (2014). Infinite beams on stone column reinforced tensionless earth beds under moving loads, International Journal of Geotechnical Engineering, 8(1), 21-25.

Matsunaga, H. (2000). Vibration and stability of thick plates on elastic foundations. Journal of engineering mechanics, 126(1), 27-34.

MEPDG (2004). Guide for Mechanistic-Empirical Design of New and Rehabilitated Pavement Structures, Part 2. Design Inputs, Chapter 3. Environmental Effects. ARA, Inc., ERES Consultant Division, Champaign, Illinois.

Mindess, S., Young, J. F., and Darwin, D. (2003). Concrete, 2nd edition, Pearson.

MnROAD (2017). Minnesota Department of Transportation, Minnesota's Cold Weather Pavement Testing Facility. https://www.dot.state.mn.us/mnroad/ Accessed 2017.

Nazarian, S., and I. I. Stokoe. (1986). Use of surface waves in pavement evaluation. In Transportation Research Record: Journal of the Transportation Research Board, Washington, D.C., (170), 132-144.

Ozgan, K., and Daloglu, A. T. (2009). Application of the Modified Vlasov Model to the free vibration analysis of thick plates resting on elastic foundations. Shock and Vibration, 16(5), 439-454.

Ozgan, K. (2012). Free vibration analysis of thick plates on elastic foundations using modified Vlasov model with higher order finite elements. Indian Journal of Engineering & Materials Sciences, (19), 279-291.

Ozgan, K. (2013). Dynamic analysis of thick plates including deep beams on elastic foundations using modified Vlasov model. Shock and Vibration, 20(1), 29-41.

Pasternak, P. L. (1954). On a New Method of Analysis of an Elastic Foundation by Means of Two Foundation Constants. Gosudarstvennoe Izdatel'stvo Litearturi po Stroitel'stvu i Arkhitekture, Moscow, USSR (in Russian).

Patil, V., Sawant, V. and Kousik D. (2012). Finite element analysis of rigid pavement on a nonlinear two parameter foundation model. International Journal of Geotechnical Engineering, 6(3), 275-286.

Pouget, S., Sauzéat, C., Benedetto, H. D., and Olard, F. (2011). Viscous energy dissipation in asphalt pavement structures and implication for vehicle fuel consumption. Journal of Materials in Civil Engineering, 24(5), 568-576.

Pouget, S., Sauzeat, C., Di Benedetto, H., and Olard, F. (2014). Calculation of viscous energy dissipation in asphalt pavements. The Baltic Journal of Road and Bridge Engineering, 9(2), 123-123.

Pozhuev, V. I. (1986). Steady-state reaction to the effect of a moving load in a system consisting of a cylindrical shell and a viscoelastic filler. Soviet Applied Mechanics, 22(5), 415-421.

Pradhan, M., Mishra, M. K. and Dash, P. R. (2016). Free Vibration Analysis of an Asymmetric Sandwich Beam Resting on a Variable Pasternak Foundation, Procedia Engineering, 144, 116-123.

Read, W. T. (1950). Stress analysis for compressible viscoelastic materials. Journal of Applied Physics, 21(7), 671-674.

Saito, H., Terasawa, T. (1980). Steady-state Vibrations of a Beam on a Pasternak Foundation for Moving Loads, Journal of Applied Mechanics, 47(4), 879-883.

Sebaaly, B., Davis, T. G., and Mamlouk, M. S. (1985). Dynamics of falling weight deflectometer. Journal of Transportation Engineering, 111(6), 618-632.

Sebaaly, B. E., Mamlouk, M. S., and Davies, T. G. (1986). Dynamic analysis of falling weight deflectometer data. Transportation Research Record, 1070, 63-68.

Selvadurai, A. P. (1979). Elastic analysis of soil-foundation interaction. Elsevier, 1st Edition.

Shi, X. P., Fwa, T. F., Tan, S. A. (1993). Warping Stresses in Concrete Pavements on Pasternak Foundation. Journal of transportation engineering, 119(6), 905-913.

Shi, X. P., Tan, S. A., Fwa, T. F. (1994). Rectangular Thick Plate with Free Edges on Pasternak Foundation, Journal of engineering mechanics, 120(5), 971-988.

Silva, A. R., Silveira, R. A., and Gonçalves, P. B. (2001). Numerical methods for analysis of plates on tensionless elastic foundations. International Journal of Solids and Structures, 38(10), 2083-2100.

Sireesh, S., Faby Mole, P. A., Madhav, M. R., and Vijay Kumar, R. (2016). Non-linear response of geocell reinforced dense granular layer over weak soil under circular loading. International Journal of Geotechnical Engineering, 10(1), 23-30.

Smith, K. D., Bruinsma, J. E., Wade, M. J., Chatti, K., Vandenbossche, J. M., and Yu, H. T. (2010). Using Falling Weight Deflectometer Data with Mechanistic-Empirical Design and Analysis, Volume 1: Final Report. Federal Highway Administration, 1200.

Stet, M. T. B. V. J., Thewessen, B., and Verbeek, J. (2002). Structural assessment of flexible and rigid airfield pavements. In Proc., Int. Workshop on the "PNC Calcultions for Heavier Aircraft.

Stolle, D. F. E. (1991). Modelling of dynamic response of pavements to impact loading. Computers and Geotechnics, 11(1), 83-94.

Swaminathan, K., Naveenkumar, D. T., Zenkour, A. M., and Carrera, E. (2015). Stress, vibration and buckling analyses of FGM plates—a state-of-the-art review. Composite Structures, 120, 10-31.

Tanahashi, H. (2004). Formulas for an infinitely long Bernoulli-Euler beam on the Pasternak model. Soils and foundations, 44(5), 109-118.

Tanyu, B.F., Kim, W.H., Edil, T.B. and Benson, C.H., (2003). Comparison of laboratory resilient modulus with back-calculated elastic moduli from large-scale model experiments and FWD tests on granular materials. In Resilient Modulus Testing for Pavement Components. ASTM International.

Teodoru, I. B., and Muşat, V. (2010). The modified Vlasov foundation model: an attractive approach for beams resting on elastic supports. EJGE, 15.

Tholen O, Sharma J, and Terrel RL. (1985). Comparison of FWD with other deflection testing devices. Transportation research record, TRB. Washington, DC: National Research Council, 1007, 20-26.

Tornabene, F., Fantuzzi, N., Viola, E. and Reddy, J. N. (2014). Winkler–Pasternak foundation effect on the static and dynamic analyses of laminated doubly-curved and degenerate shells and panels, Composites Part B: Engineering, 57, 269-296.

Turhan, A. (1992). A consistent Vlasov model for analysis of plates on elastic foundations using the finite element method. Doctoral dissertation, Texas Tech University.

Ullidtz, P. (2000). Will nonlinear backcalculation help. In: Tayabji SD, Lukanen EO, editors. NDT of pavements and backcalculation of moduli, 3. Special technical publication, STP 1375. Pennsylvania: ASTM Publication, 14-22.

Uzan, J. (1994a). Advanced backcalculation techniques. In Nondestructive Testing of Pavements and Backcalculation of Moduli: Second Volume. ASTM International.

Uzan, J. (1994b). Dynamic Linear Backcalculation of Pavement Material Parameters. Transportation Research Record: Journal of the Transportation Research Board, 120(1), 109-126.

Vallabhan, C. V., and Das, Y. C. (1988). An improved model for beams on elastic foundations. ASME Pressure Vessel and Piping Conference.

Vallabhan, C. V., and Das, Y. C. (1991). Modified Vlasov model for beams on elastic foundations. Journal of geotechnical engineering , 117(6), 956-966.

Vallabhan, C. G., and Daloglu, A. T. (1999). Consistent FEM-Vlasov model for plates on layered soil. Journal of Structural Engineering, 125(1), 108-113.

Van Cauwelaert, F. (2003). Pavement Design and Evaluation. The required mathematics and its applications. Federation of the Belgian Cement Industry, Brussels.

Varma, S. (2015). Viscoelastic inverse analysis of FWD data using genetic algorithms. Doctorate dissertation, Michigan State University.

Vlasov, V. Z., and Leontiev, U. N. (1966). Beams, plates and shells on elastic foundations. Israel Program for Scientific Translations, Jerusalem, Isreal.

Von Quintus, H. L., and A. L. Simpson. (2002). Back-Calculation of Layer Parameters for LTPP Test Sections, Volume II: Layered Elastic Analysis for Flexible and Rigid Pavements. No. FHWA-RD-01-113.

Von Quintus, H. L., Rao, C., and Irwin, L. (2015). Long-Term Pavement Performance Program Determination of In-Place Elastic Layer Modulus: Backcalculation Methodology and Procedures (No. FHWA-HRT-15-036).

Wang, F., and Lytton, R. L. (1993). System identification method for backcalculating pavement layer properties. Transportation Research Record, 1384, 1-7.

Wang, Y. H., Tham, L. G. and Cheung, Y. K. (2005). Beams and plates on elastic foundations: a review. Progress in Structural Engineering and Materials, 7(4), 174-182.

Wang, T., Harvey, J., and Kendall, A. (2014). Reducing greenhouse gas emissions through strategic management of highway pavement roughness. Environmental Research Letters, 9(3), 034007.

Westergaard, H. M. (1926). Stresses in concrete pavements computed by theoretical analysis. Public Roads, 7(2), 25-35.

Worku, A. (2010). Part I: A generalized formulation of continuum models for elastic foundations. In GeoFlorida 2010: Advances in Analysis, Modeling & Design (1641-1650).

Worku, A., and Degu, Y. (2010). Part II: Application of newly derived and calibrated continuum subgrade models in the analysis of beams on elastic foundations. In GeoFlorida 2010: Advances in Analysis, Modeling & Design (1651-1660).

Worku, A. (2013). Calibrated analytical formulas for foundation model parameters, International Journal of Geomechanics, ASCE, 13(4), 340-347.

Worku, A. (2014). Development of a calibrated Pasternak foundation model for practical use, International Journal of Geotechnical Engineering, 8(1), 26-33.

Xing, Y. F. and Liu, B. (2009). New exact solutions for free vibrations of thin orthotropic rectangular plates, Composite Structures, 89(4), 567-574.

Xu, Q. (2014). Development of a computational method for inverting dynamic moduli of multilayer systems with applications to flexible pavements. Doctorate dissertation, The University of Texas at Austin.

Yang, Y., Ding, H., and Chen, L. Q. (2013). Dynamic Response to a Moving Load of a Timoshenko Beam Resting on a Nonlinear Viscoelastic Foundation. Acta Mechanica Sinica, 29(5), 718-727.

Yau, A., and Von Quintus, H. L. (2002). Study of LTPP laboratory resilient modulus test data and response characteristics. US Department of Transportation, Federal Highway Administration, No. FHWA-RD-02-051.

Yin, J. H. (2000). Closed-form solution for reinforced Timoshenko beam on elastic foundation, Journal of Engineering Mechanics, 126(8), 868-874.

Younesian, D., Kargarnovin, M. H., Thompson, D. J., and Jones, C. J. C. (2006). Parametrically Excited Vibration of a Timoshenko Beam on Random Viscoelastic Foundation Subjected to a Harmonic Moving Load. Nonlinear Dynamics, 45(1-2), 75-93.

Zaabar, I., and Chatti, K. (2010). Calibration of HDM-4 models for estimating the effect of pavement roughness on fuel consumption for US conditions. Transportation Research Record: Journal of the Transportation Research Board, 2155, 105-116.

Zaabar, I., and Chatti, K. (2011). New mechanistic-empirical approach for estimating the effect of roughness on vehicle durability. Transportation Research Record: Journal of the Transportation Research Board, 2227, 180-188.

Zaabar, I., Chatti, K., Lee, H. S., and Lajnef, N. (2014). Backcalculation of asphalt concrete modulus master curve from field measured falling weight deflectometer data using a new time domain viscoelastic dynamic solution and genetic algorithm. Transportation Research Record: Journal of the Transportation Research Board, 2475, 80-92.

Zheng, D. Y., Au, F. T. K. and Cheung, Y. K. (2000). Vibration of Vehicle on Compressed Rail on Viscoelastic Foundation, Journal of Engineering Mechanics, 126(11), 1141-1147.

Zhang, C., Zhu, H., Shi, B., and Liu, L. (2014). Theoretical investigation of interaction between a rectangular plate and fractional viscoelastic foundation. Journal of Rock Mechanics and Geotechnical Engineering, 6(4), 373-379.